Power Quality
Prof. Bhim Singh
Department of Electrical Engineering
Indian Institute of Technology, Delhi

Chapter - 15
Module - 04
Lecture - 45
Power Quality Improvement in Distributed Generation Sources Based Microgrids

Welcome to the course on Power Quality. Today we will be discussing Power Quality Improvement in Distributed Generation Sources Based Microgrid.

(Refer Slide Time: 00:27)

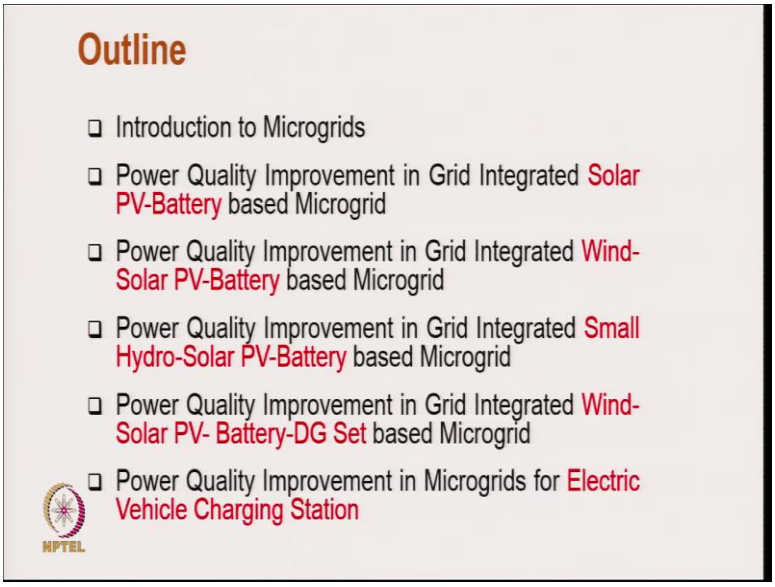

The outline of presentation is:

- Introduction to microgrid
- Power quality improvement in grid integrated solar PV based microgrid
- Power quality improvement in grid integrated wind solar PV and battery based microgrid
- Power quality improvement in grid connected small hydro solar PV and battery based microgrid

- Power quality improvement in grid connected wind solar battery and DG set based microgrid

- Power quality improvement in microgrid for electric vehicle charging station

(Refer Slide Time: 00:54)

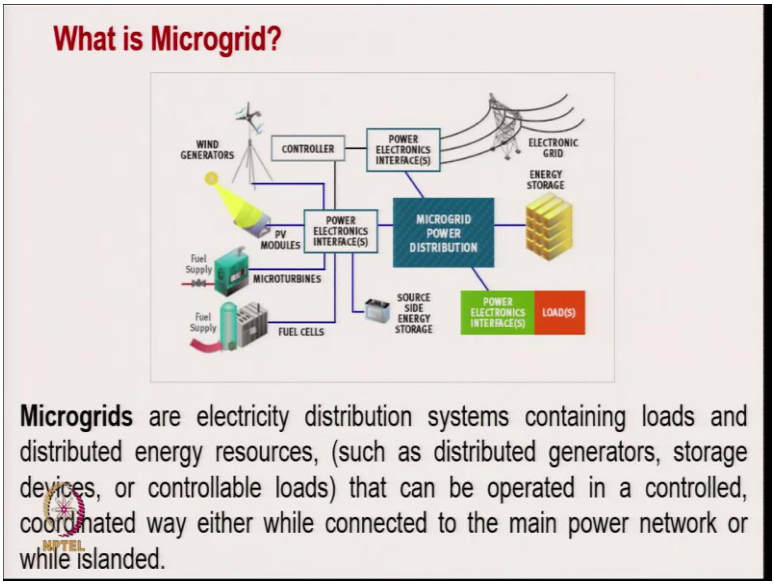

This is typically the concept of microgrid. Microgrids are electrically distributed system containing loads, distributed energy sources; such as distributed generator storage device and controllable load, that can be operated in a control coordinated way either while connecting to the main power network or while islanded.

(Refer Slide Time: 01:42)

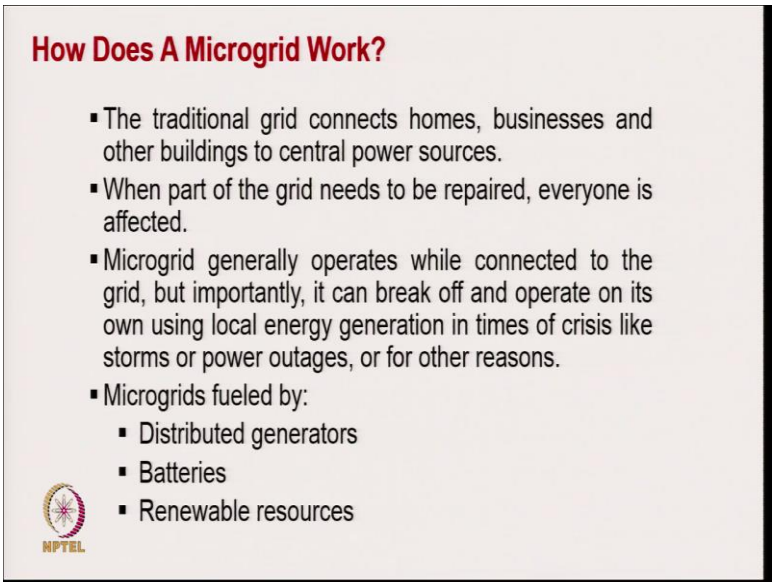

And how does microgrid work? The traditional grid connect homes business and other buildings to central power sources and when part of the grid needs to be repaired everyone is affected.

And microgrid generally operate while connected to the grid, but importantly it can break off and operate on its own using the local energy generation in times of crisis like a storm or power outage or for other reasons. And microgrid may be fueled by distributed generators, batteries and renewable energy sources.

(Refer Slide Time: 02:11)

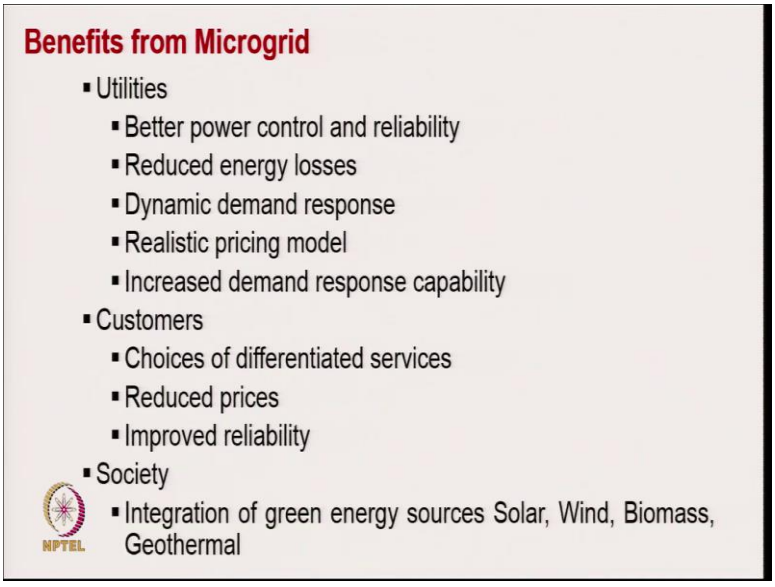

And benefits from the microgrid for the utility are: better power control and reliability, reduced energy losses, dynamic demand response, realistic pricing model and increased demand response capability. And for customer it provides choices for differentiated services and reduce prices and improved reliability. And for society it is an integration of green energy sources like solar, wind, biomass, geothermal.

(Refer Slide Time: 03:15)

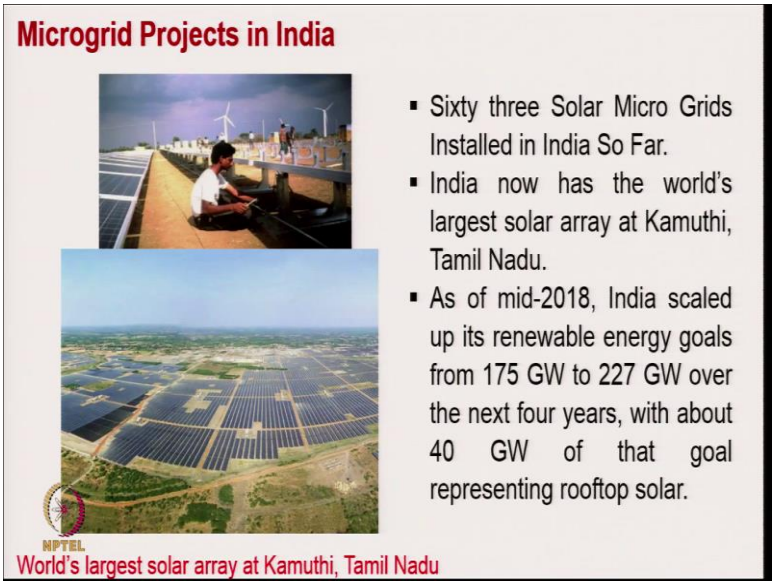

There are 63 solar microgrids installed in India. India now has the world's largest solar farm at Kamuthi, Tamil Nadu. As of 2018, India scaled up renewable energy goals from 175 gigawatt to 277 gigawatt over the next 4 years with about 40 gigawatt of the goal representing rooftop solar.

(Refer Slide Time: 05:45)

Now, coming to the power quality improvement in grid integrated solar PV based microgrid.

(Refer Slide Time: 05:51)

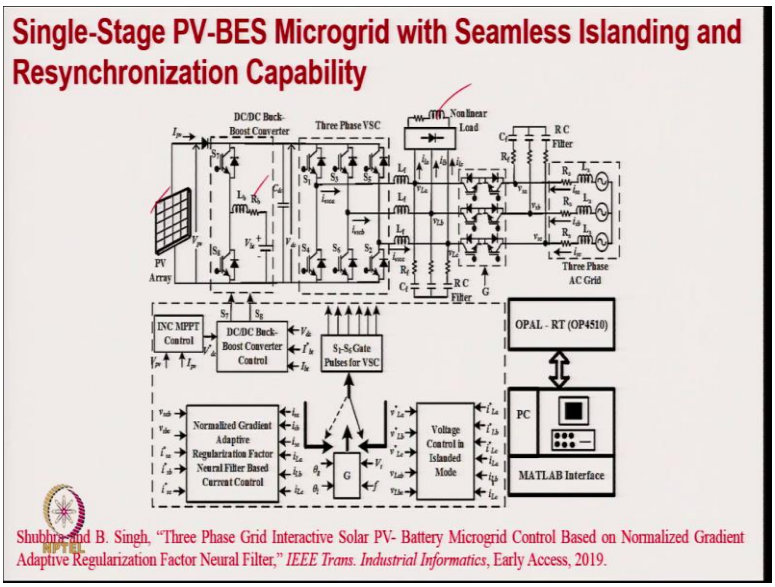

We have a single-stage solar PV array and BES is connected with the buck boost converter.

(Refer Slide Time: 07:05)

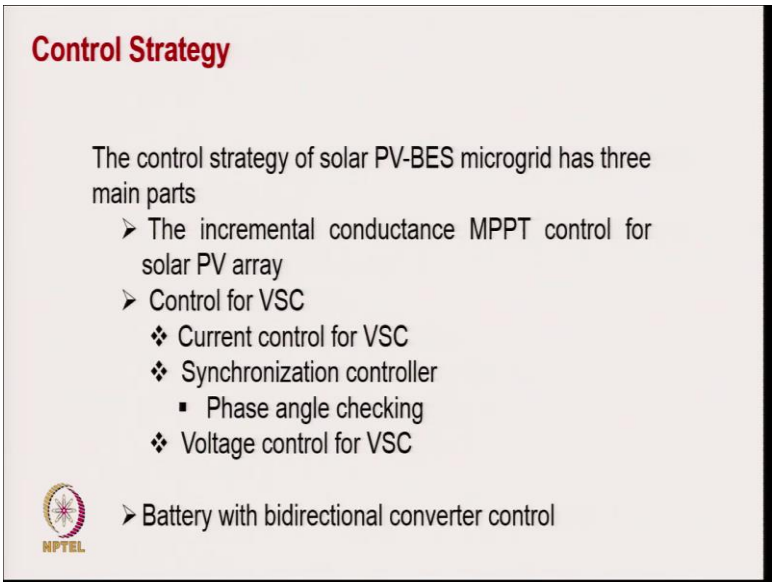

The details of the control strategy are provided in the screenshots herein.

(Refer Slide Time: 07:43)

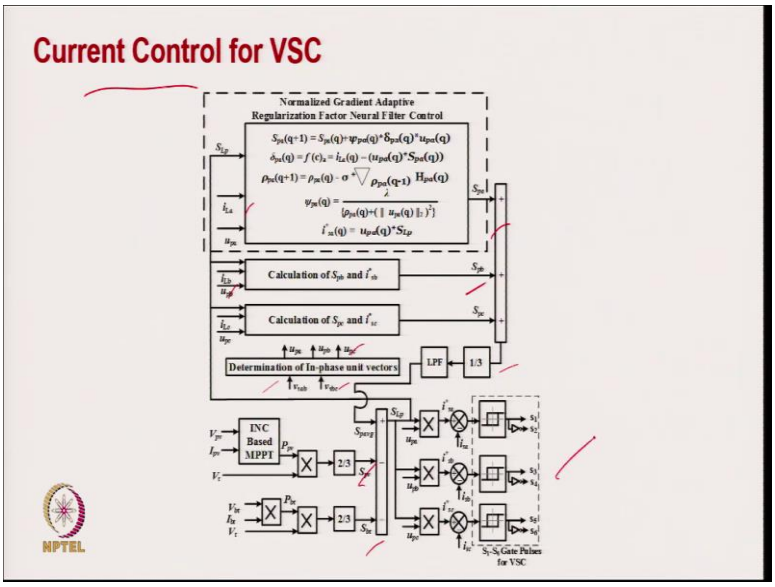

(Refer Slide Time: 08:21)

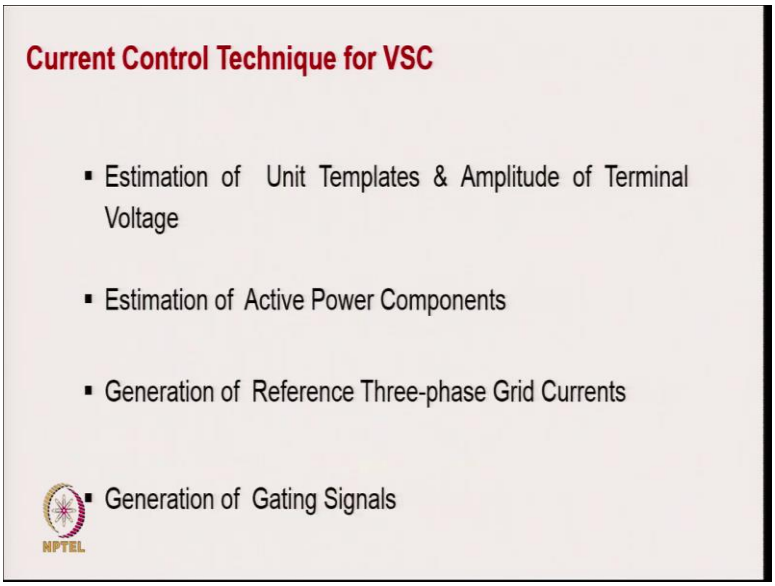

(Refer Slide Time: 08:31)

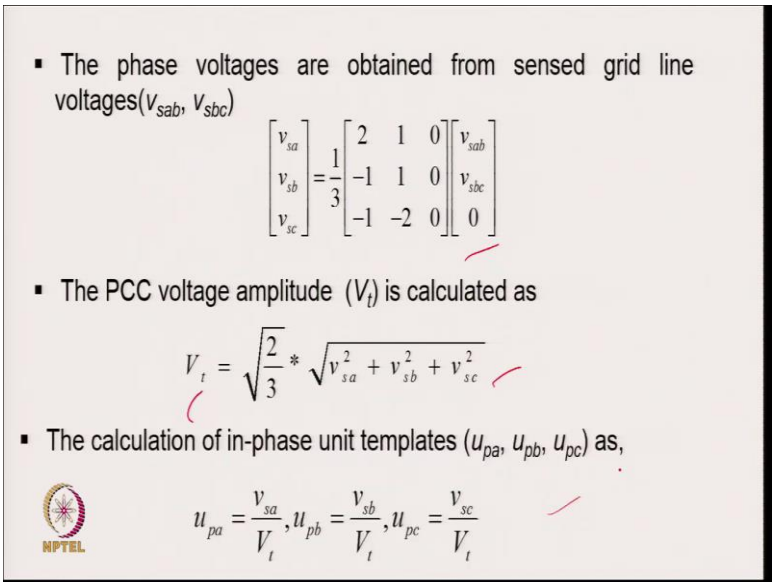

(Refer Slide Time: 08:41)

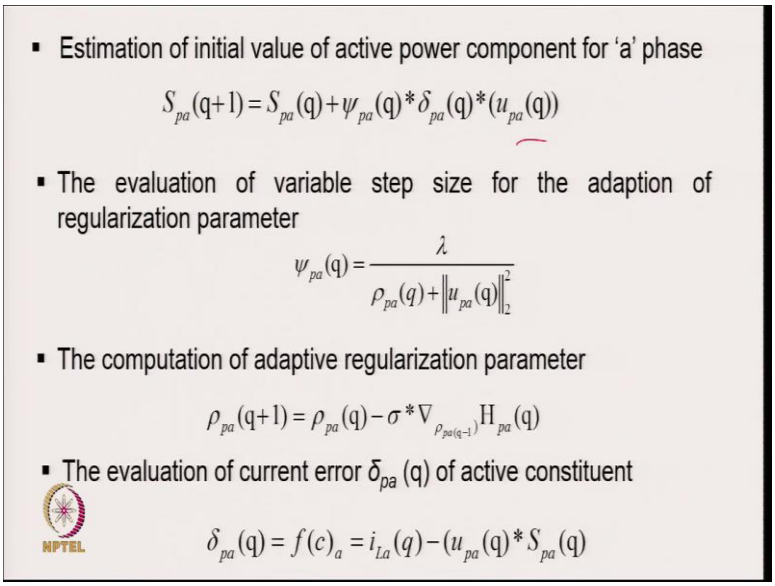

(Refer Slide Time: 09:02)

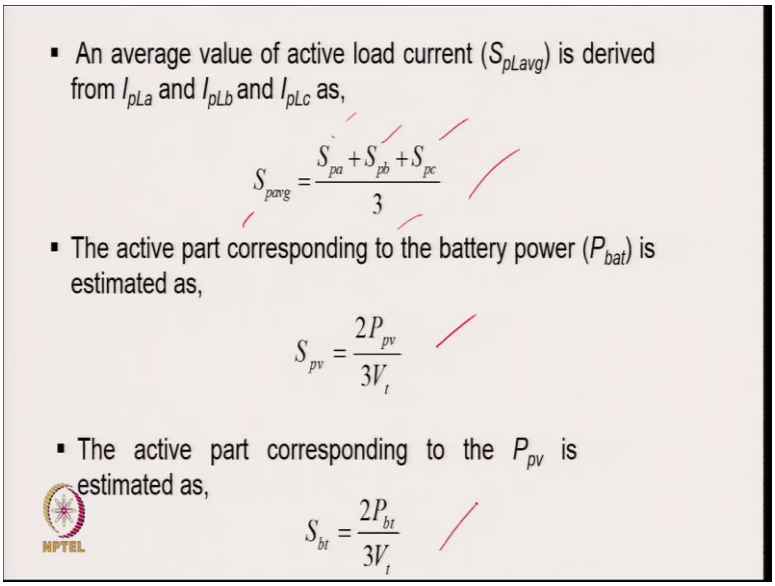

(Refer Slide Time: 09:17)

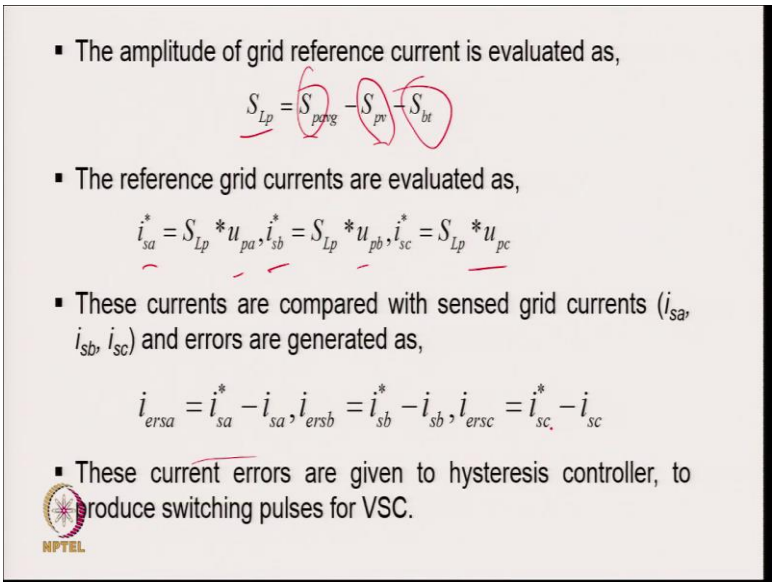

(Refer Slide Time: 09:44)

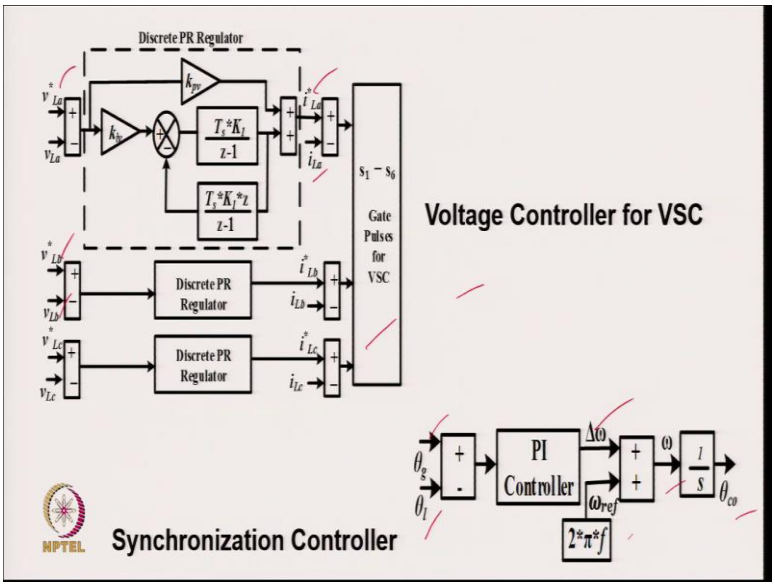

(Refer Slide Time: 10:33)

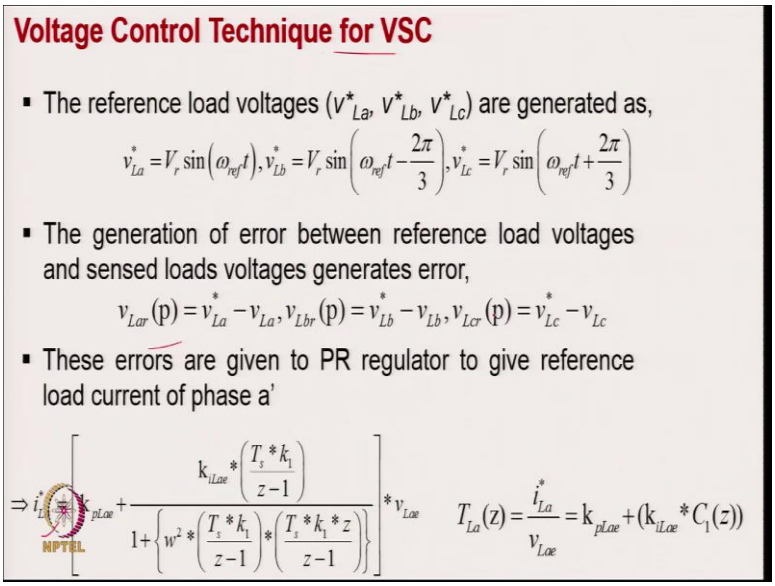

(Refer Slide Time: 10:46)

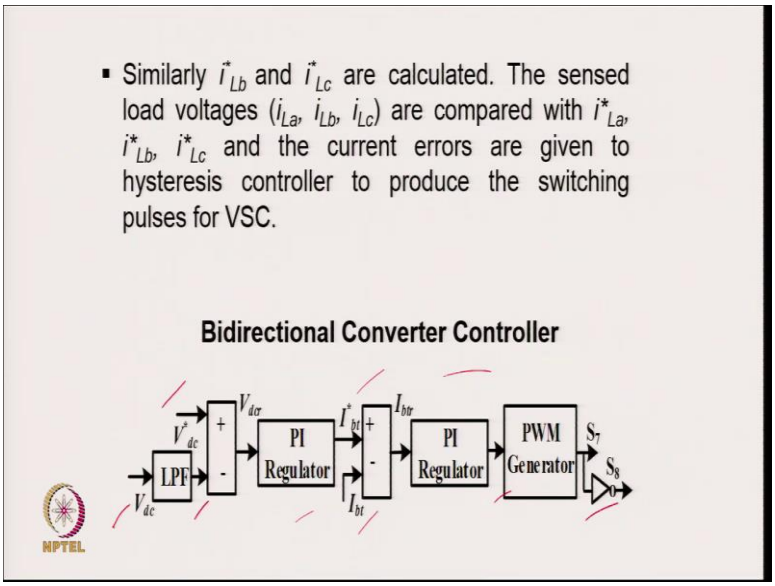

(Refer Slide Time: 11:12)

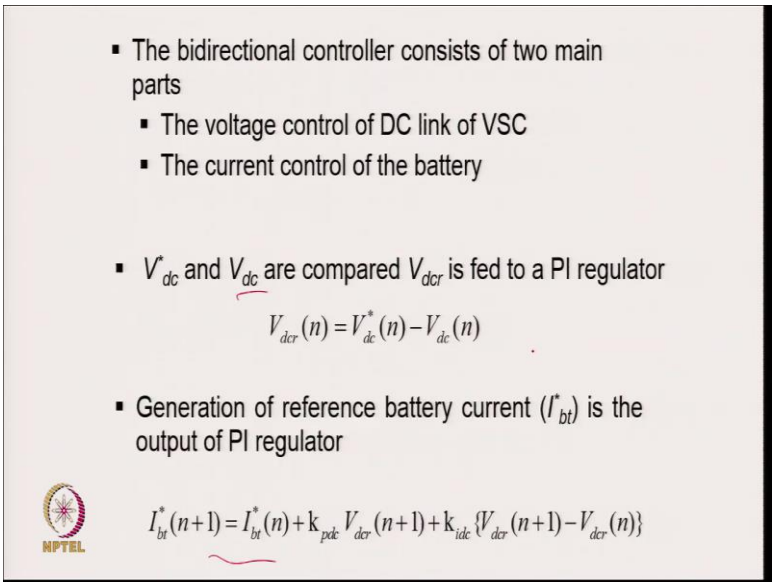

(Refer Slide Time: 11:26)

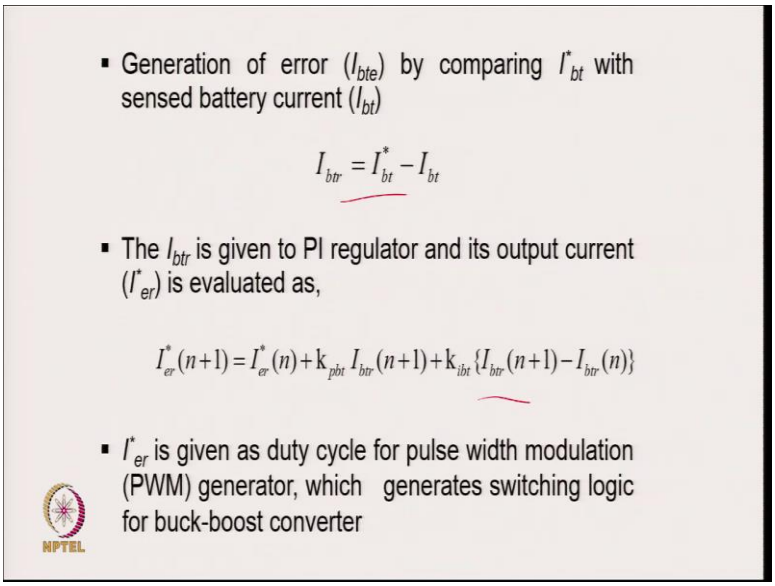

(Refer Slide Time: 11:37)

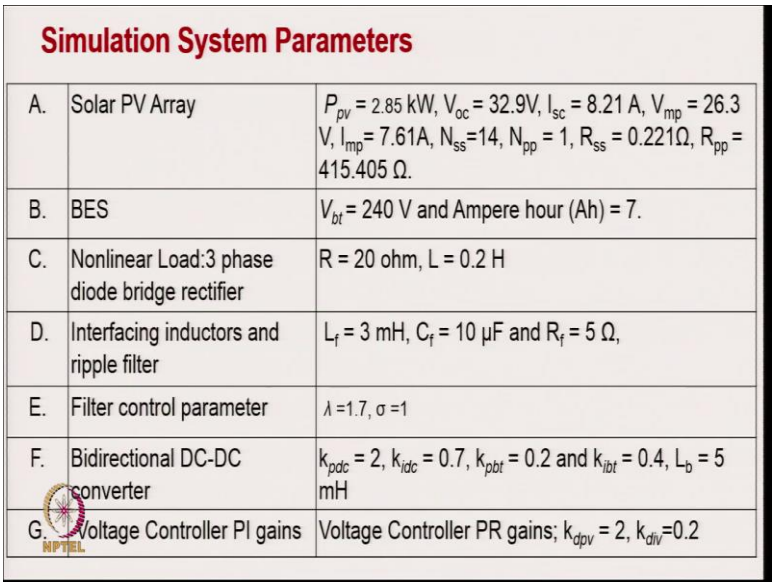

The parameters used for the simulation analysis are provided here.

(Refer Slide Time: 11:41)

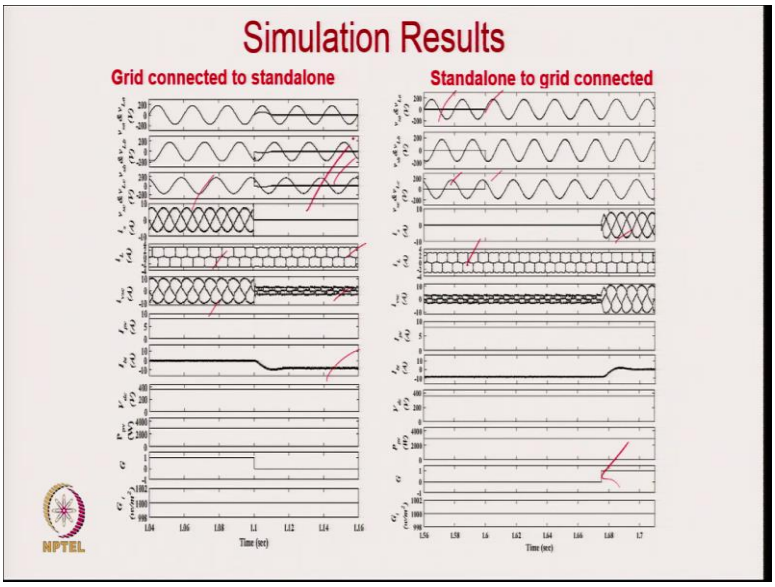

The simulation results are provided in the screenshots herein.

(Refer Slide Time: 12:26)

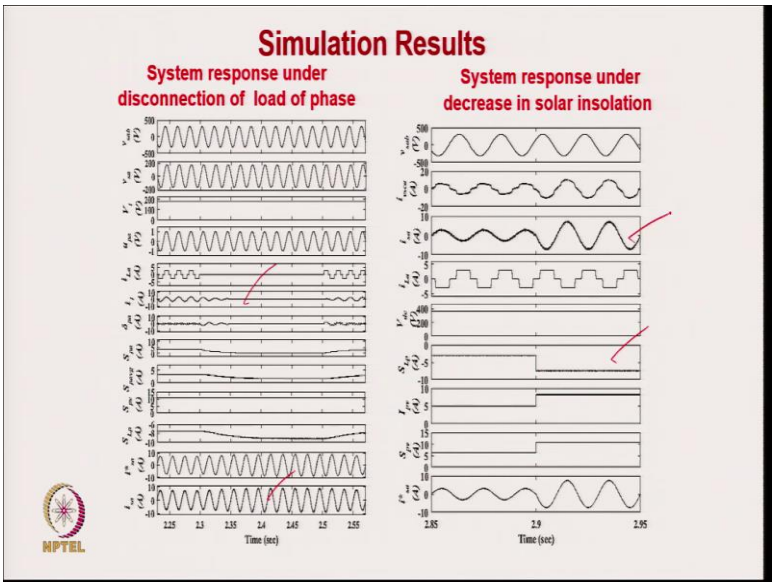

(Refer Slide Time: 12:41)

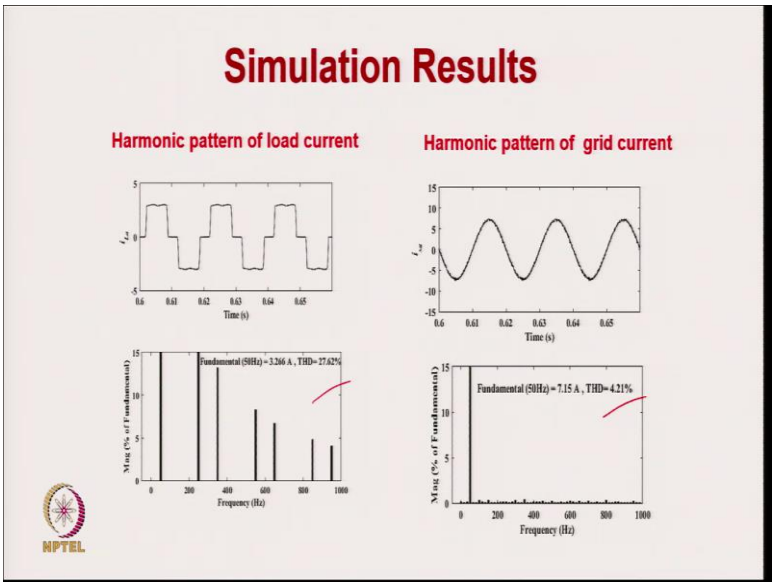

(Refer Slide Time: 12:58)

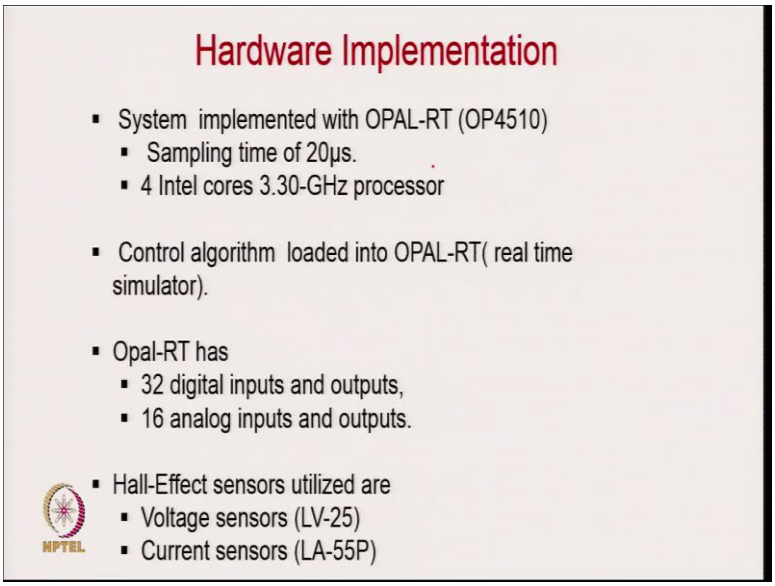

The parameters used for the experimental analysis are provided here.

(Refer Slide Time: 13:10)

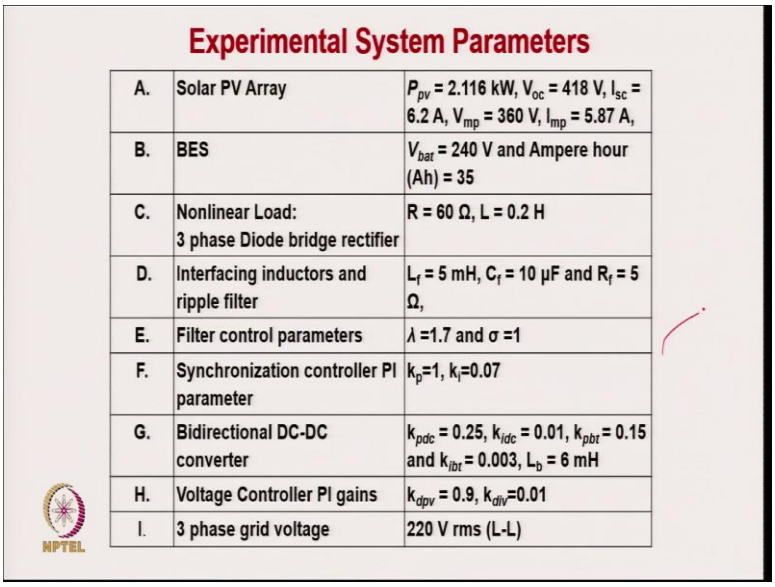

And these are the data of practical system.

(Refer Slide Time: 13:13)

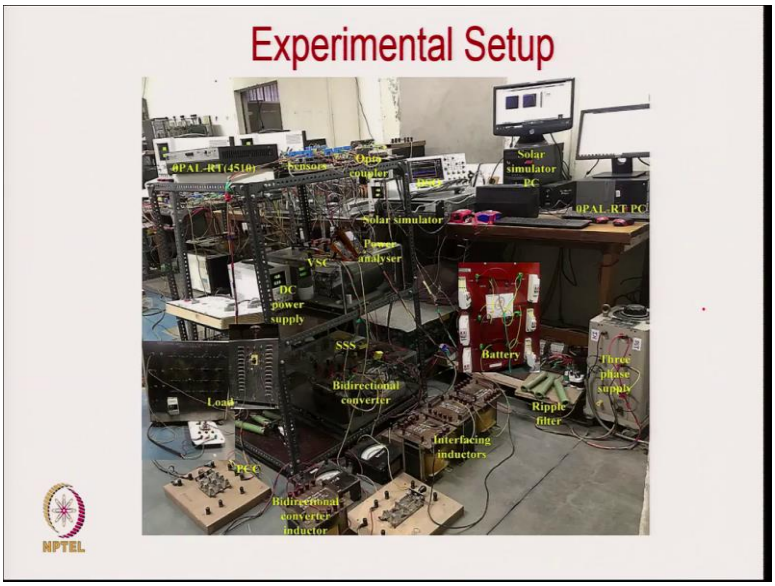

This is the photograph of the practical system.

(Refer Slide Time: 13:15)

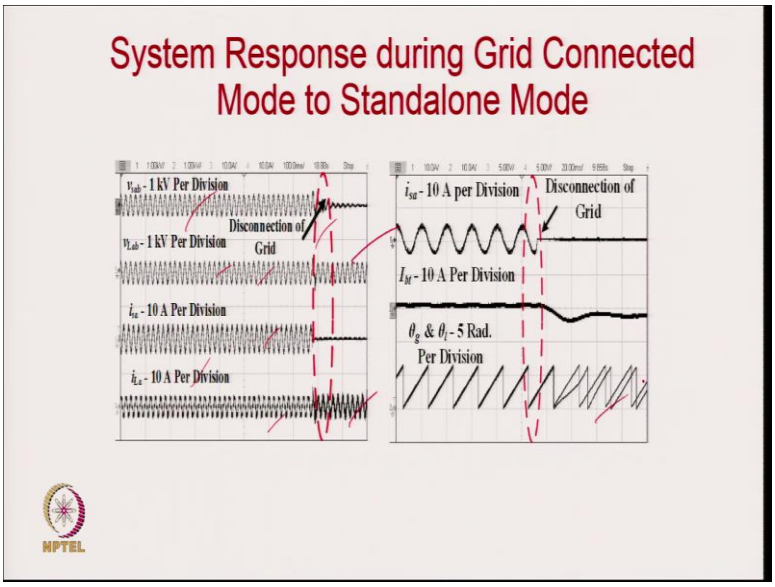

The simulation results are provided in the screenshots herein.

(Refer Slide Time: 13:33)

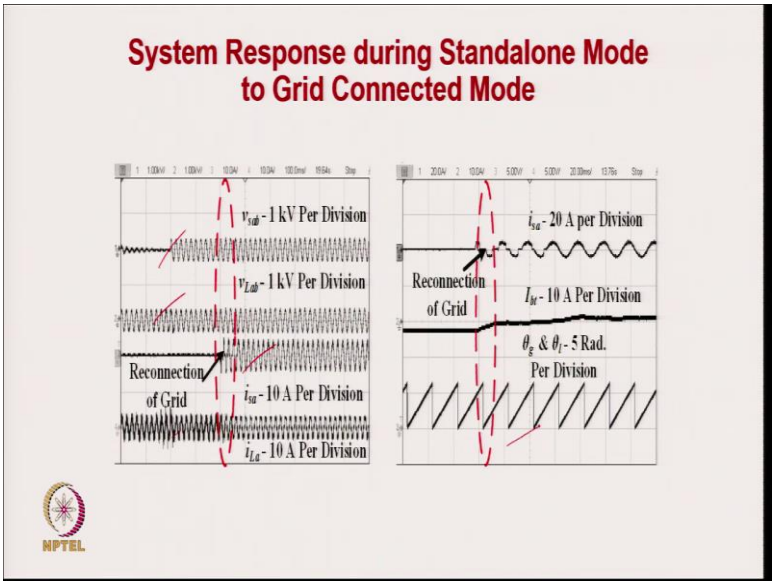

(Refer Slide Time: 13:52)

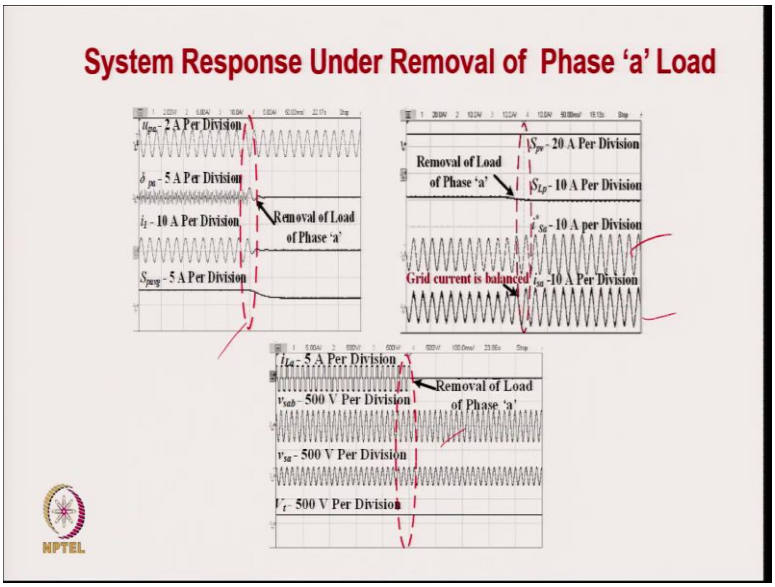

(Refer Slide Time: 14:07)

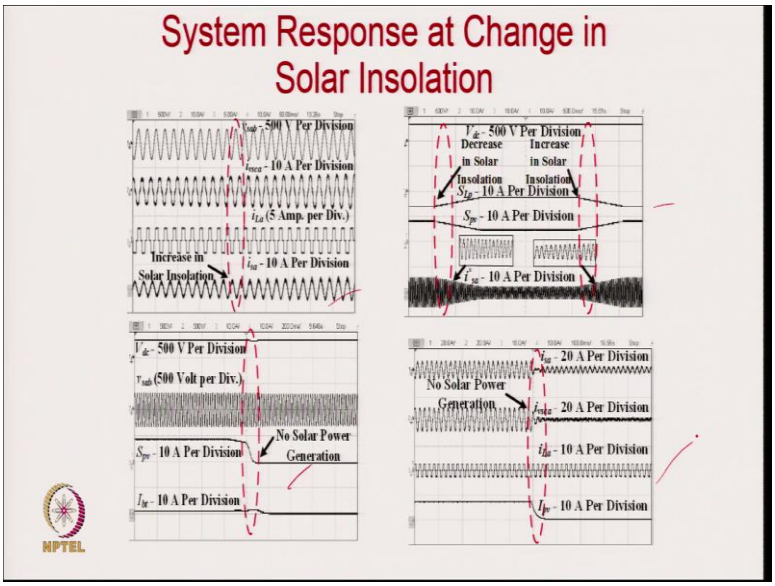

(Refer Slide Time: 14:27)

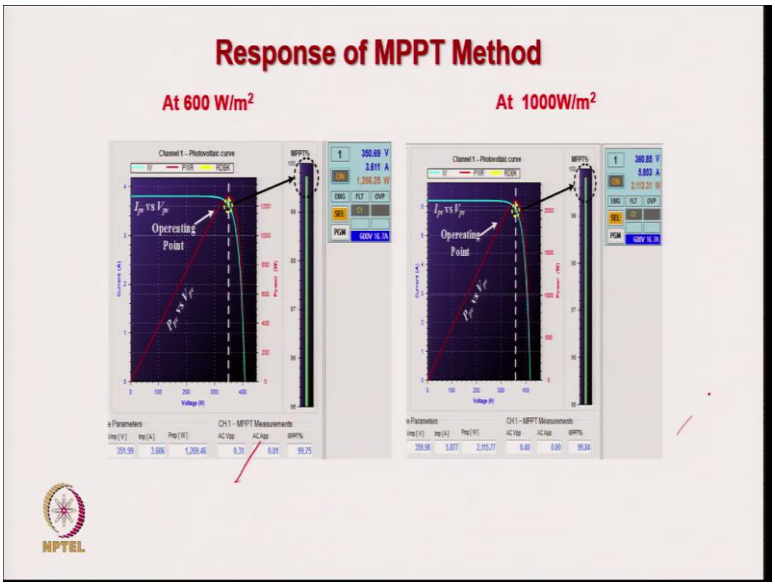

(Refer Slide Time: 14:35)

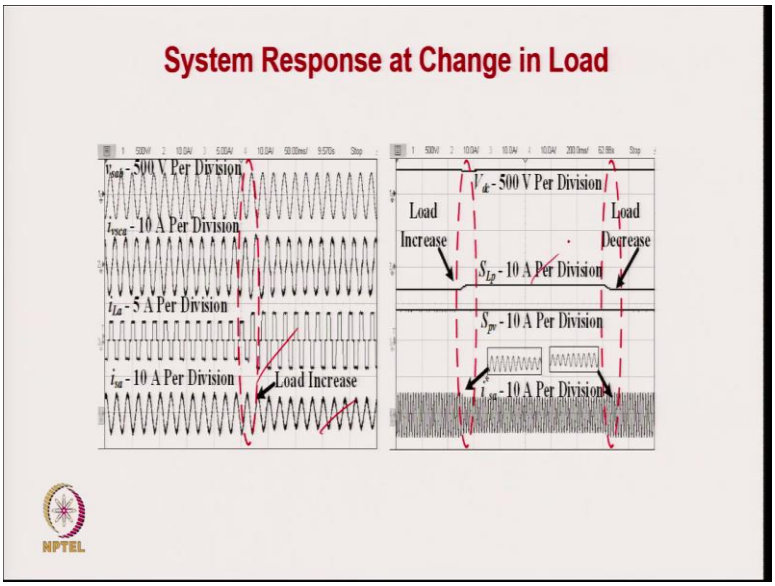

(Refer Slide Time: 14:51)

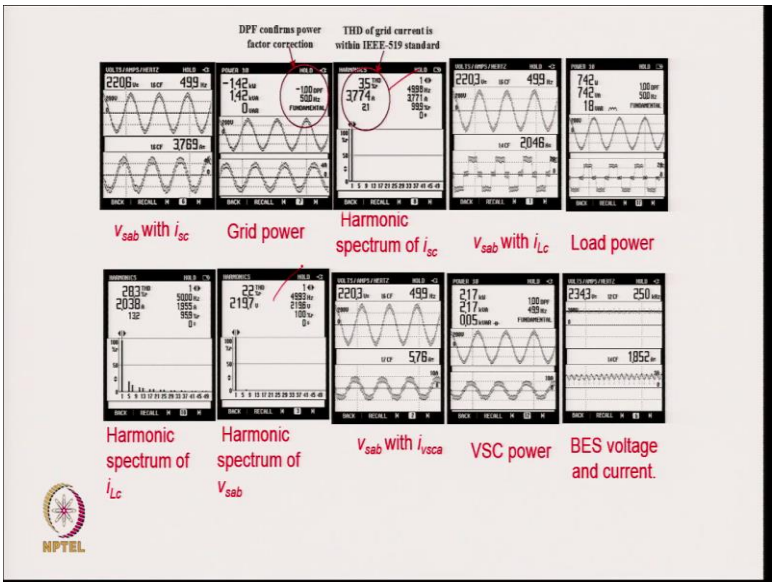

(Refer Slide Time: 15:01)

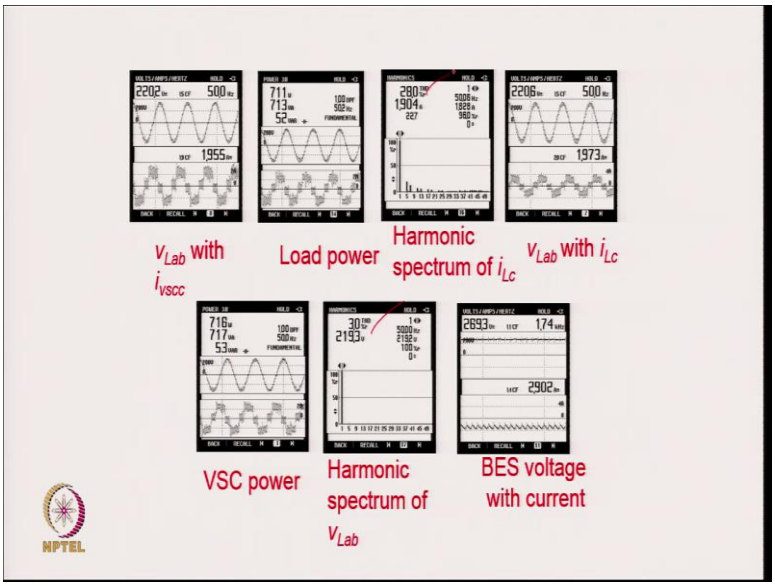

(Refer Slide Time: 15:50)

Now, coming to power quality improvement in the wind solar PV with battery based microgrid.

(Refer Slide Time: 15:56)

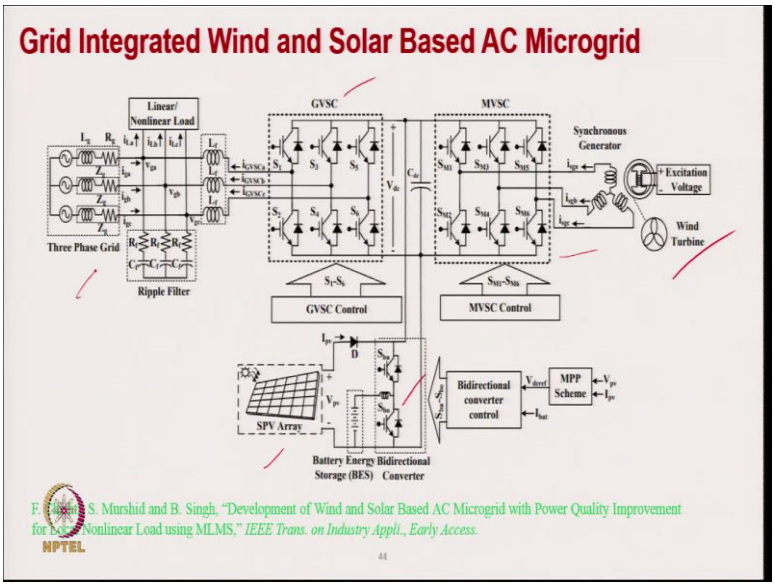

Here is the system where we have wind generation from synchronous generator with variable speed generation. SPV array is connected at DC link. And here on the DC link we are keeping a battery with the buck boost converter.

(Refer Slide Time: 16:18)

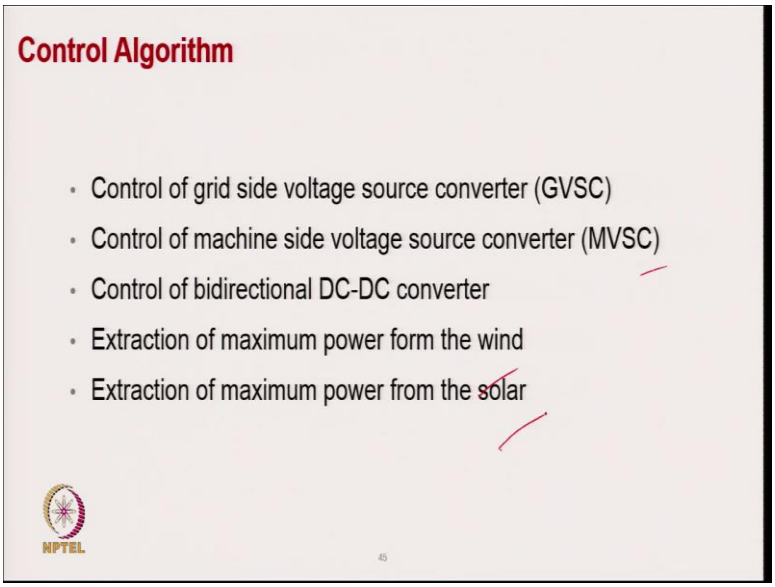

The control algorithm is explained herein.

(Refer Slide Time: 16:28)

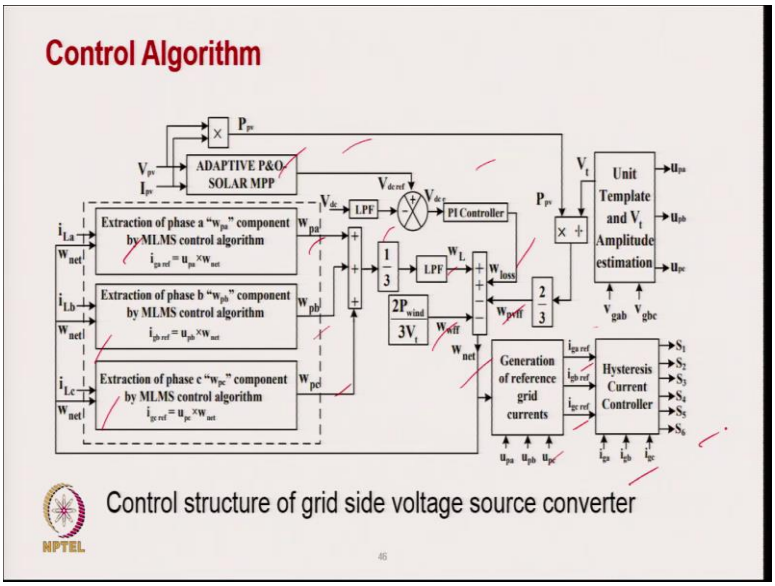

(Refer Slide Time: 17:07)

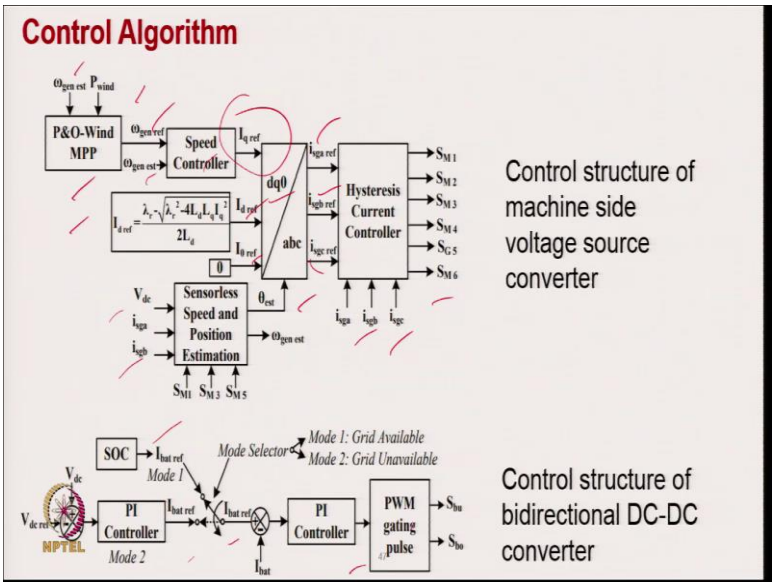

(Refer Slide Time: 18:07)

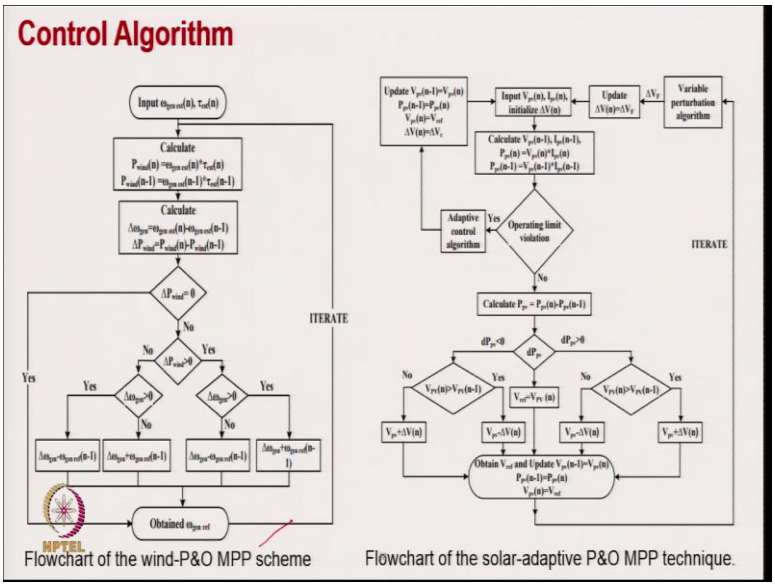

(Refer Slide Time: 18:19)

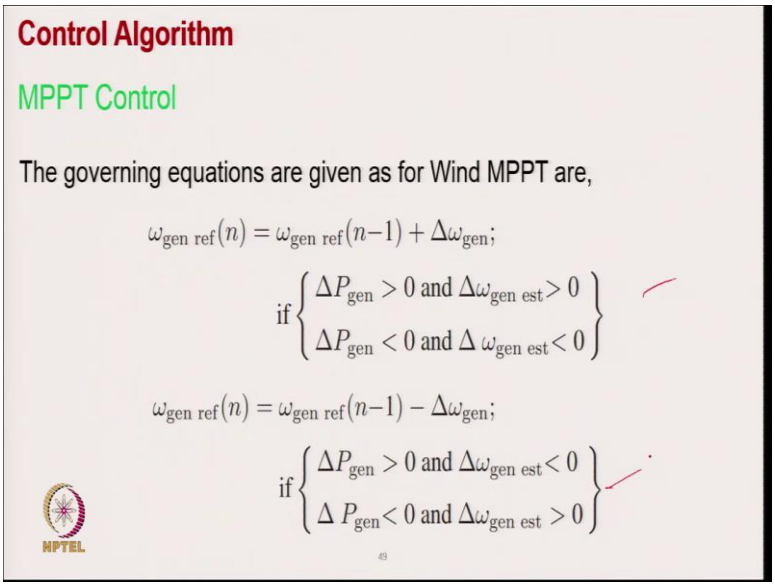

(Refer Slide Time: 18:26)

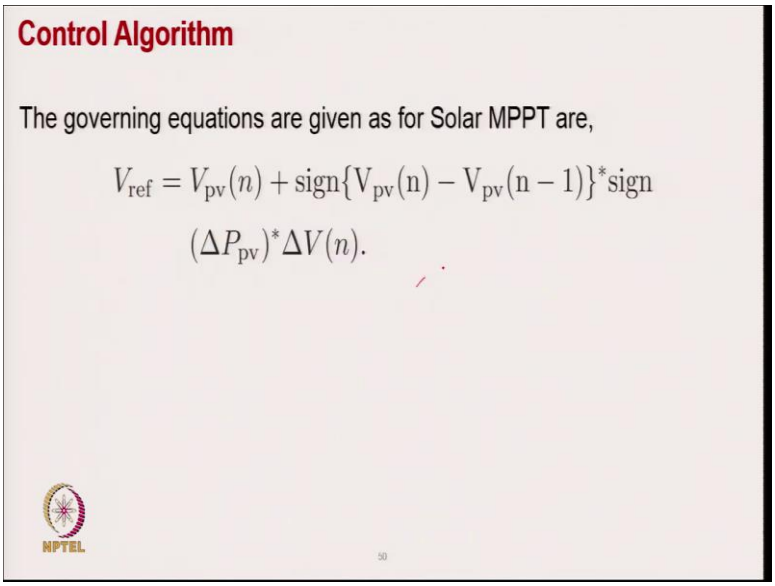

(Refer Slide Time: 18:35)

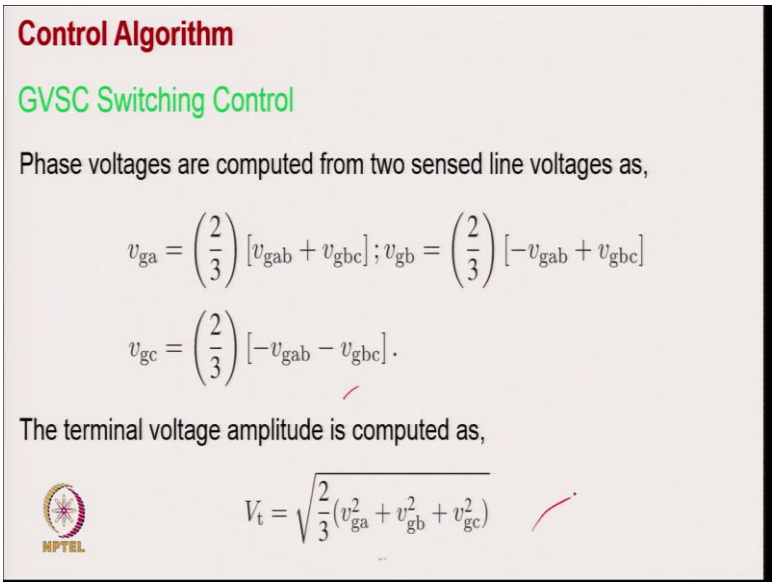

(Refer Slide Time: 18:42)

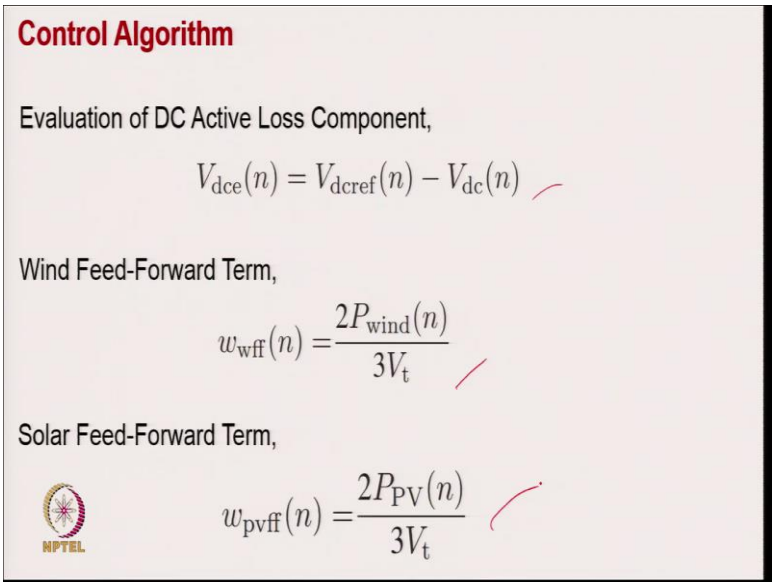

(Refer Slide Time: 18:53)

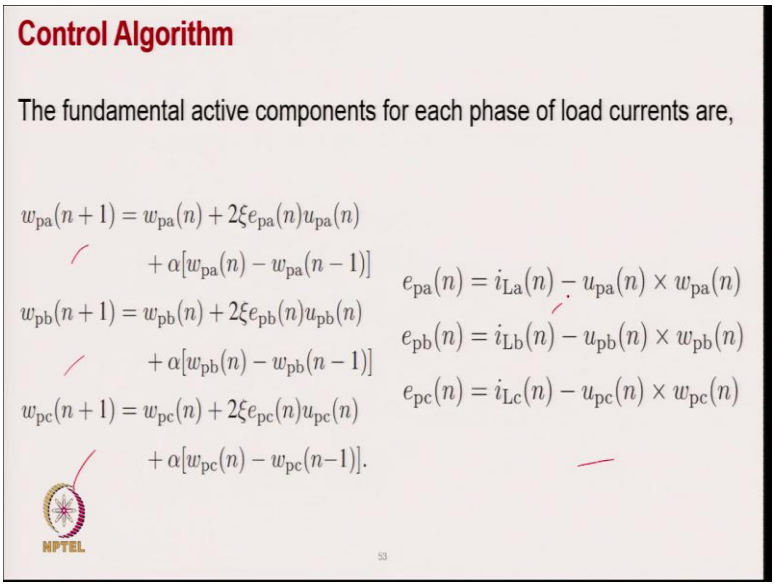

(Refer Slide Time: 19:03)

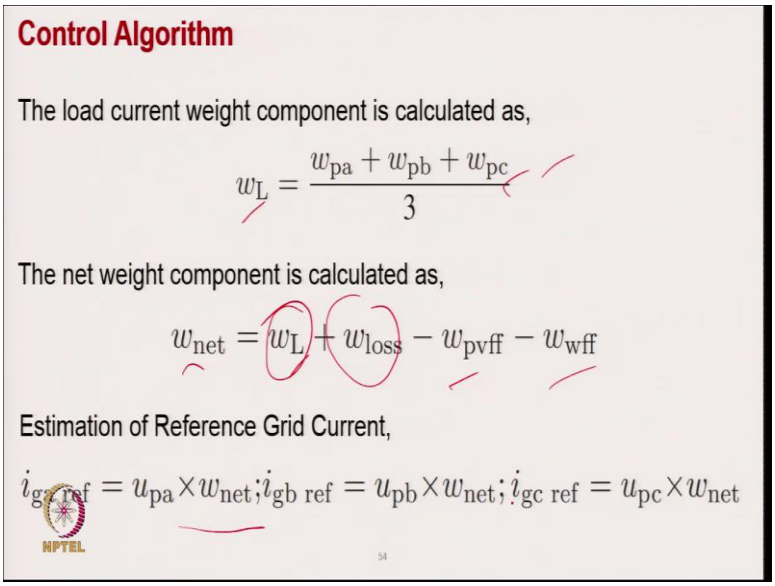

(Refer Slide Time: 19:27)

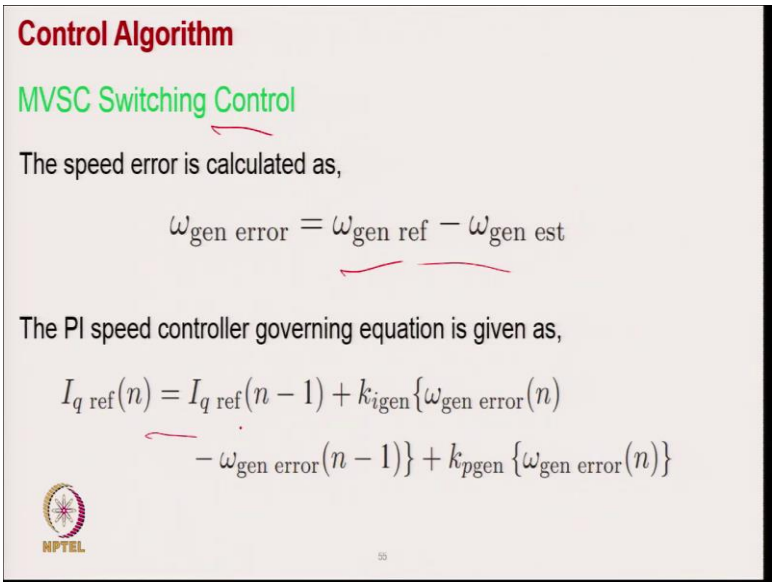

(Refer Slide Time: 19:48)

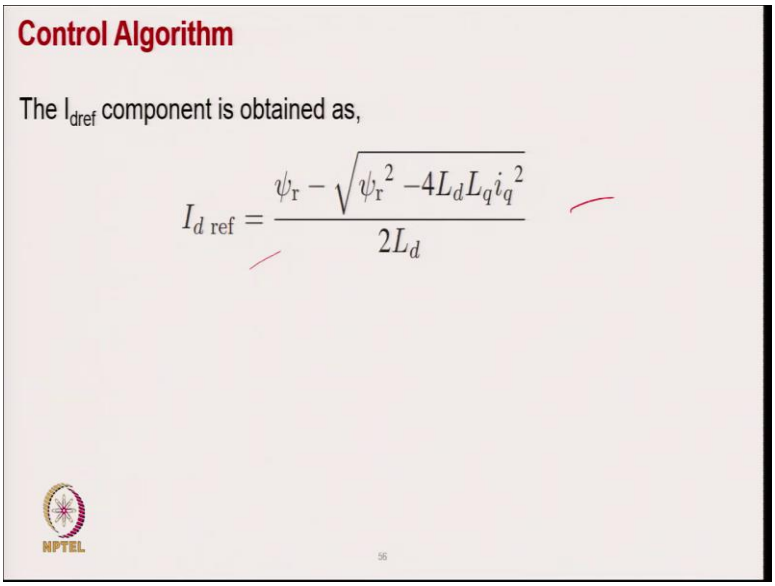

(Refer Slide Time: 20:04)

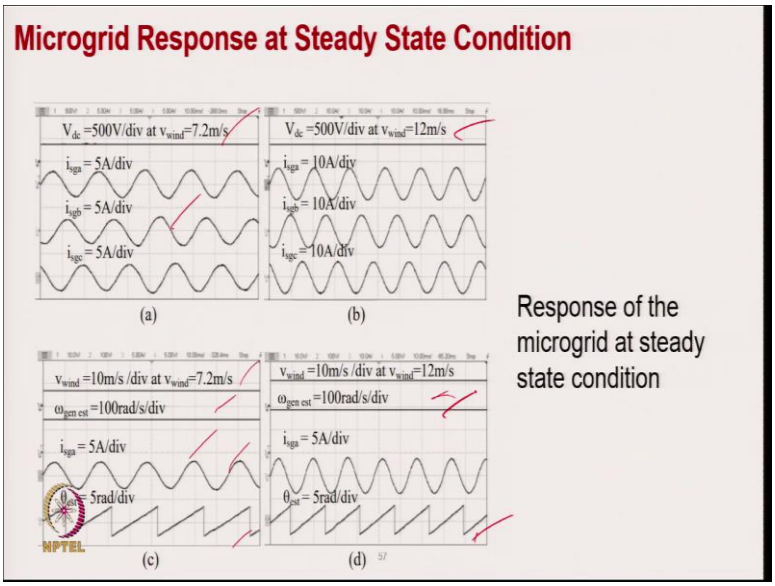

The experimental results are displayed in the screenshots herein.

(Refer Slide Time: 20:32)

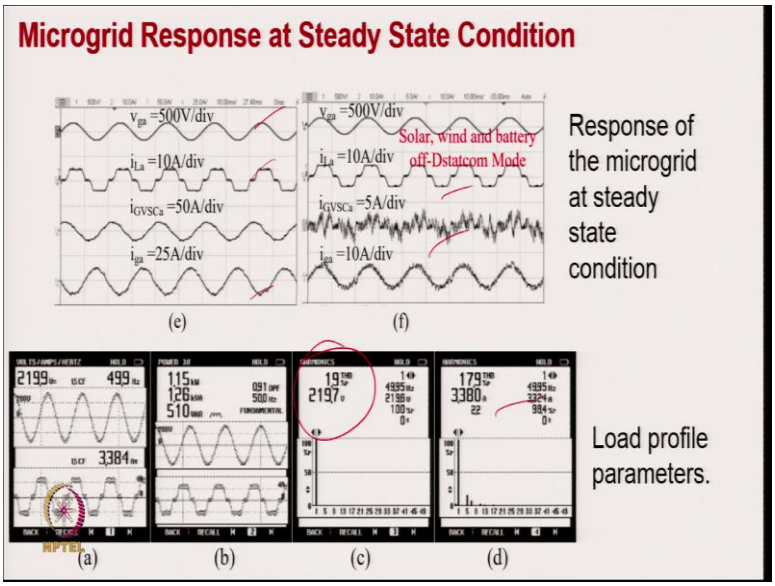

(Refer Slide Time: 20:53)

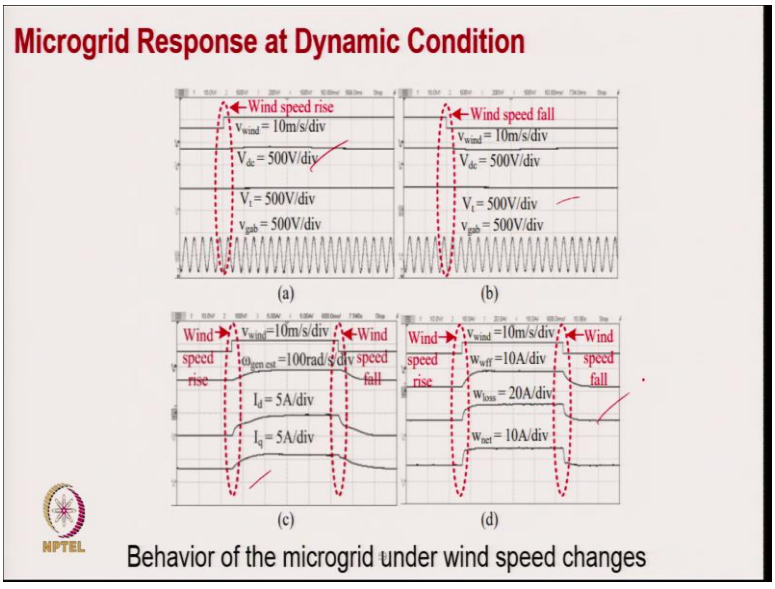

.

(Refer Slide Time: 21:09)

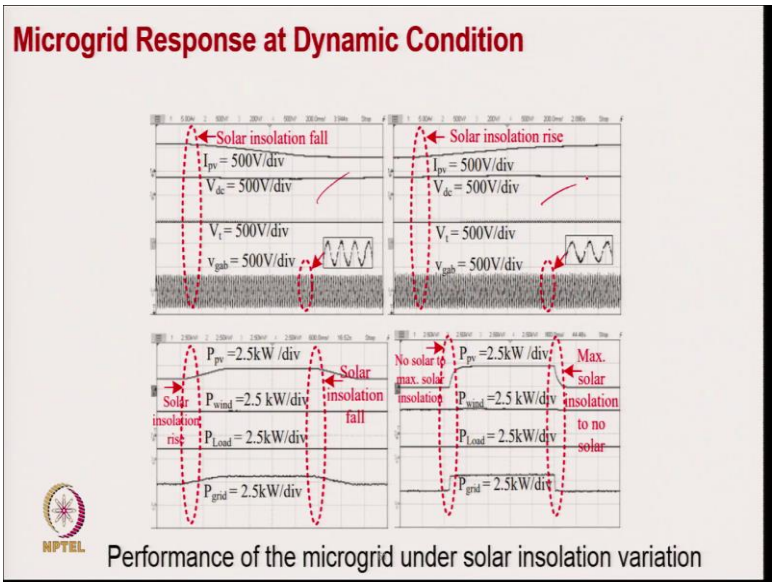

(Refer Slide Time: 21:20)

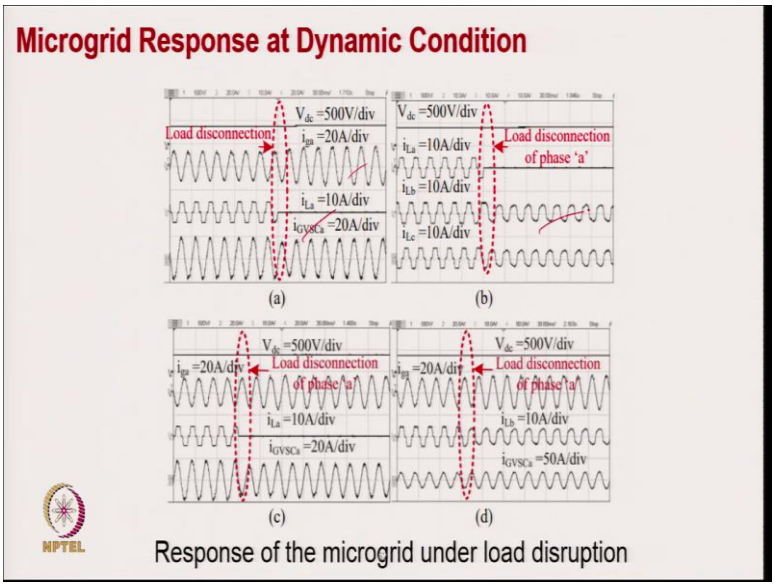

(Refer Slide Time: 21:34)

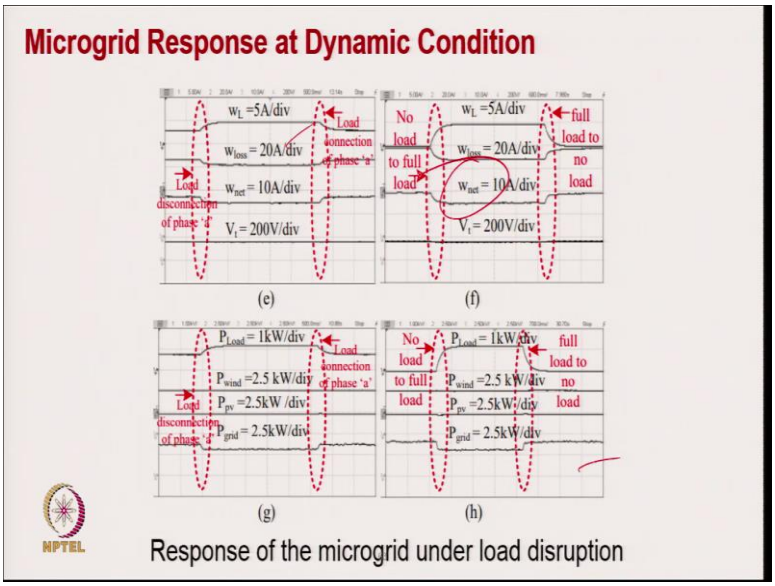

(Refer Slide Time: 21:47)

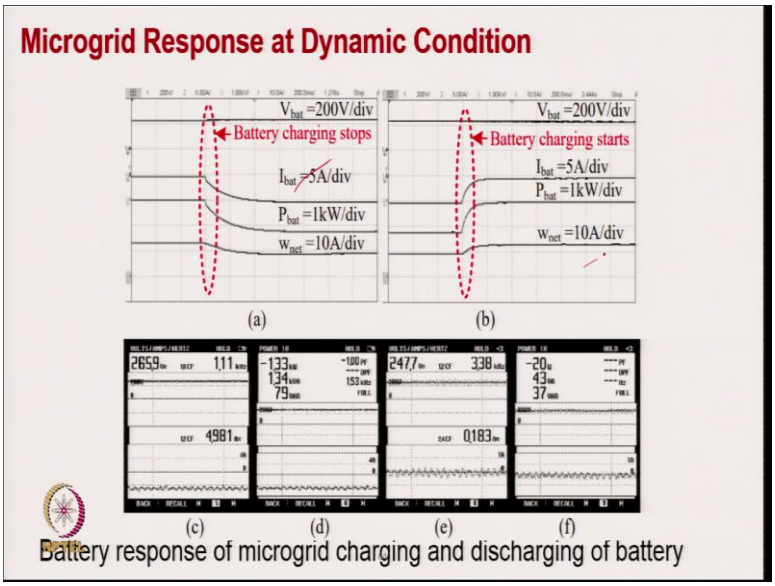

(Refer Slide Time: 21:57)

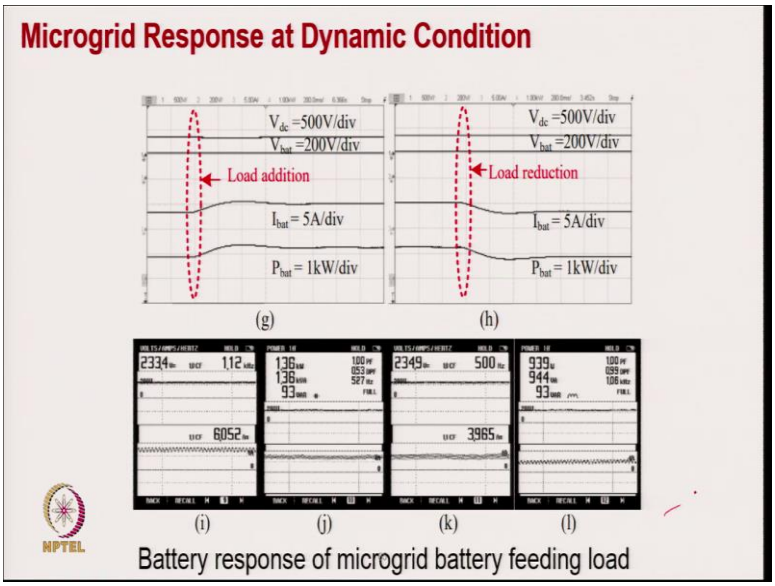

(Refer Slide Time: 22:03)

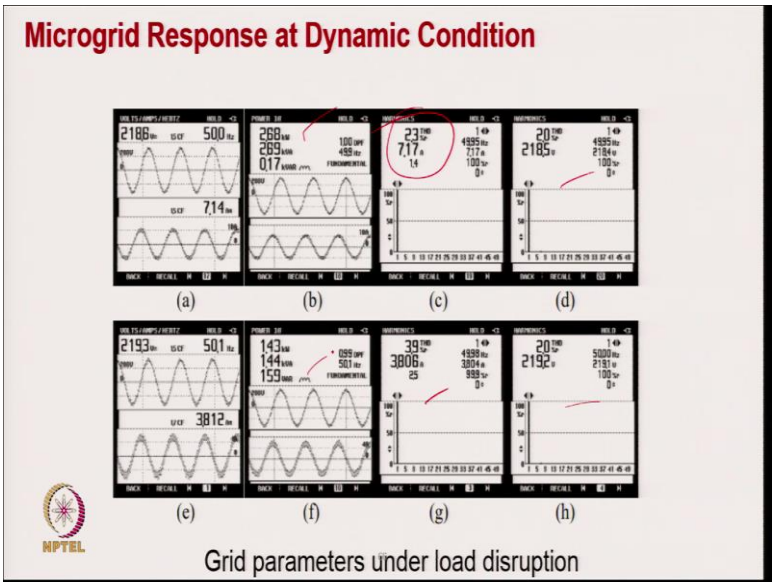

(Refer Slide Time: 22:19)

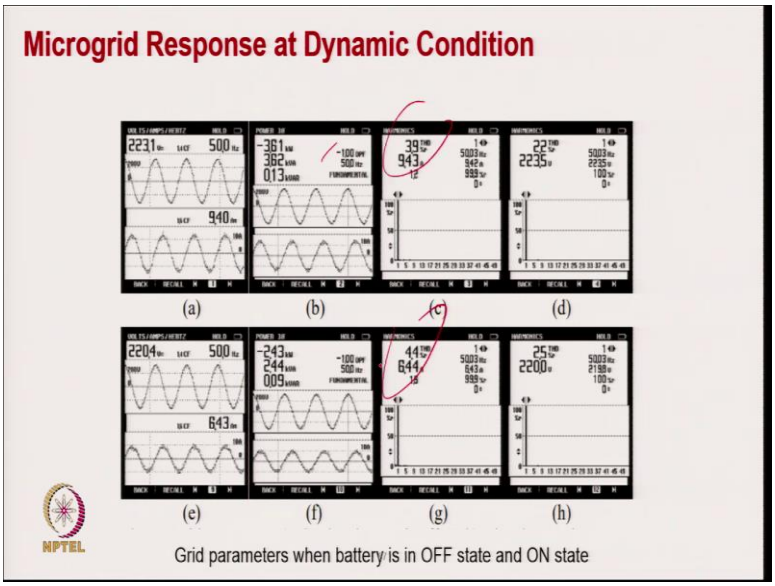

(Refer Slide Time: 22:29)

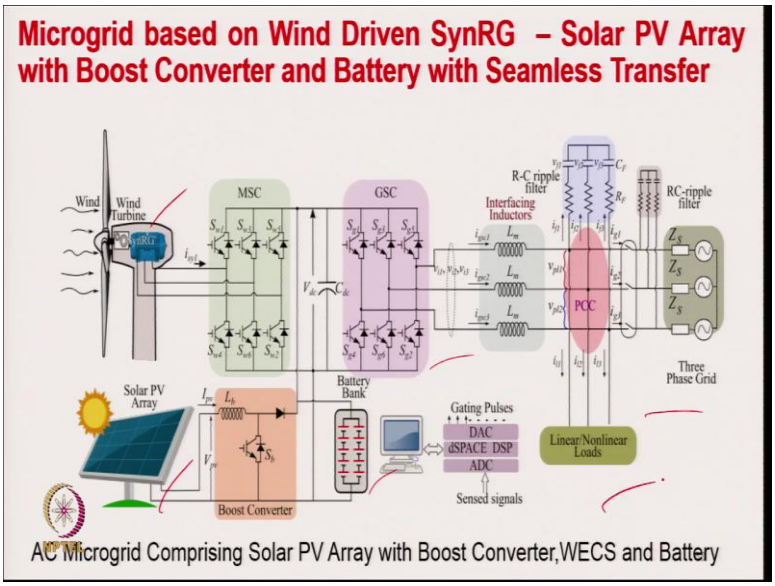

Now coming to another topology of microgrid; microgrid based on wind driven synchronous reluctance generator and solar PV array. And then we have a the battery here connected on the DC link.

(Refer Slide Time: 22:48)

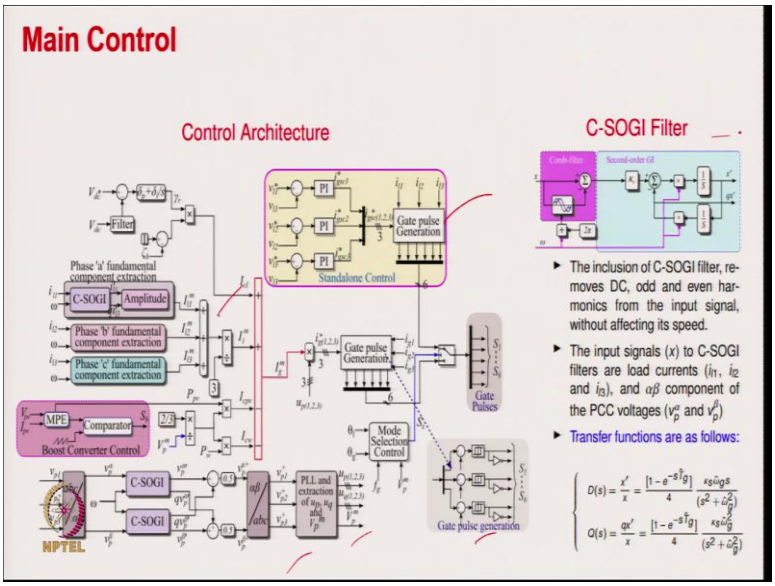

The control strategy and experimental results are displayed in the screenshots herein.

(Refer Slide Time: 23:06)

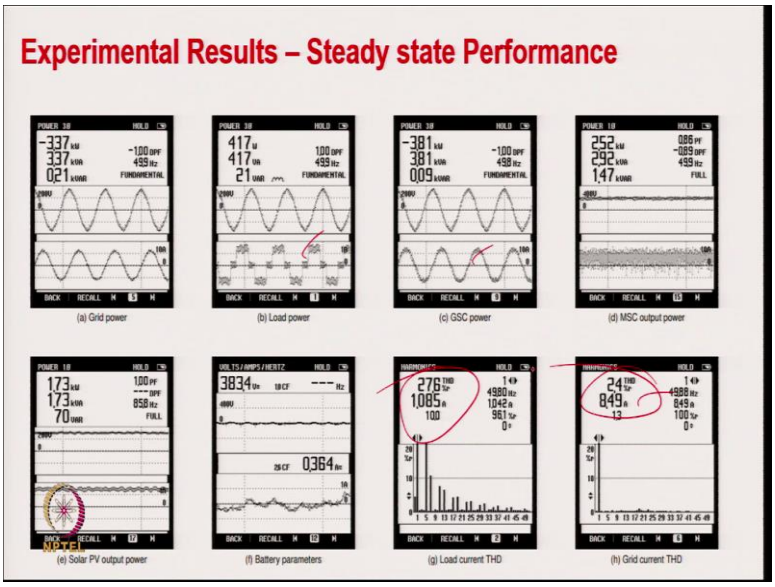

(Refer Slide Time: 23:19)

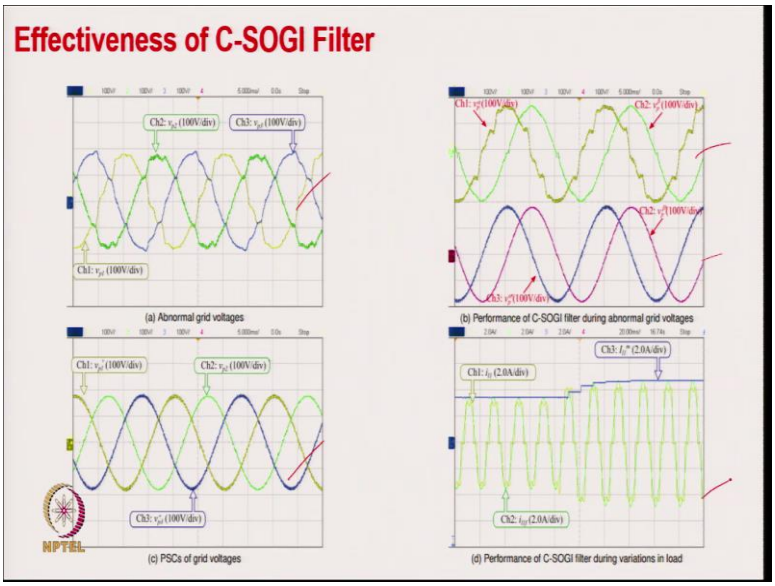

(Refer Slide Time: 23:37)

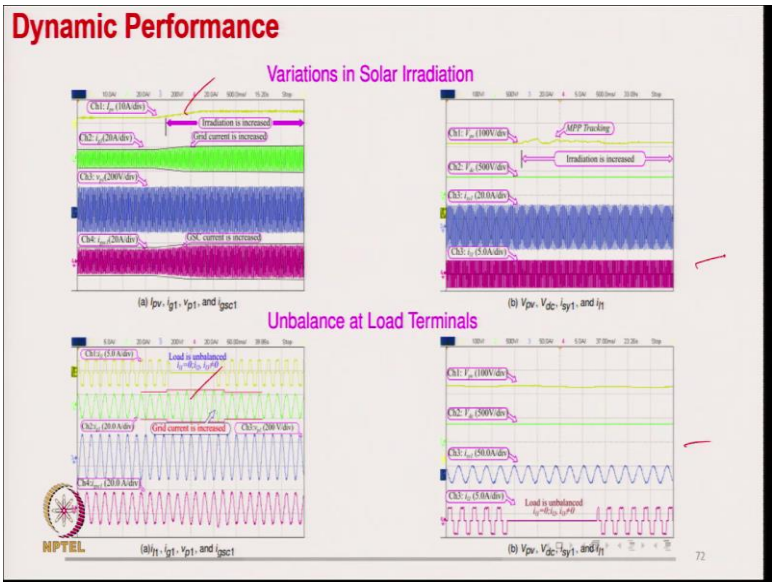

(Refer Slide Time: 23:52)

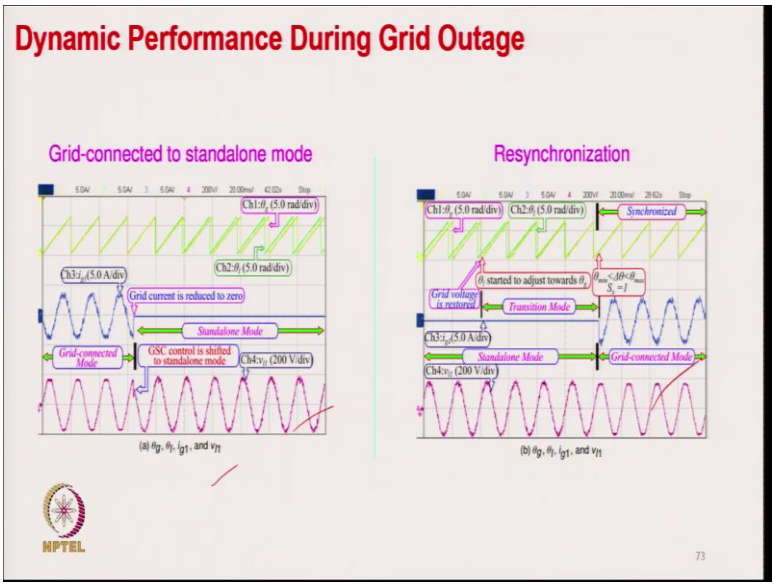

(Refer Slide Time: 24:08)

Coming to the power quality improvement in grid integrated small hydro solar PV battery microgrid.

(Refer Slide Time: 24:14)

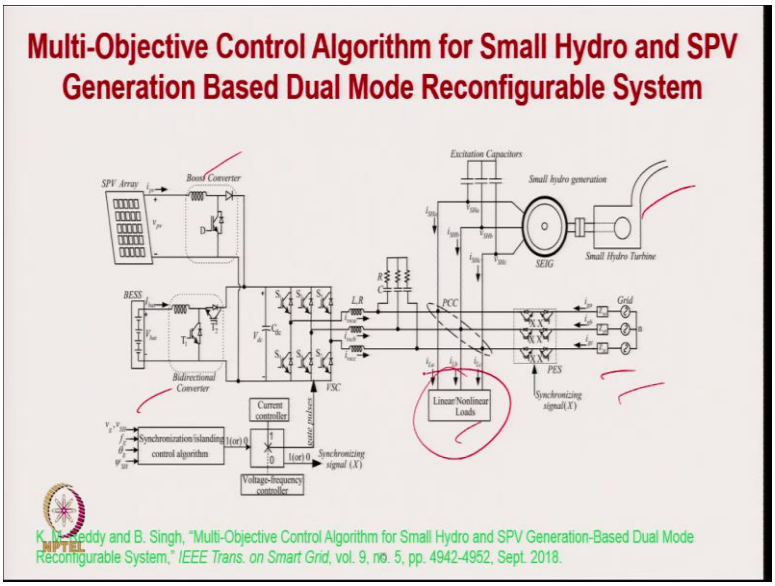

Here is a small hydro connected to the solar PV, and we have a battery connected to the system.

(Refer Slide Time: 24:47)

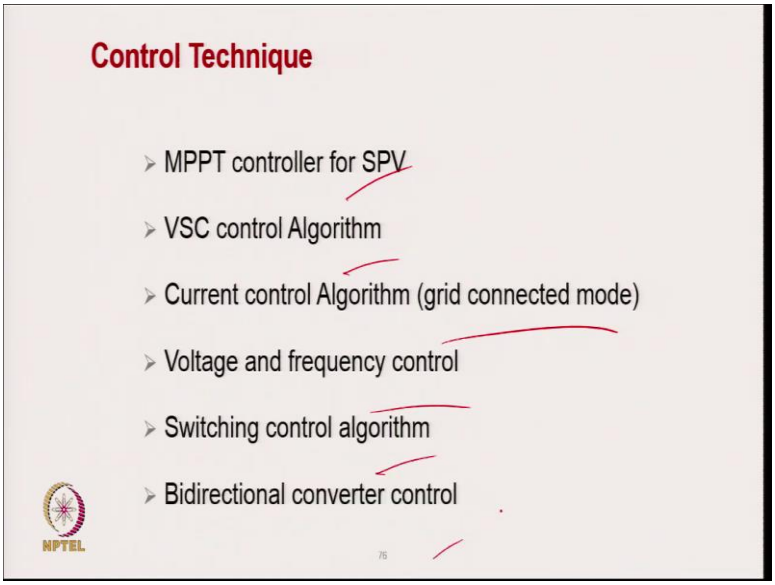

The control strategy is described in the screenshots herein.

(Refer Slide Time: 25:05)

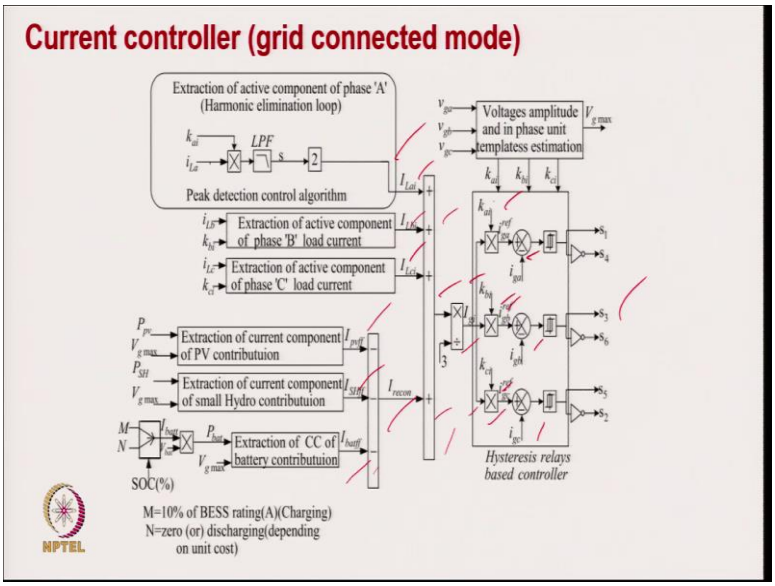

(Refer Slide Time: 25:49)

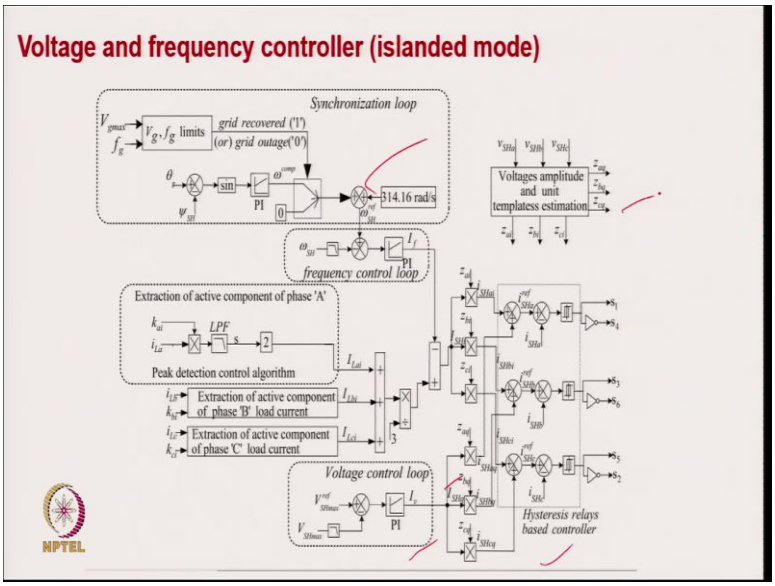

(Refer Slide Time: 26:06)

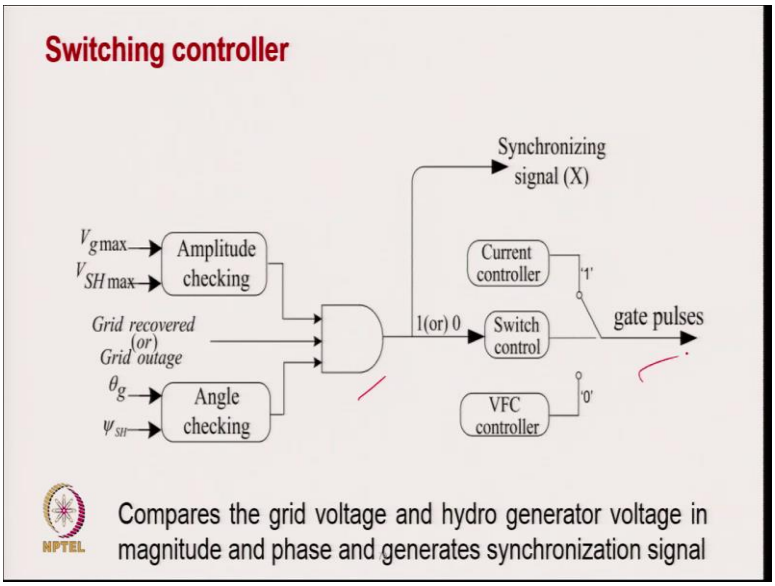

(Refer Slide Time: 26:19)

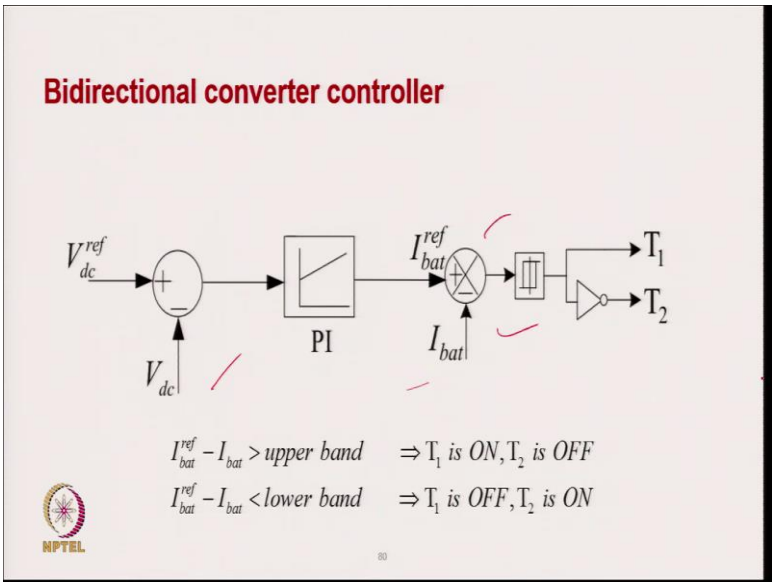

(Refer Slide Time: 26:24)

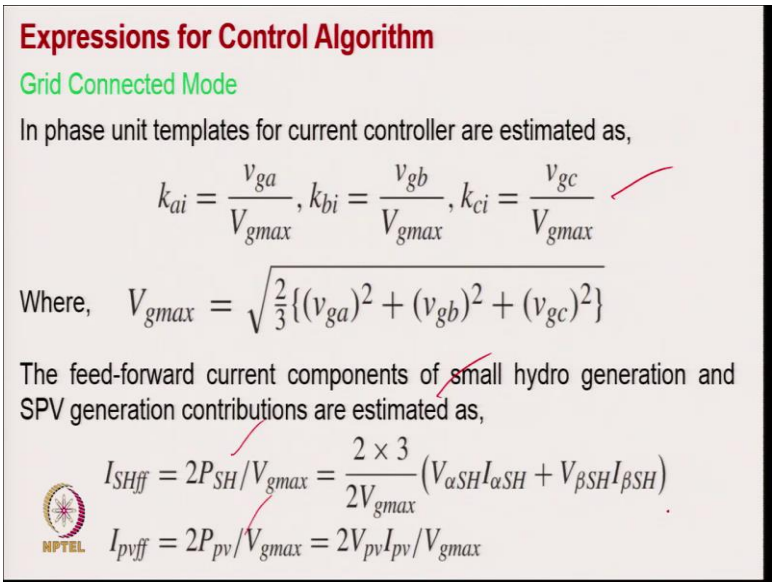

(Refer Slide Time: 26:35)

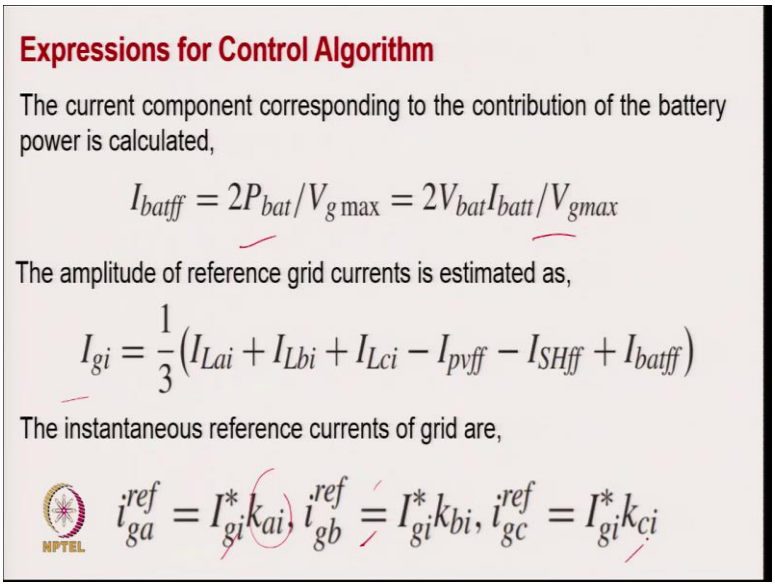

(Refer Slide Time: 26:49)

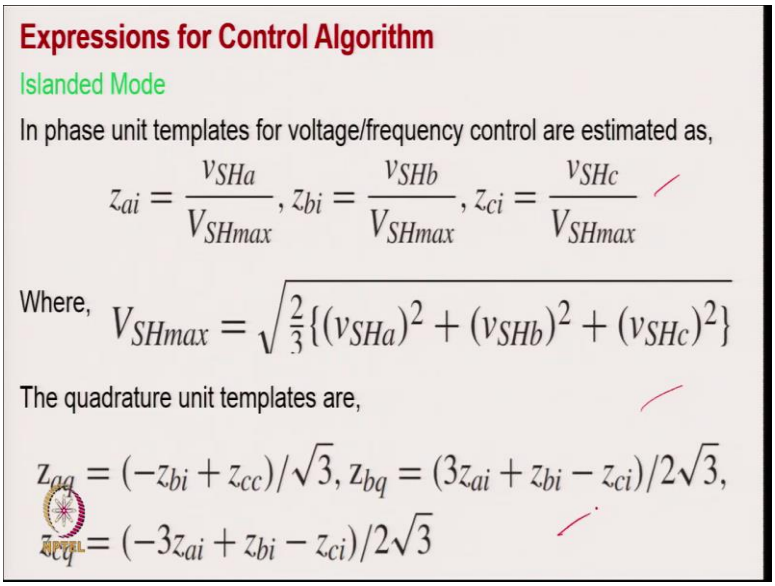

(Refer Slide Time: 27:00)

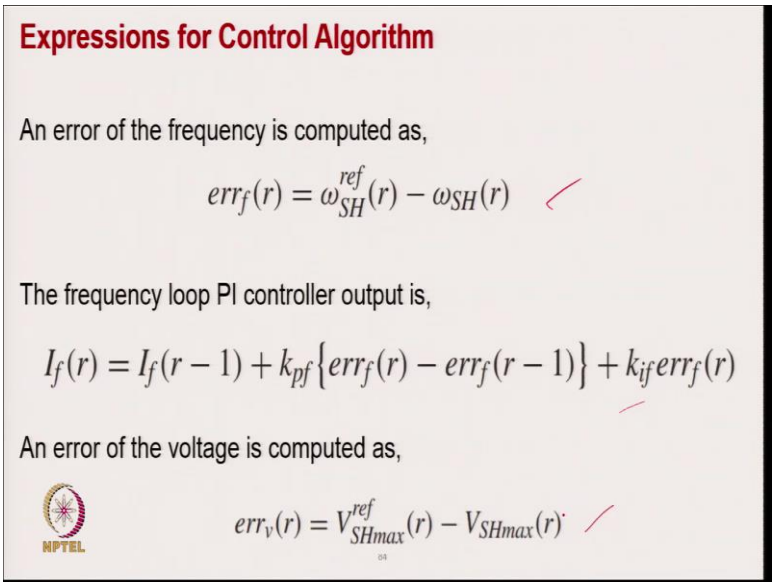

(Refer Slide Time: 27:09)

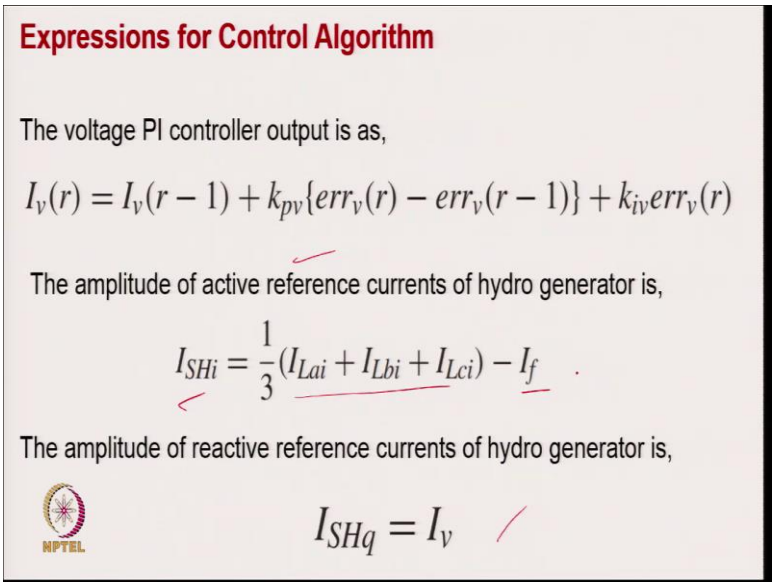

(Refer Slide Time: 27:28)

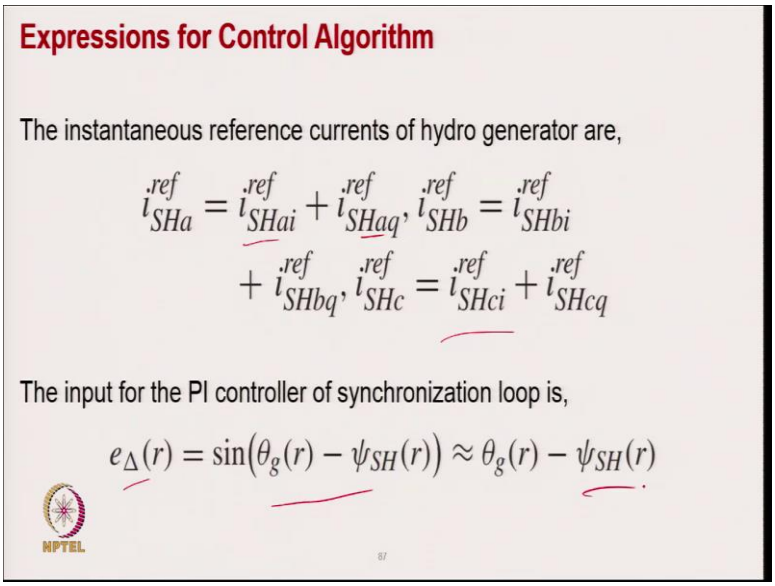

(Refer Slide Time: 27:42)

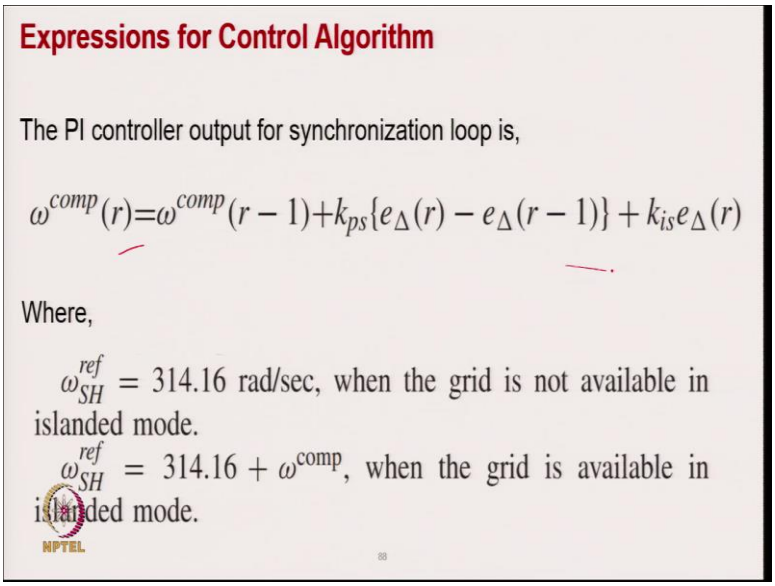

(Refer Slide Time: 27:49)

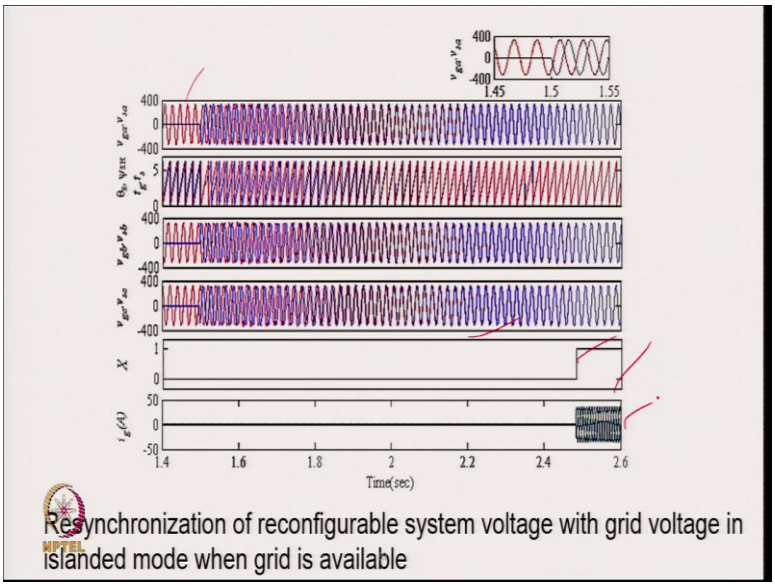

The simulation results are presented in the screenshots herein.

(Refer Slide Time: 28:06)

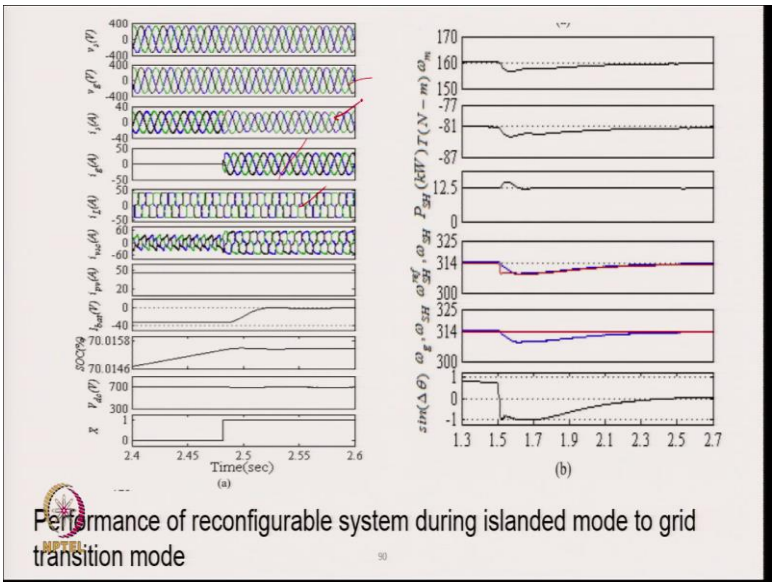

Performance of reconfigurable system during islanded mode to grid transition mode

(Refer Slide Time: 28:22)

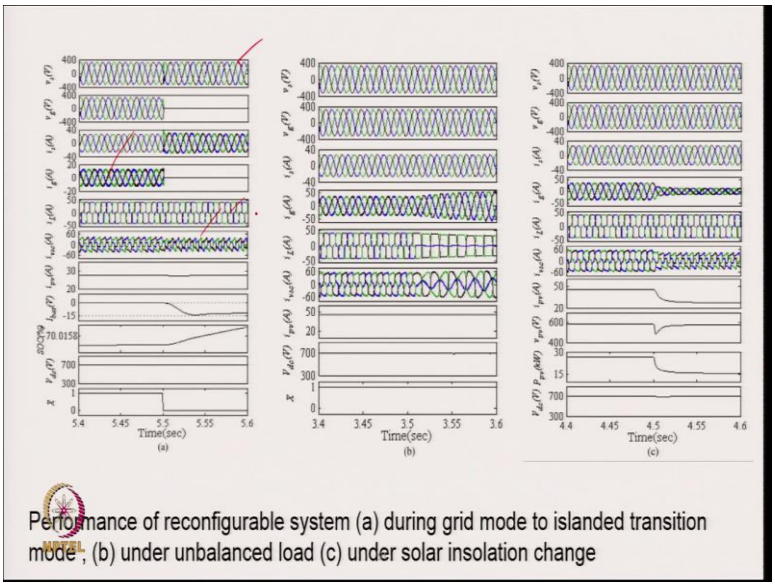

Performance of reconfigurable system (a) during grid mode to islanded transition mode, (b) under unbalanced load (c) under solar insolation change

(Refer Slide Time: 28:33)

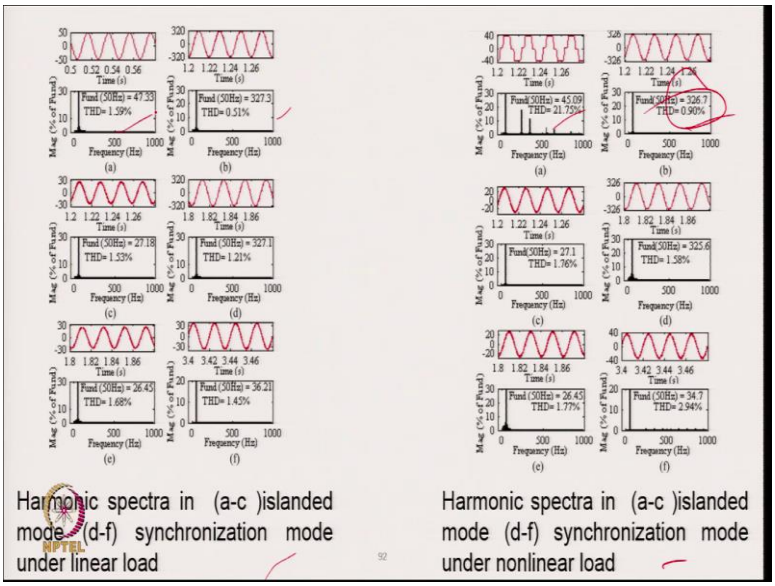

(Refer Slide Time: 28:52)

Now, coming to power quality improvement in the grid connected wind solar PV battery based DG set based microgrid.

(Refer Slide Time: 29:00)

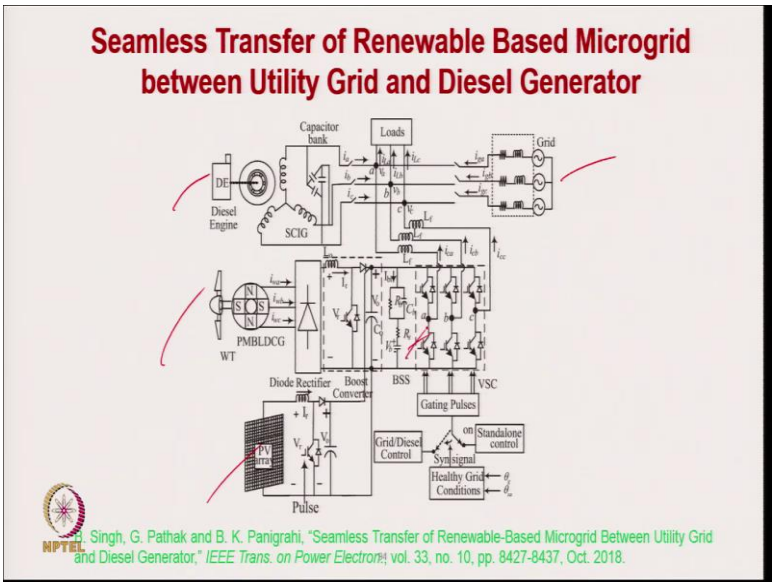

The system configuration is shown in the above screenshot.

(Refer Slide Time: 29:23)

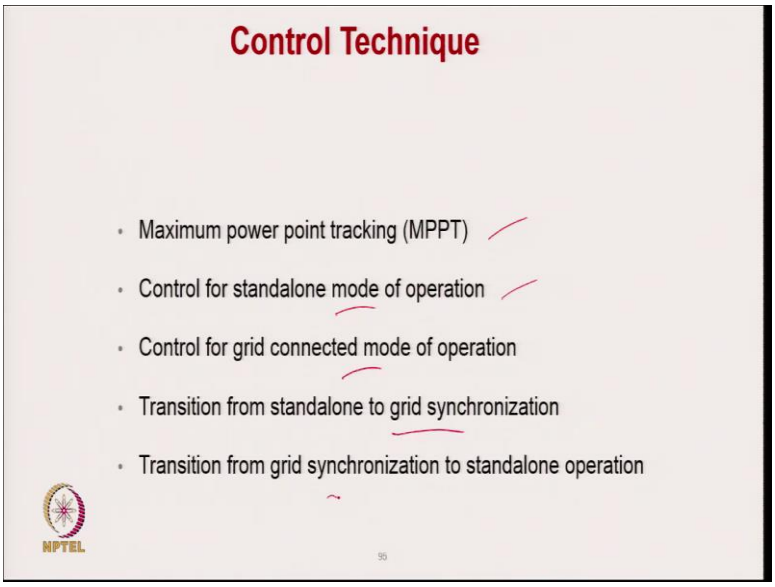

The control strategy is briefly described in the screenshots herein.

(Refer Slide Time: 29:36)

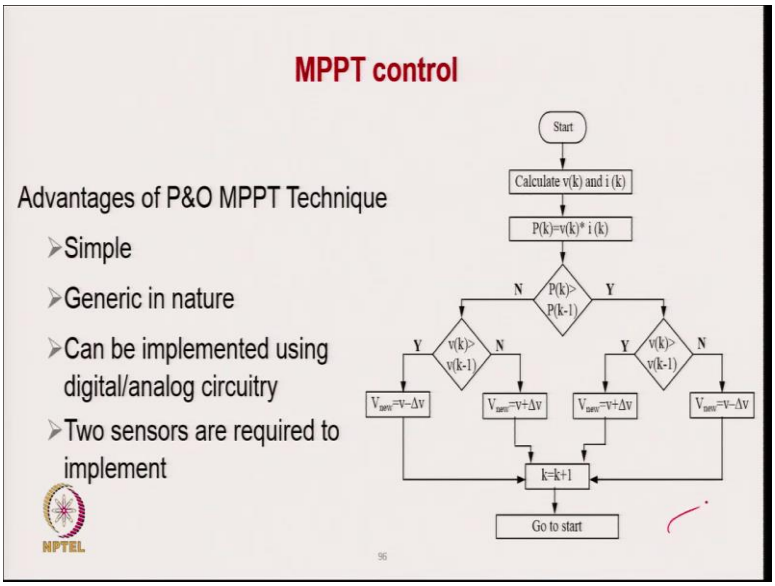

(Refer Slide Time: 29:42)

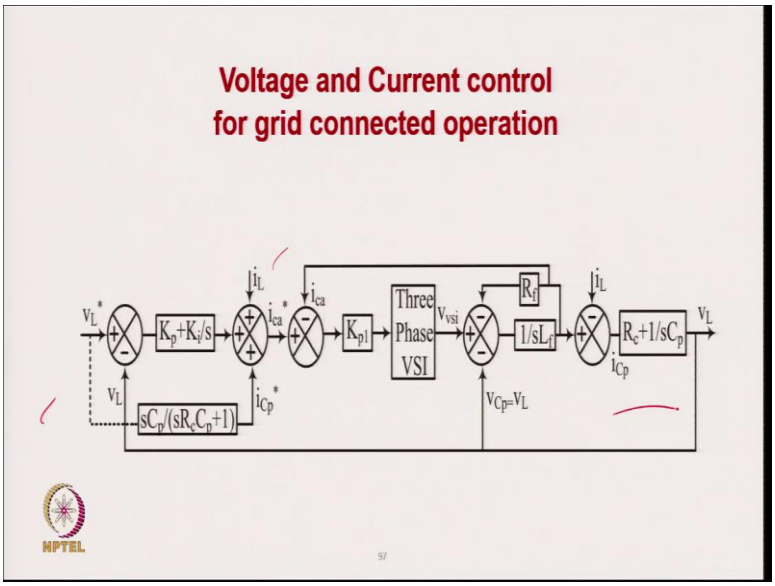

(Refer Slide Time: 29:55)

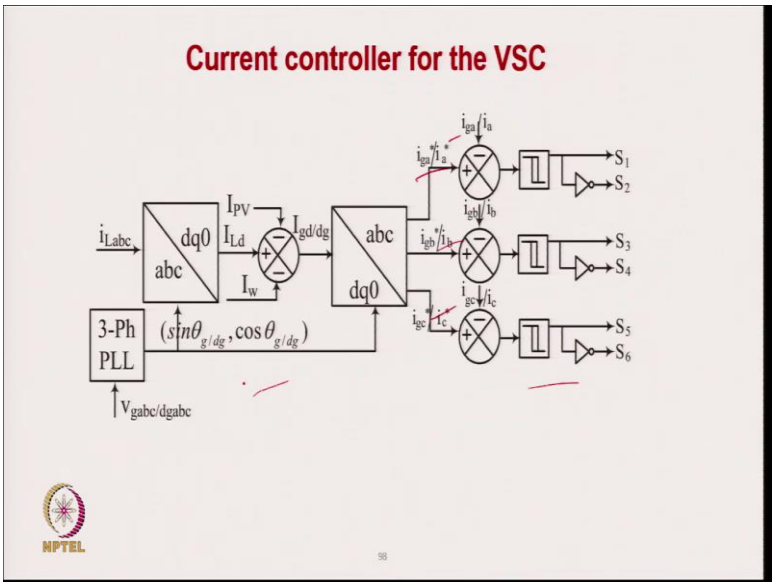

(Refer Slide Time: 30:06)

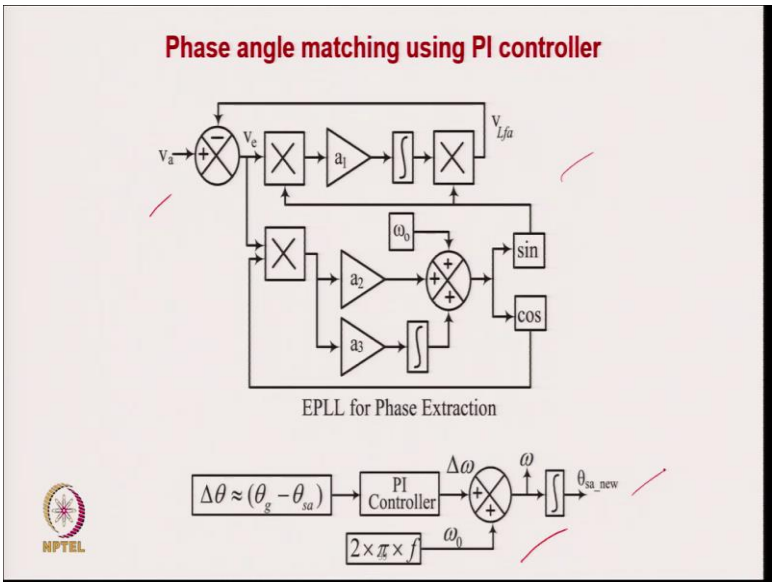

(Refer Slide Time: 30:20)

Control Algorithm Expressions

The reference voltages for an islanded mode are derived as,

$$v_{La}^{*} = V_{p}^{*} \sin(\omega_0 t)$$

$$v_{Lb}^{*} = V_{p}^{*} \sin\left(\omega_0 t - \frac{2\pi}{3}\right)$$

$$v_{Lc}^{*} = V_{p}^{*} \sin\left(\omega_0 t + \frac{2\pi}{3}\right)$$

The load currents in the three phases are converted into the d-q-0 frame using,

$$\begin{bmatrix} i_{Ld} \\ i_{Lq} \\ i_{L0} \end{bmatrix} = \frac{2}{3} \begin{bmatrix} \cos\theta_g & -\sin\theta_g & \frac{1}{2} \\ \cos\left(\theta_g - \frac{2\pi}{3}\right) & -\sin\left(\theta_g - \frac{2\pi}{3}\right) & \frac{1}{2} \\ \cos\left(\theta_g + \frac{2\pi}{3}\right) & \sin\left(\theta_g + \frac{2\pi}{3}\right) & \frac{1}{2} \end{bmatrix} \begin{bmatrix} i_{La} \\ i_{Lb} \\ i_{Lc} \end{bmatrix}$$

(Refer Slide Time: 30:27)

Control Algorithm Expressions

The reference active components of source is estimated as,

$$I_{Tp} = (I_{Ld} - I_w - I_{PV})$$

The active component of wind current is,

$$I_w = \frac{P_w}{3V_t}$$

The active component of solar PV current is,

$$I_{PV} = \frac{P_{PV}}{3V_t}$$

(Refer Slide Time: 30:40)

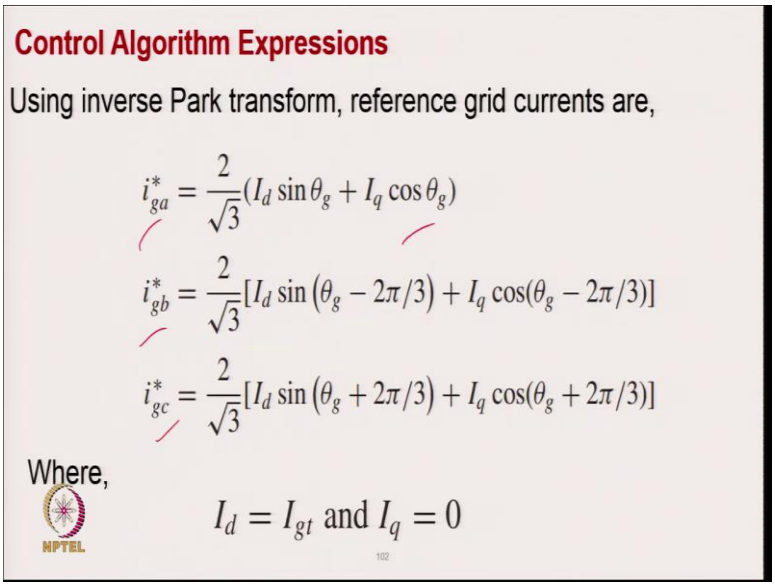

(Refer Slide Time: 30:49)

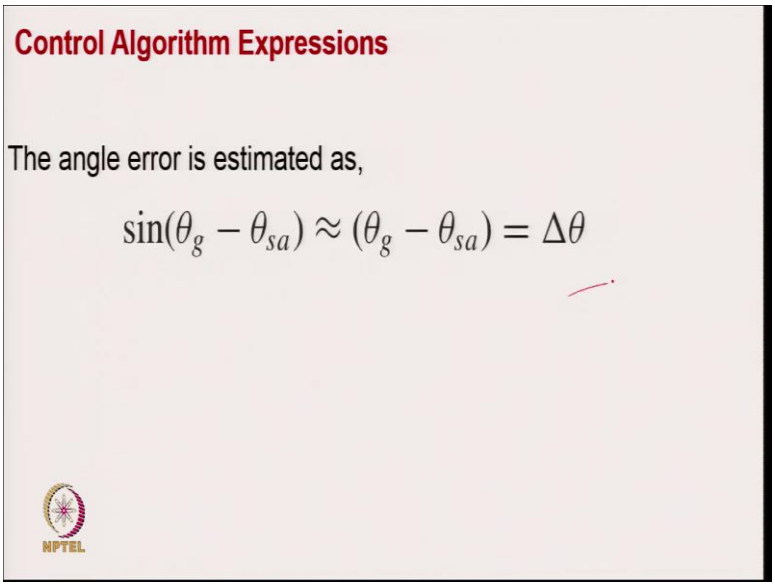

(Refer Slide Time: 30:53)

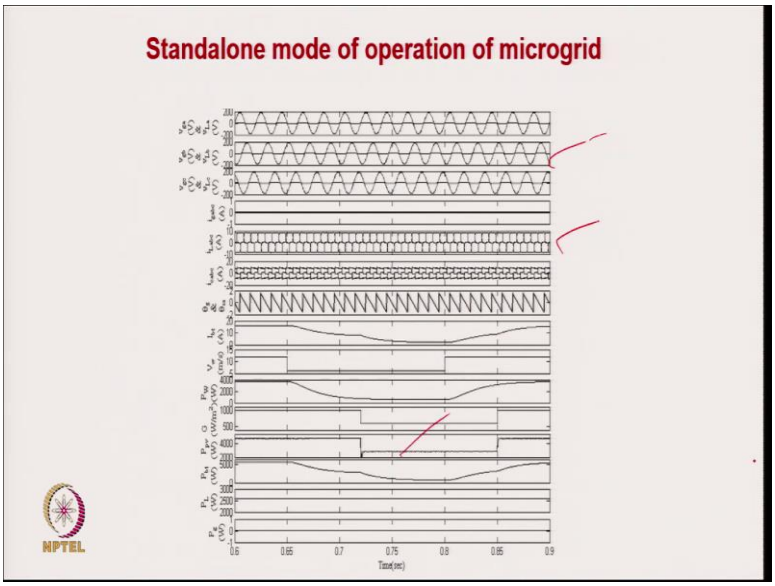

The simulation results are provided in the screenshots herein.

(Refer Slide Time: 31:14)

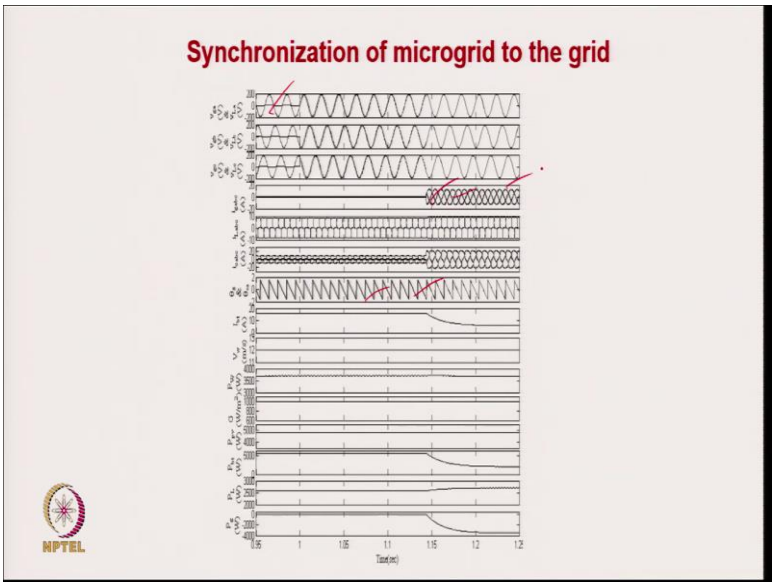

(Refer Slide Time: 31:28)

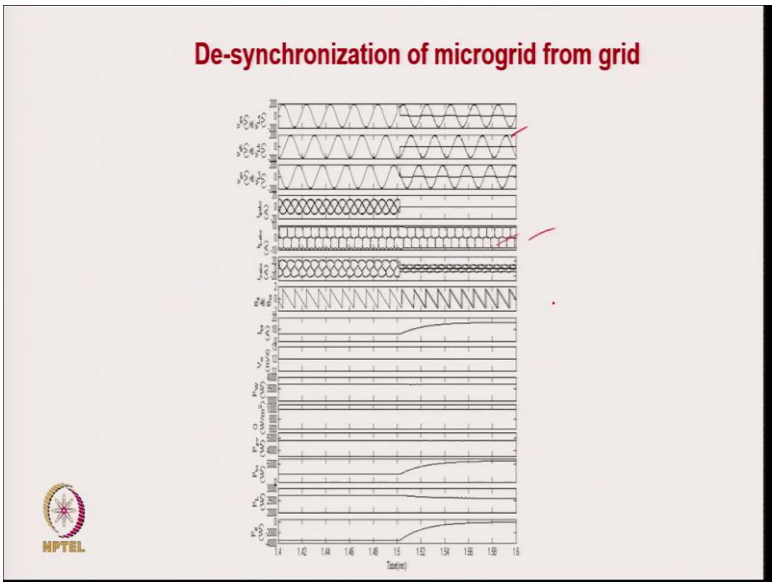

(Refer Slide Time: 31:34)

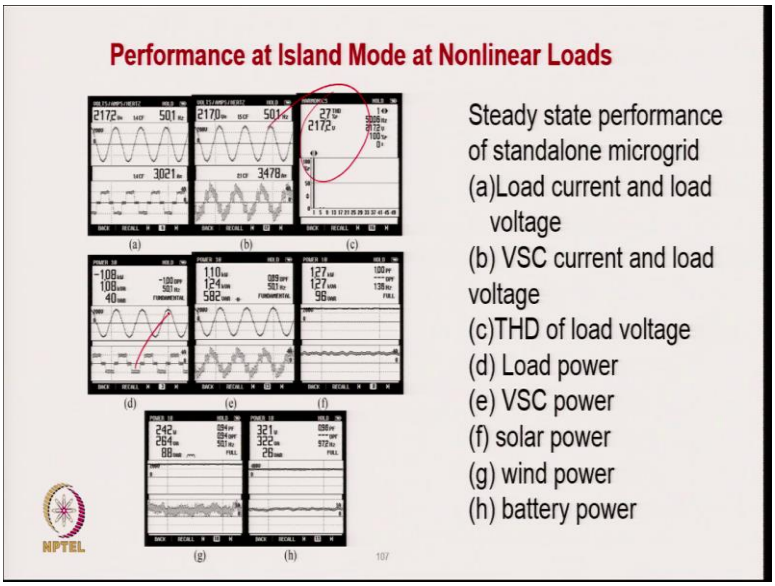

The experimental results are provided in the screenshots herein.

(Refer Slide Time: 31:47)

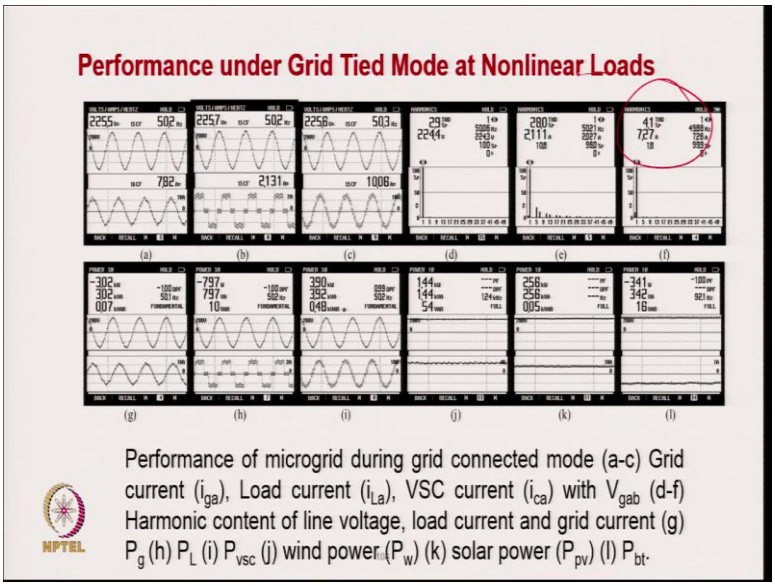

(Refer Slide Time: 31:55)

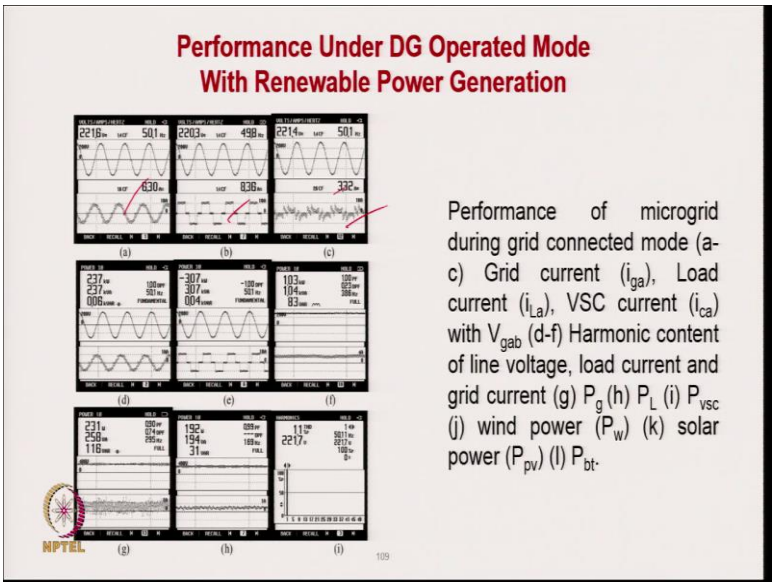

(Refer Slide Time: 32:11)

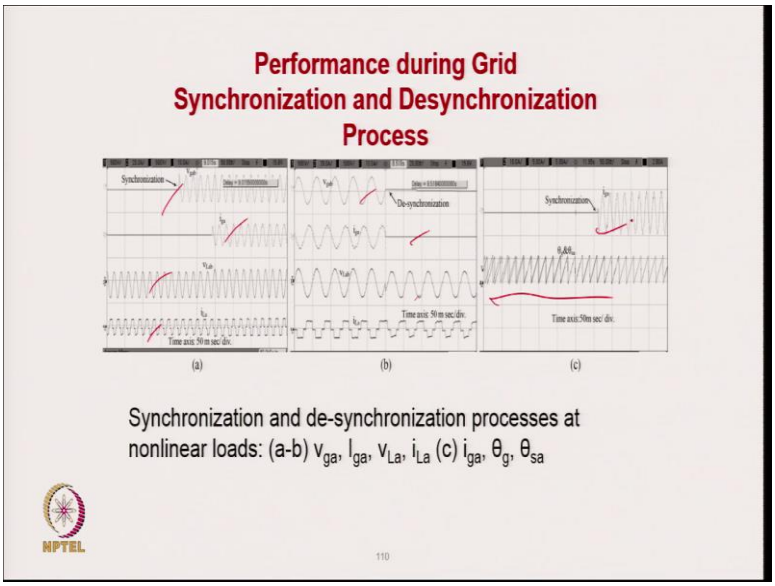

(Refer Slide Time: 32:31)

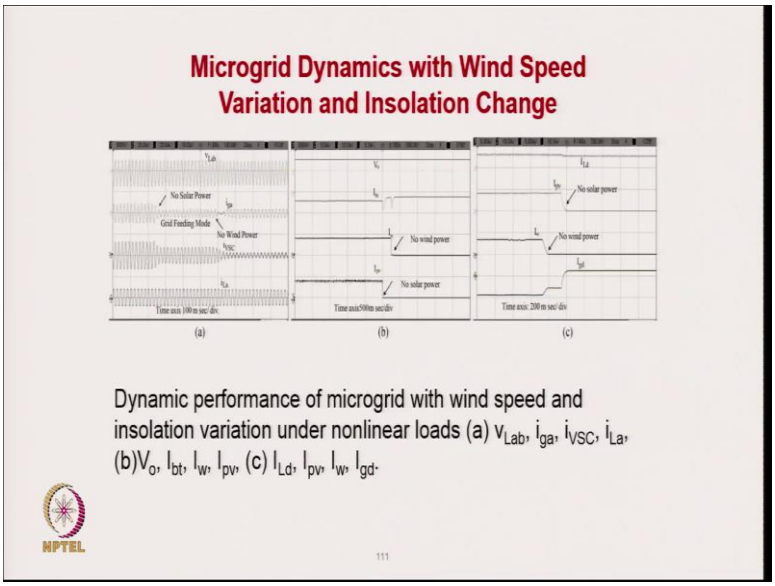

(Refer Slide Time: 32:36)

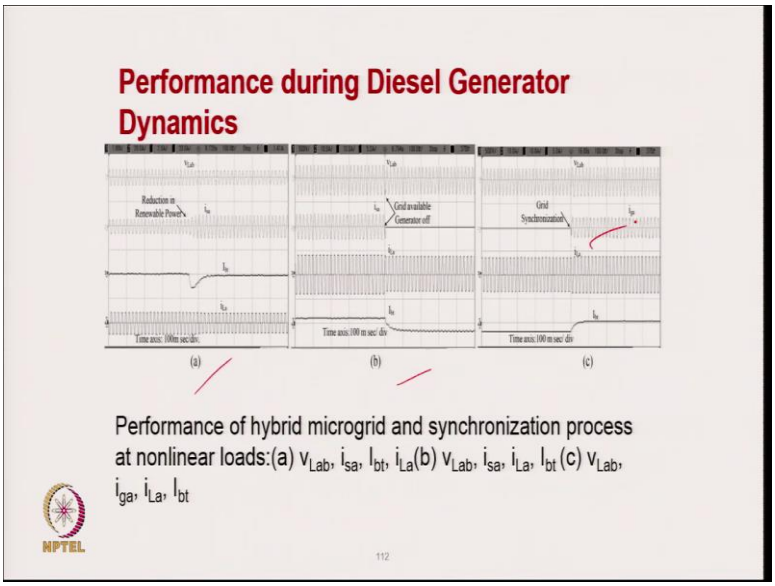

(Refer Slide Time: 32:53)

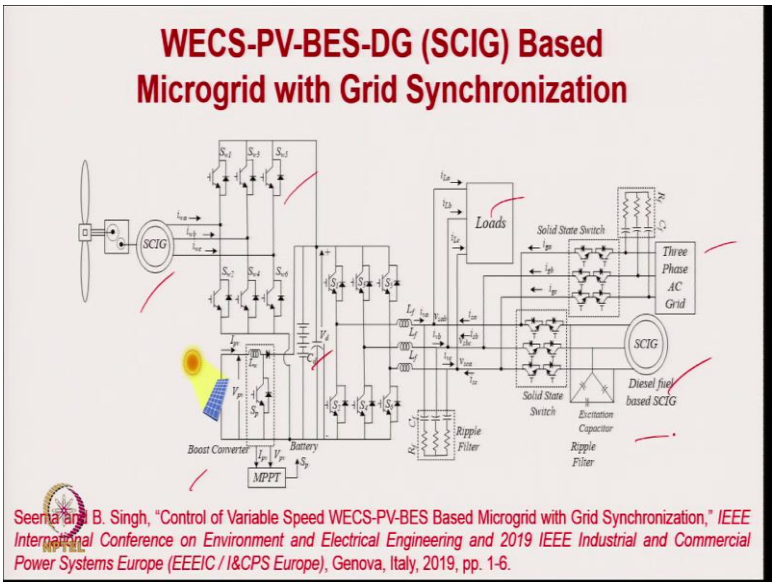

This is another configuration whose control strategy, simulation results and experimental results are described in the screenshots herein.

(Refer Slide Time: 33:33)

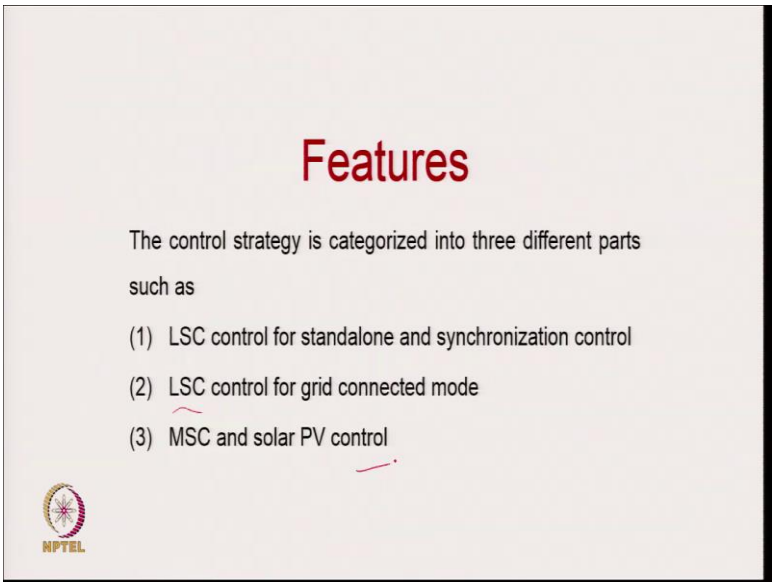

(Refer Slide Time: 33:41)

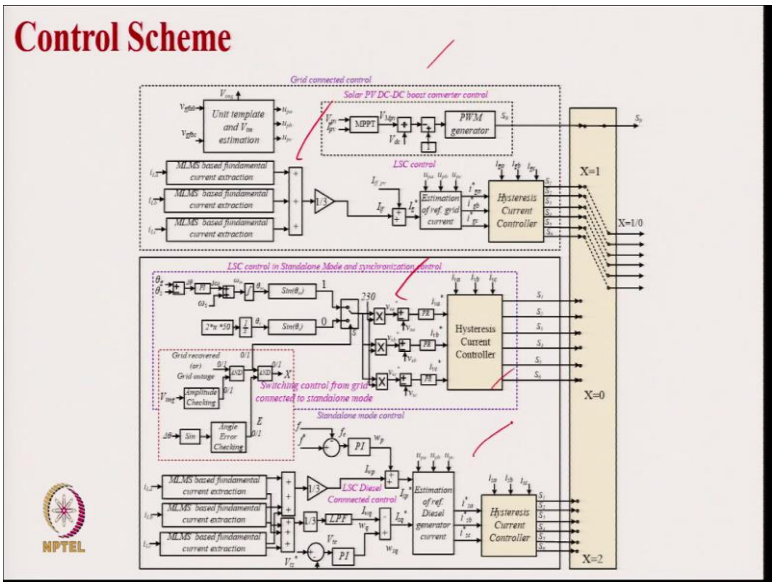

(Refer Slide Time: 33:53)

Machine Side VSC Control Algorithm

- The machine side VSC is controlled through indirect FOC (Field Oriented Control), and this algorithm is based on flux inverse dynamic of the model.
- In indirect FOC, the rotor flux is orientation is in d- axis of the frame. Since the rotor flux is aligned to the d-axis, therefore,

$$\psi_r = \psi_{dr} \qquad \psi_{qr} = 0 \qquad T_{em} = \frac{3}{2} P \frac{L_m}{L_r} \left[\psi_r I_{qs} \right]$$

- In FOC, the torque and flux are used for estimating the reference (I_{ds}^* and I_{qs}^*) current, which are given as follows,

$$I_{ds}^* = \left(\frac{1 + s\tau_r}{L_m} \right) \psi_r^* \qquad I_{qs}^* = \frac{2 L_r T_e}{3 P L_m \psi_r^*}$$

$$T_e(m) = T_e(m-1) + k_{pw}\{(\omega_{re}(m) - \omega_{re}(m-1)\} + k_{iw}\{\omega_{re}(m)\}$$

(Refer Slide Time: 34:13)

Machine Side VSC Control Algorithm

- The reference three-phase generator currents are estimated as,

$$i_{sa}^* = \left(\sin(\theta_e) I_{ds}^* + \cos(\theta_e) I_{qs}^* \right) \quad i_{sb}^* = \left(\sin\left(\theta_e - \frac{2\pi}{3}\right) I_{ds}^* + \cos\left(\theta_e - \frac{2\pi}{3}\right) I_{qs}^* \right) \quad i_{sc}^* = \left(\sin\left(\theta_e + \frac{2\pi}{3}\right) I_{ds}^* + \cos\left(\theta_e + \frac{2\pi}{3}\right) I_{qs}^* \right)$$

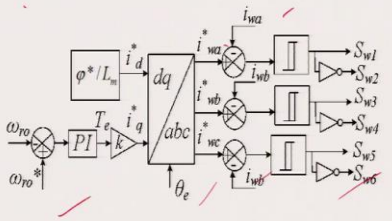

Block diagram of machine side VSC control

- Where θ_e is the synchronous frame rotor axis angle and it is estimated as,

$$\theta_e = \int \omega_r dt + \int (\omega_e - \omega_r) dt = \theta_{ro} + \int S\omega_e dt = \theta_{ro} + \frac{R_r}{L_r} \int I_{qs}^* \frac{L_m}{\psi_{dr}} dt = \theta_{ro} + \frac{1}{T_r} \int \frac{I_{qs}^*}{I_{ds}^*} dt$$

(Refer Slide Time: 34:33)

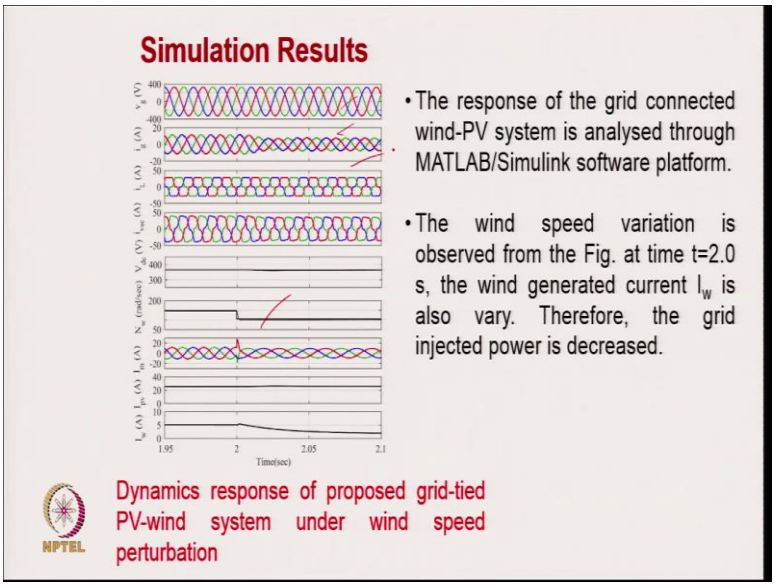

(Refer Slide Time: 34:44)

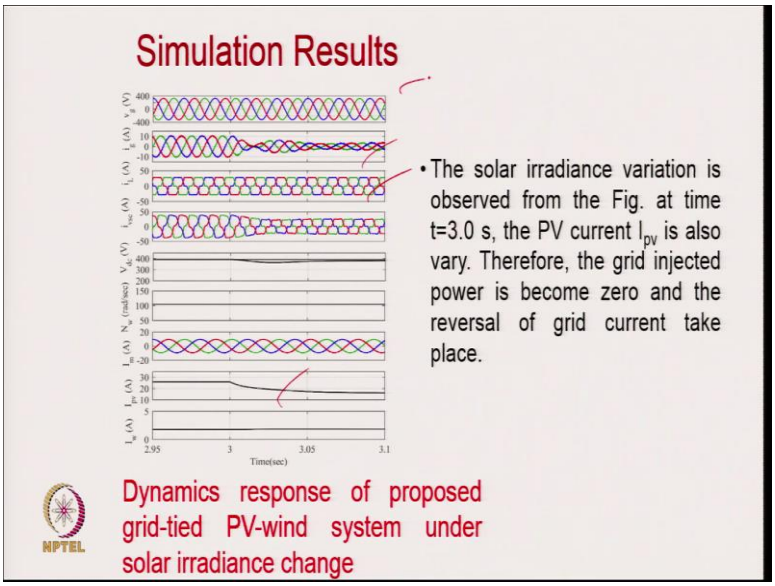

(Refer Slide Time: 34:59)

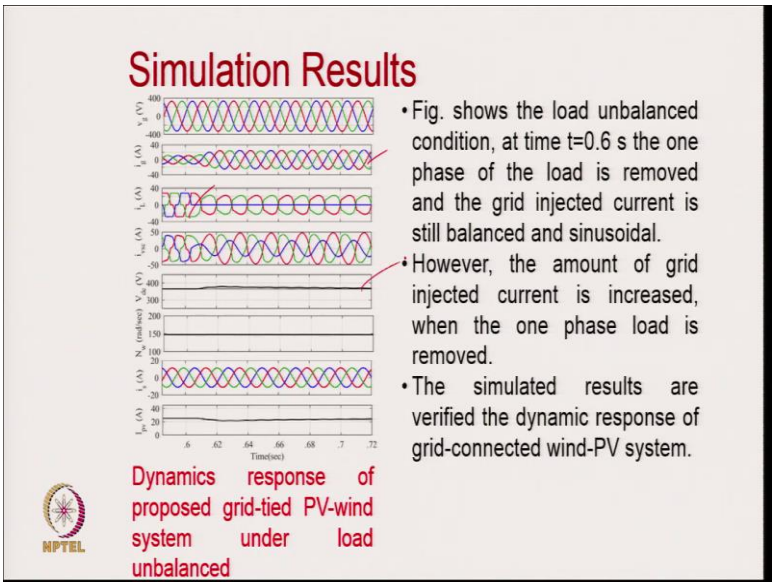

(Refer Slide Time: 35:11)

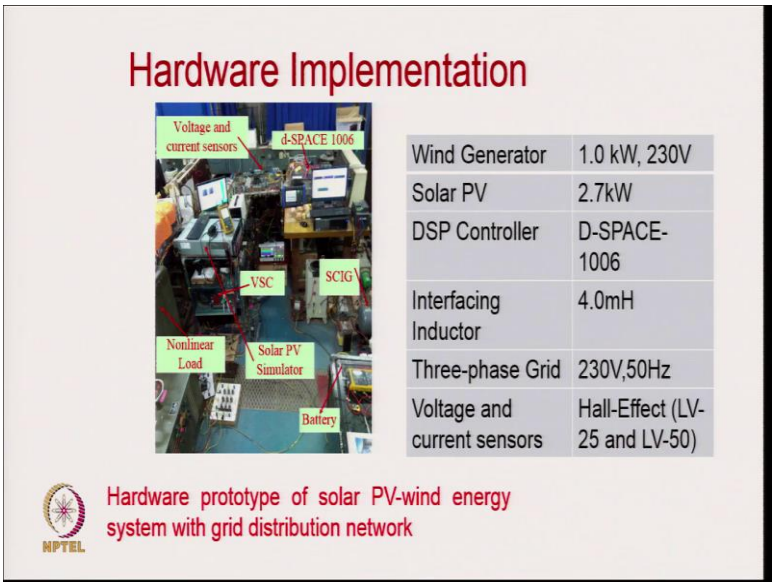

These are typically the hardware of the prototype developed for the system.

(Refer Slide Time: 35:15)

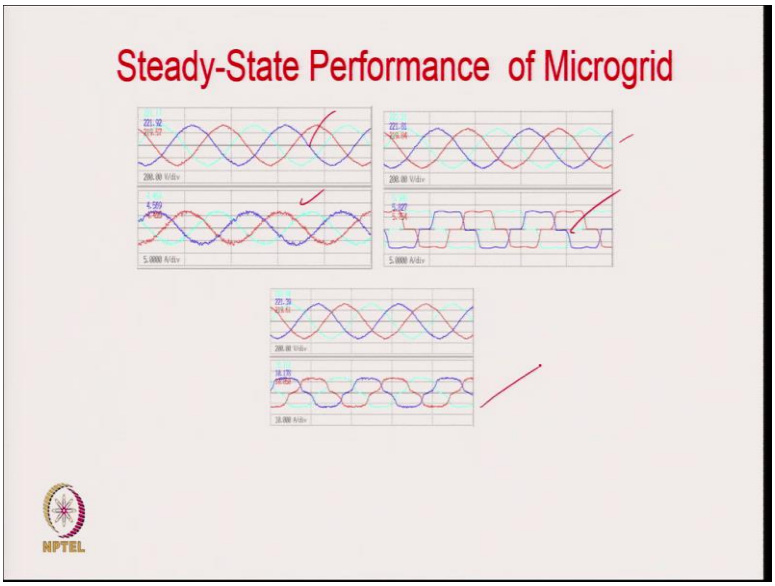

(Refer Slide Time: 35:23)

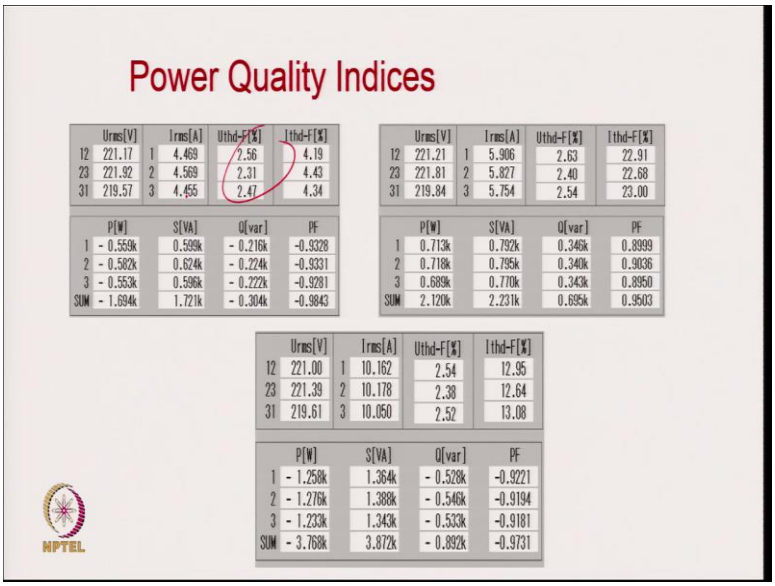

(Refer Slide Time: 35:34)

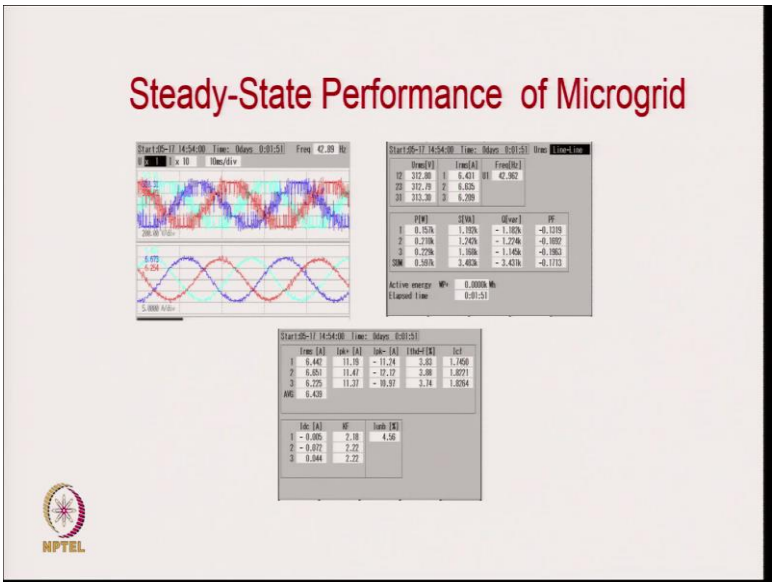

(Refer Slide Time: 35:35)

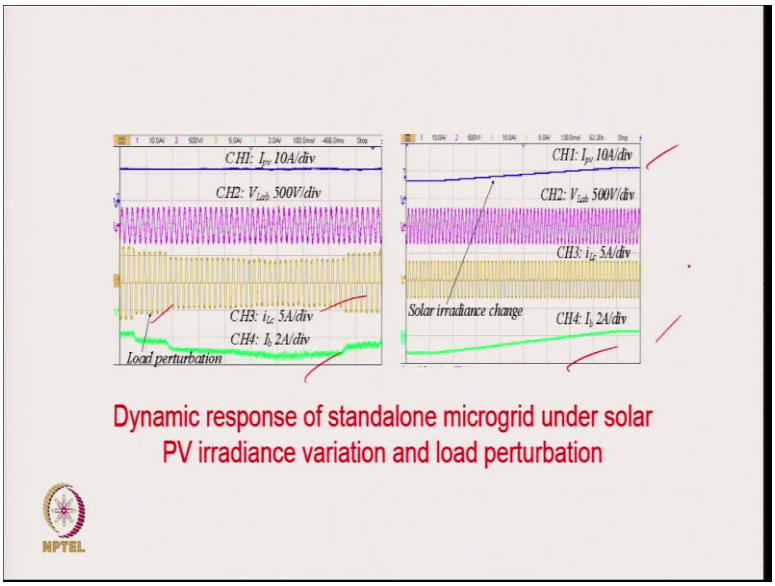

(Refer Slide Time: 35:47)

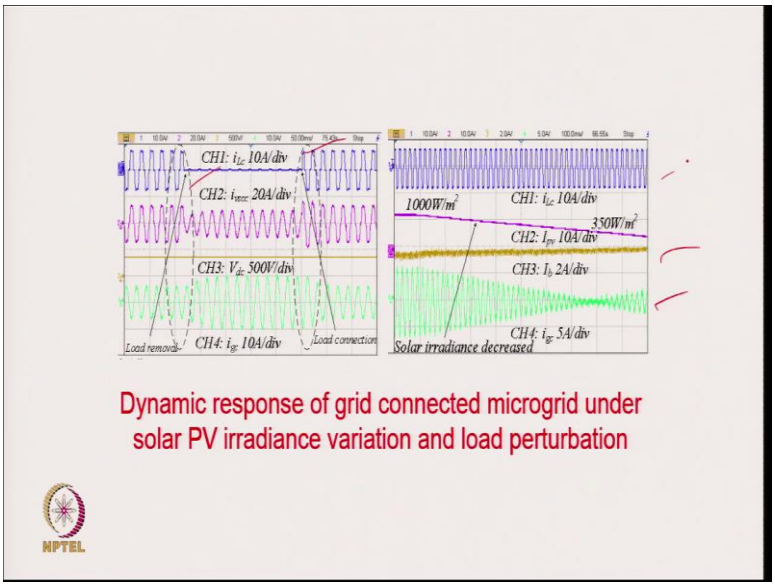

(Refer Slide Time: 36:04)

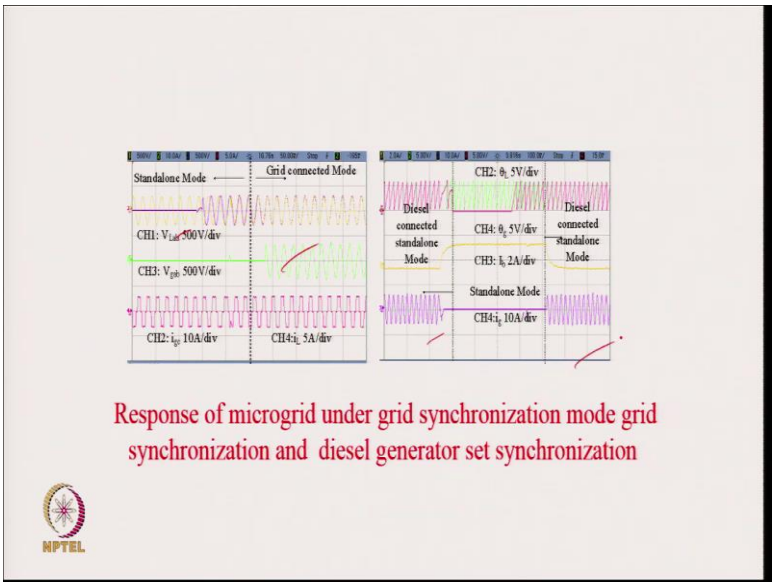

(Refer Slide Time: 36:18)

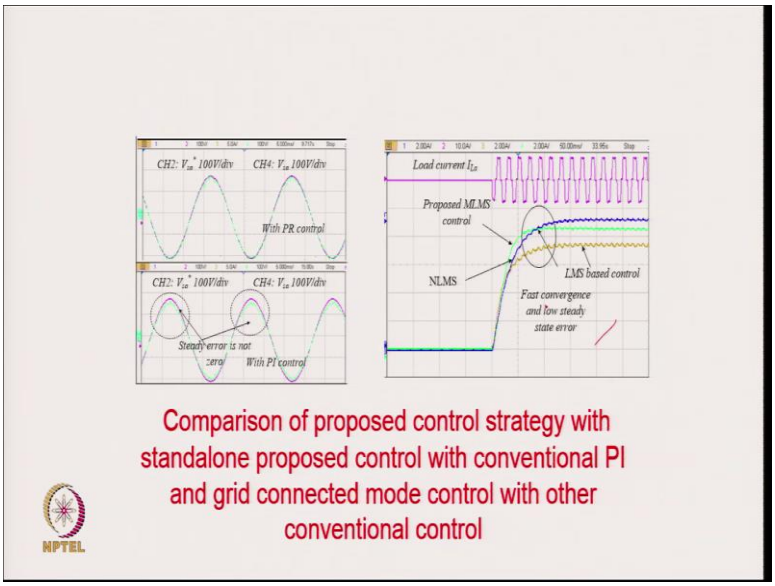

(Refer Slide Time: 36:23)

Now, coming to power quality improvement in microgrid for electric vehicle charging station.

(Refer Slide Time: 36:28)

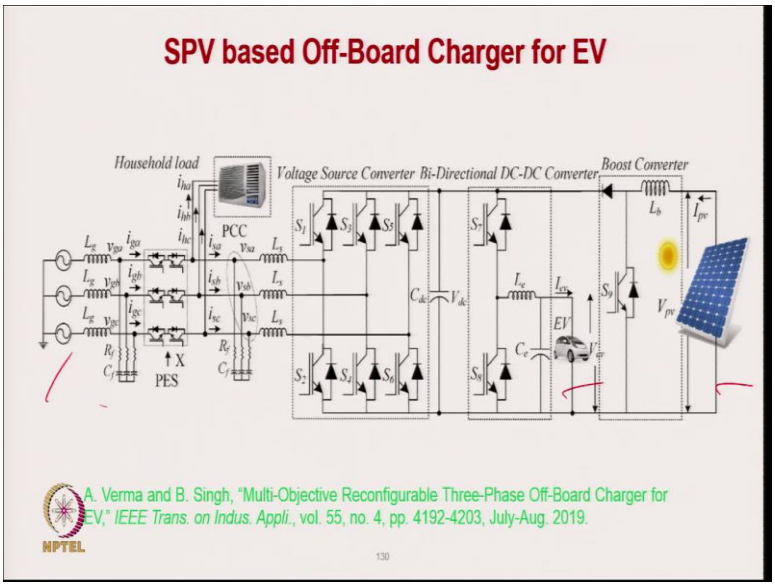

The charging station configuration is described in the screenshot herein.

(Refer Slide Time: 36:47)

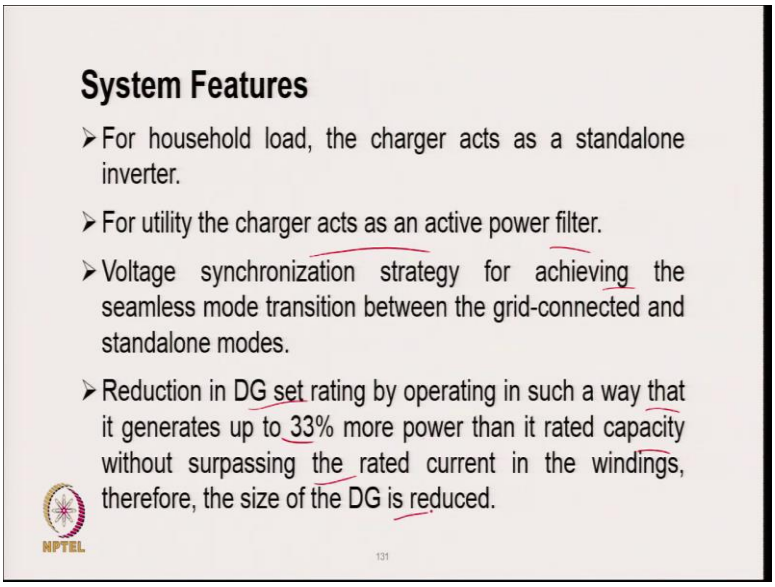

The system features and operational criterion are described here.

(Refer Slide Time: 37:10)

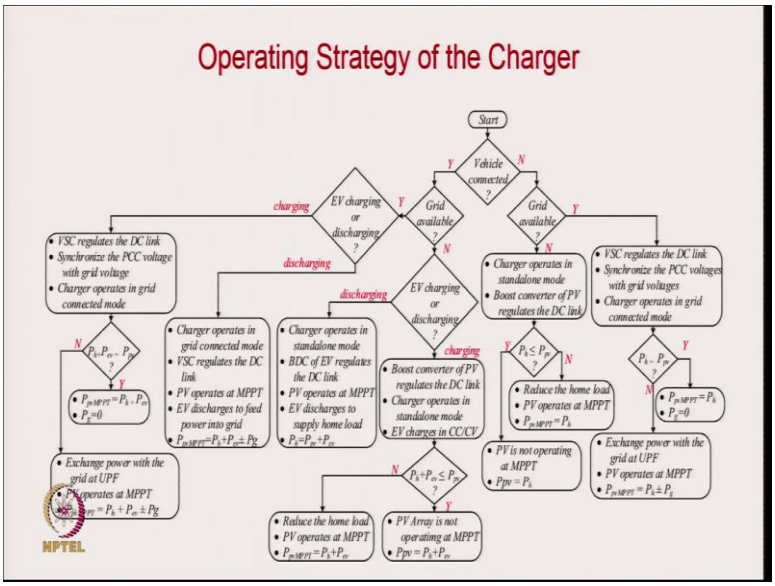

(Refer Slide Time: 36:17)

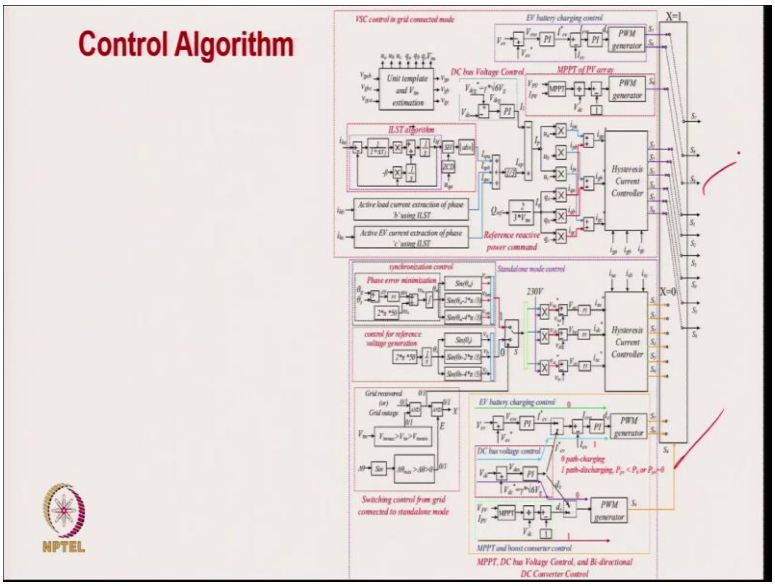

The control strategy are described in the screenshots herein.

(Refer Slide Time: 37:21)

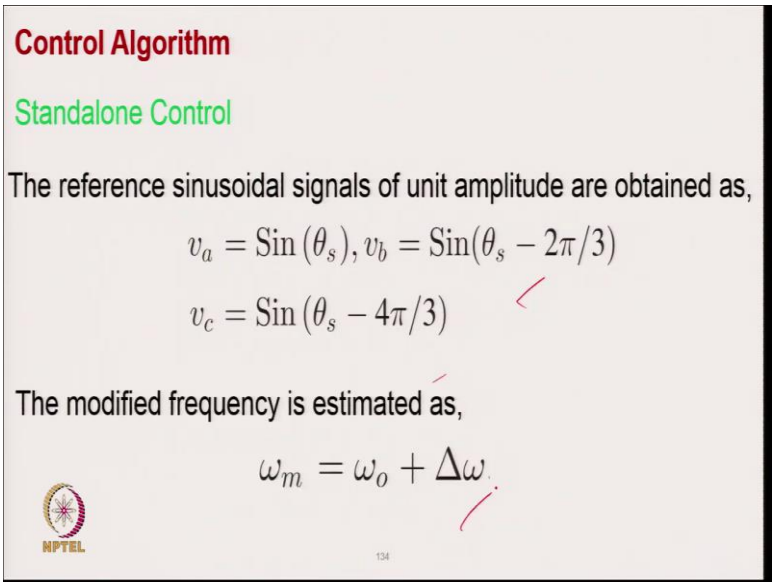

(Refer Slide Time: 37:26)

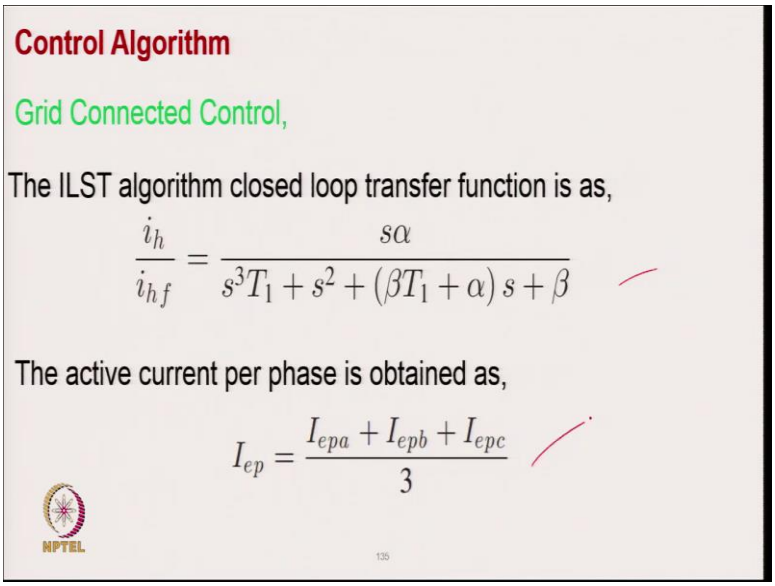

(Refer Slide Time: 37:33)

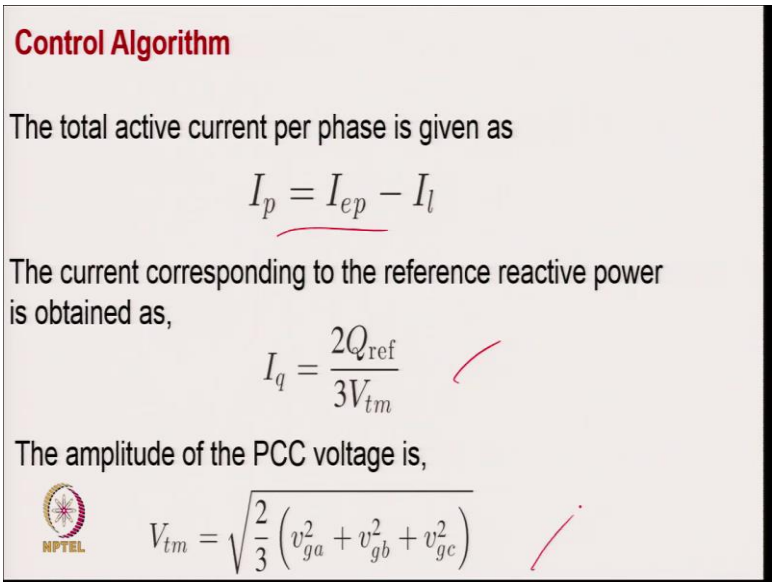

(Refer Slide Time: 37:39)

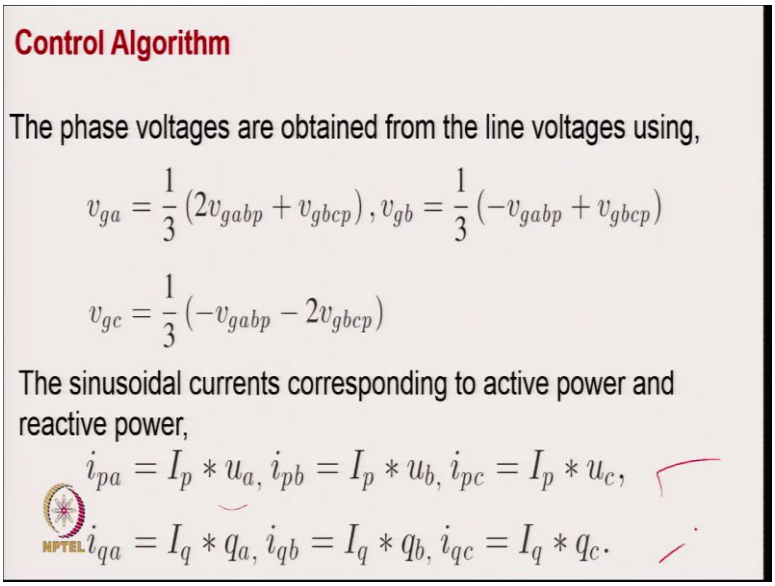

(Refer Slide Time: 37:46)

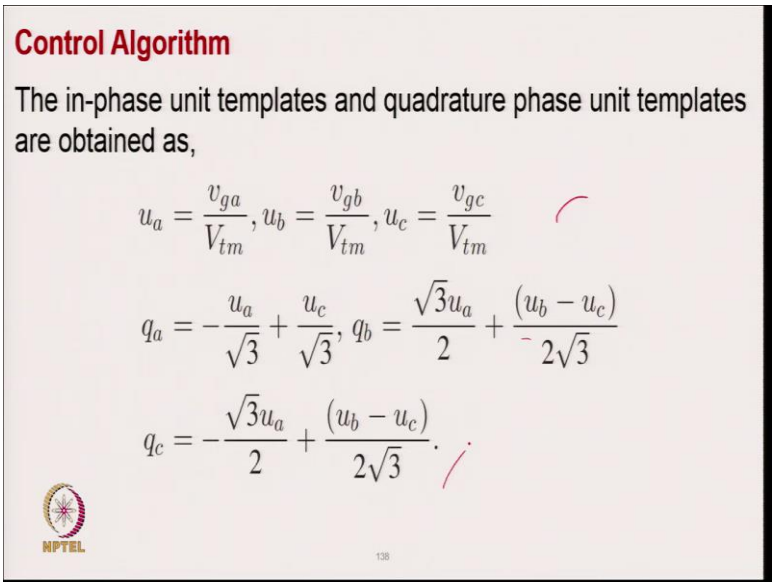

(Refer Slide Time: 37:49)

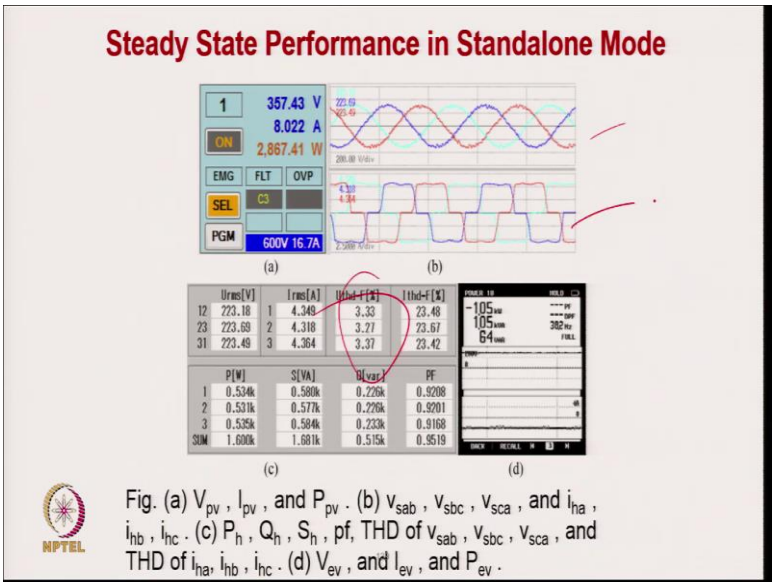

These screenshots present the experimental results.

(Refer Slide Time: 37:58)

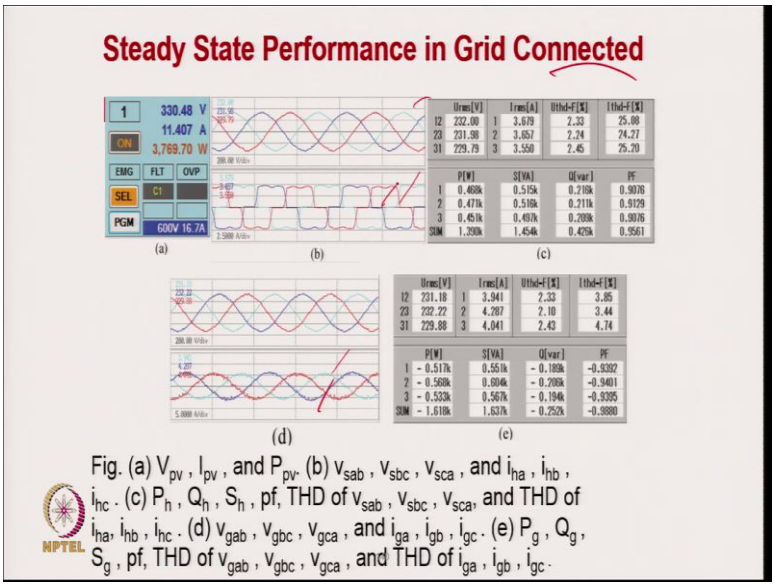

Fig. (a) V_{pv} , I_{pv} , and P_{pv}. (b) v_{sab} , v_{sbc} , v_{sca} , and i_{ha} , i_{hb} , i_{hc} . (c) P_h , Q_h , S_h , pf, THD of v_{sab} , v_{sbc} , v_{sca}, and THD of i_{ha}, i_{hb} , i_{hc} . (d) v_{gab} , v_{gbc} , v_{gca} , and i_{ga} , i_{gb} , i_{gc} . (e) P_g , Q_g , S_g , pf, THD of v_{gab} , v_{gbc} , v_{gca} , and THD of i_{ga} , i_{gb} , i_{gc} .

(Refer Slide Time: 38:07)

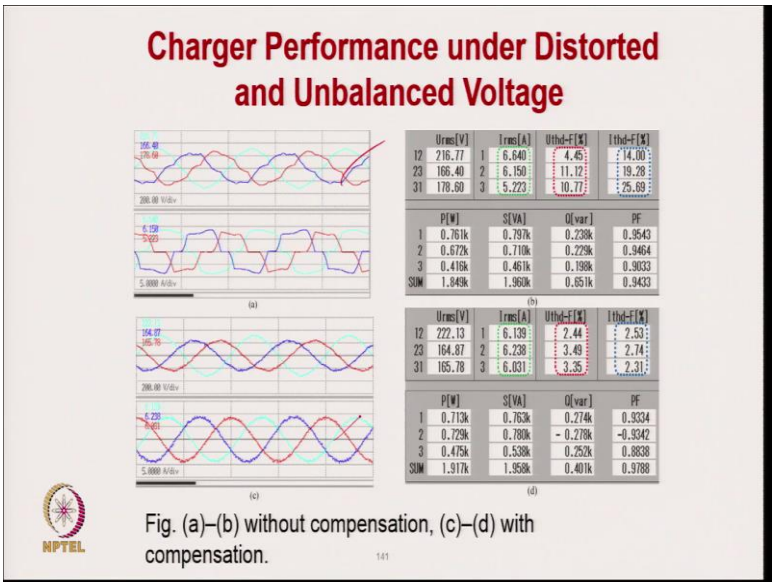

Fig. (a)–(b) without compensation, (c)–(d) with compensation.

(Refer Slide Time: 38:11)

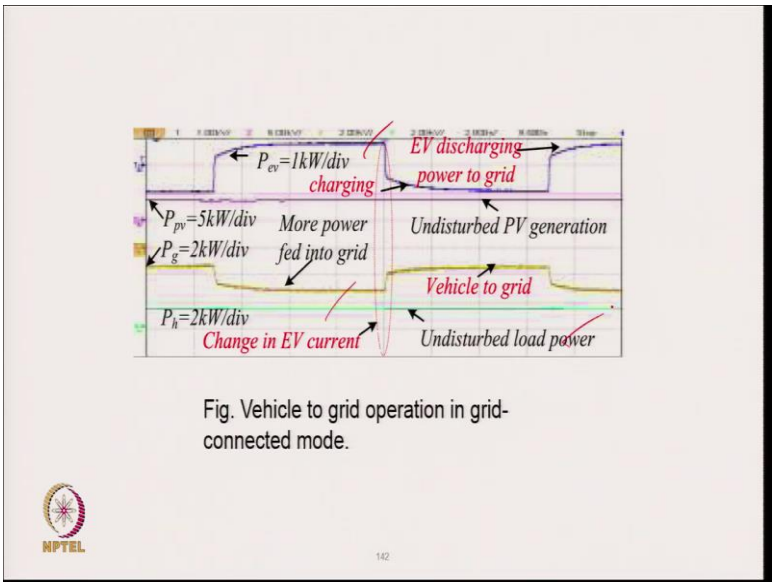

Fig. Vehicle to grid operation in grid-connected mode.

(Refer Slide Time: 38:24)

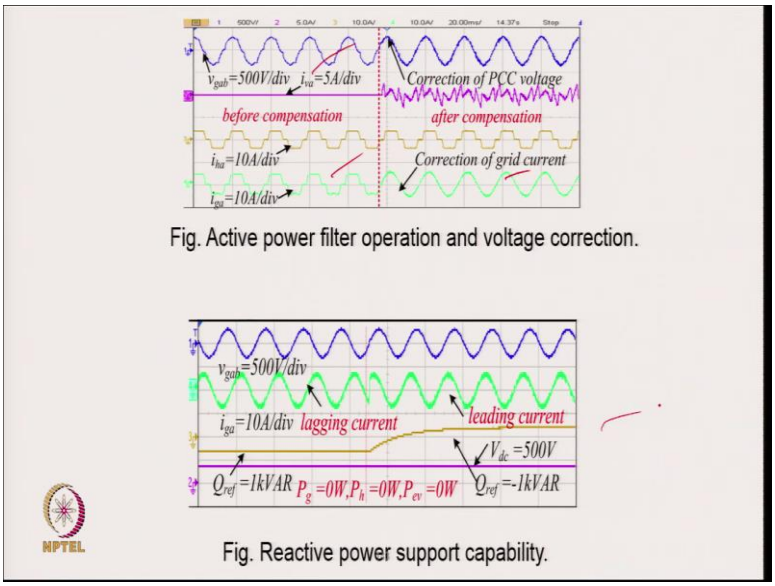

Fig. Active power filter operation and voltage correction.

Fig. Reactive power support capability.

(Refer Slide Time: 38:33)

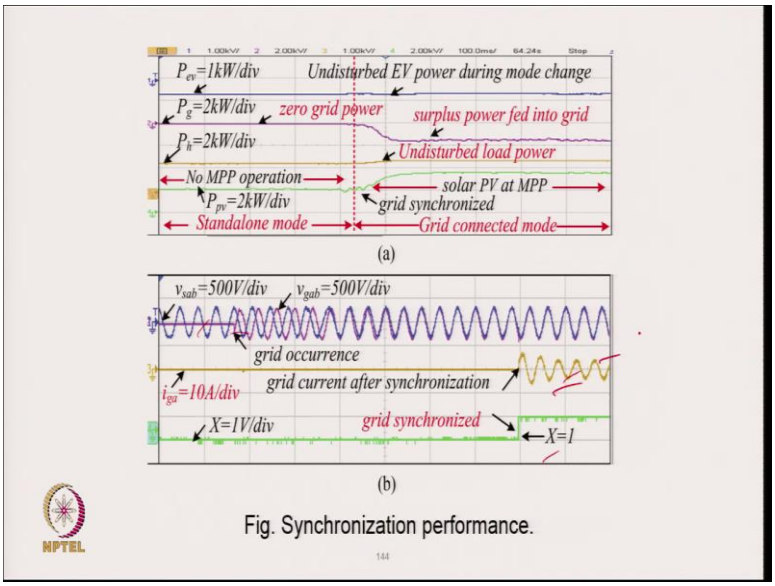

(Refer Slide Time: 38:44)

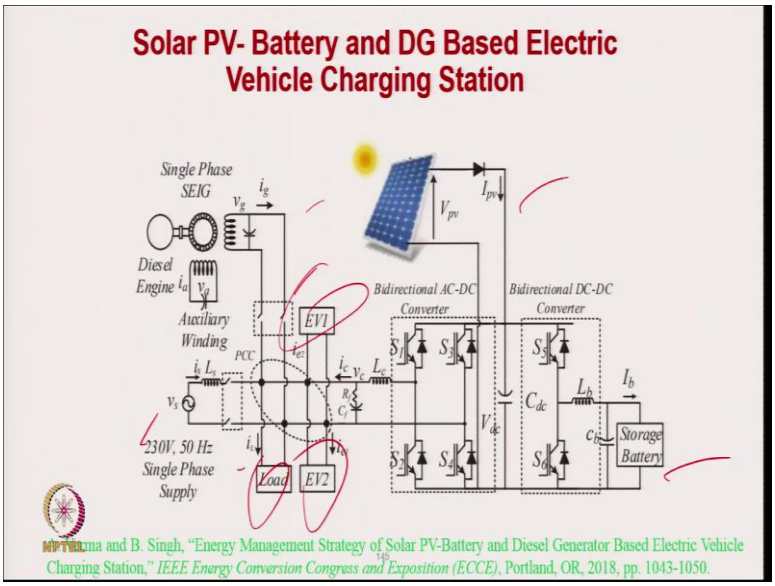

This is another charging station configuration. Its description, operational criterion, control strategy, and experimental results are presented herein.

(Refer Slide Time: 39:10)

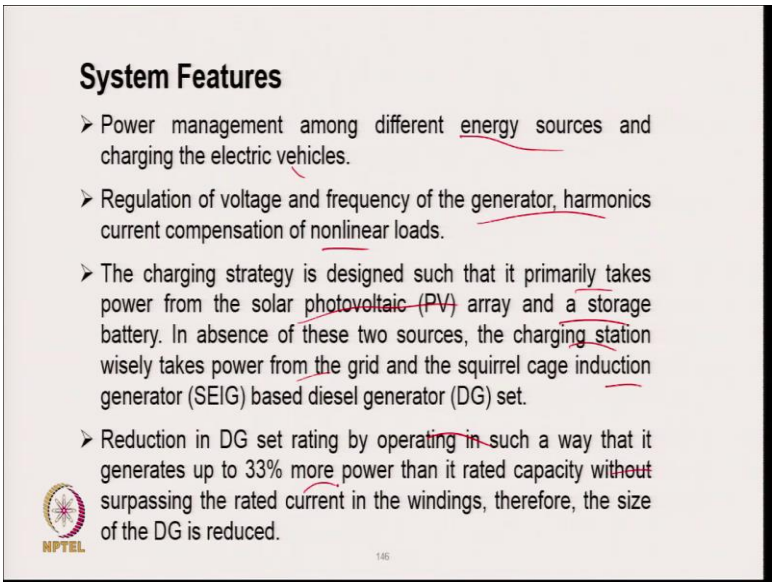

(Refer Slide Time: 39:33)

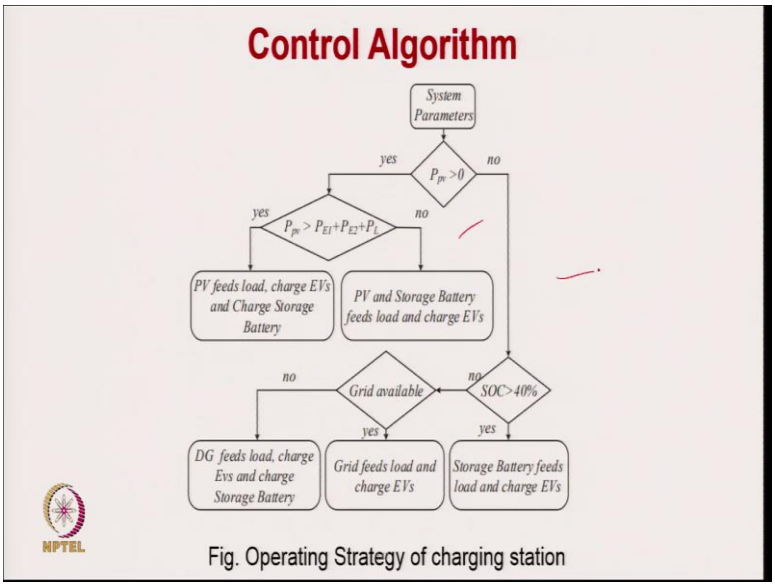

(Refer Slide Time: 39:39)

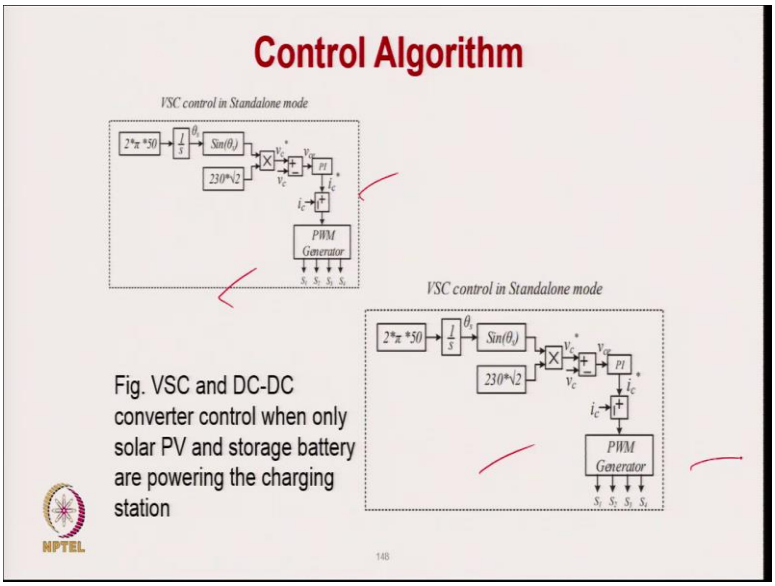

(Refer Slide Time: 39:47)

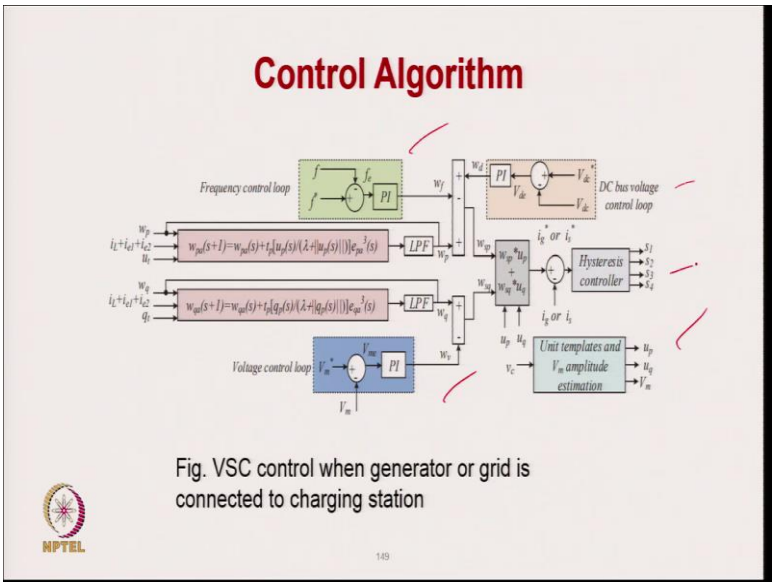

(Refer Slide Time: 39:59)

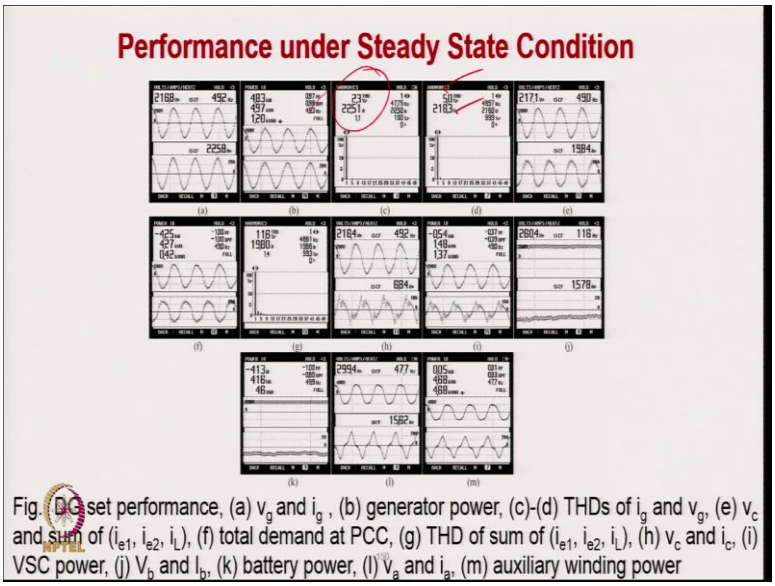

Fig. DG set performance, (a) v_g and i_g , (b) generator power, (c)-(d) THDs of i_g and v_g, (e) v_c and sum of (i_{e1}, i_{e2}, i_L), (f) total demand at PCC, (g) THD of sum of (i_{e1}, i_{e2}, i_L), (h) v_c and i_c, (i) VSC power, (j) V_b and I_b, (k) battery power, (l) V_a and i_a, (m) auxiliary winding power

(Refer Slide Time: 40:09)

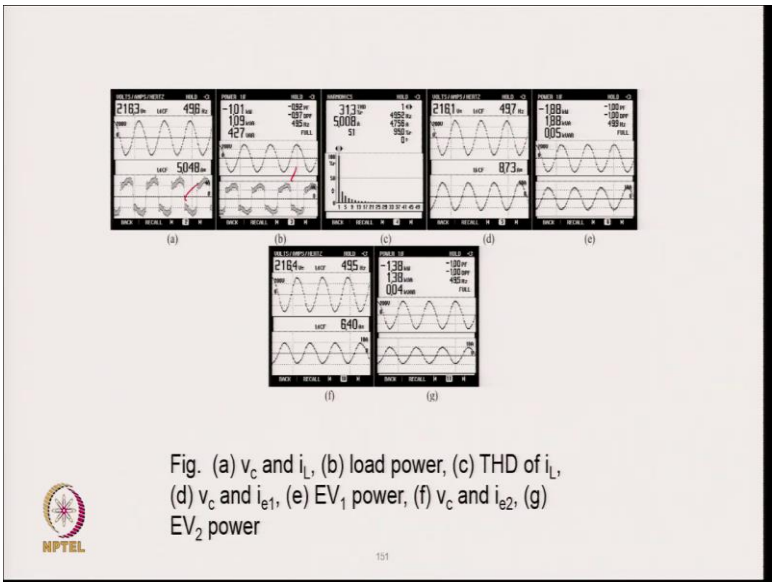

Fig. (a) v_c and i_L, (b) load power, (c) THD of i_L, (d) v_c and i_{e1}, (e) EV_1 power, (f) v_c and i_{e2}, (g) EV_2 power

(Refer Slide Time: 40:16)

Fig. Performance when storage battery is feeding load and charging EVs in absence of solar PV power, (a)V_b and I_b, (b) battery power, (c) v_c and sum of (i_{e1}, i_L), (d) total demand at PCC, (e)-(f) THDs vc and sum of (i_{e1}, i_{e2}, i_L), (g) v_c and i_L ,(h) load power, (i) THD of i_l ,(j) v_c and i_{e1}, (k) EV_1 power

(Refer Slide Time: 40:21)

Fig. Performance under grid connected mode, (a) v_s and i_s, (b) grid power, (c)-(d) THDs of v_s and i_s, (e) v_c and i_L ,(f) load power, (g) THD of i_l ,(h) v_c and i_{e1} ,(i) EV1 power, (j) v_c and i_{e2} ,(k) EV_2 power

(Refer Slide Time: 40:22)

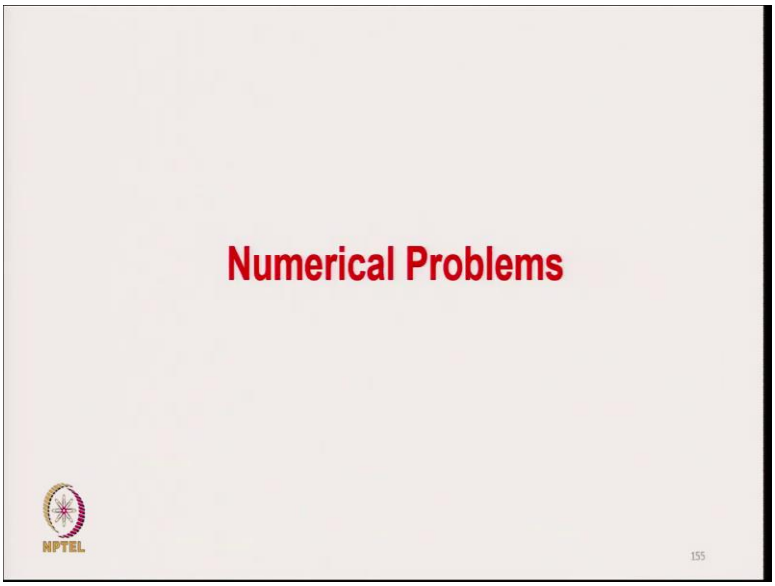

Now, coming to the numerical problems.

(Refer Slide Time: 40:25)

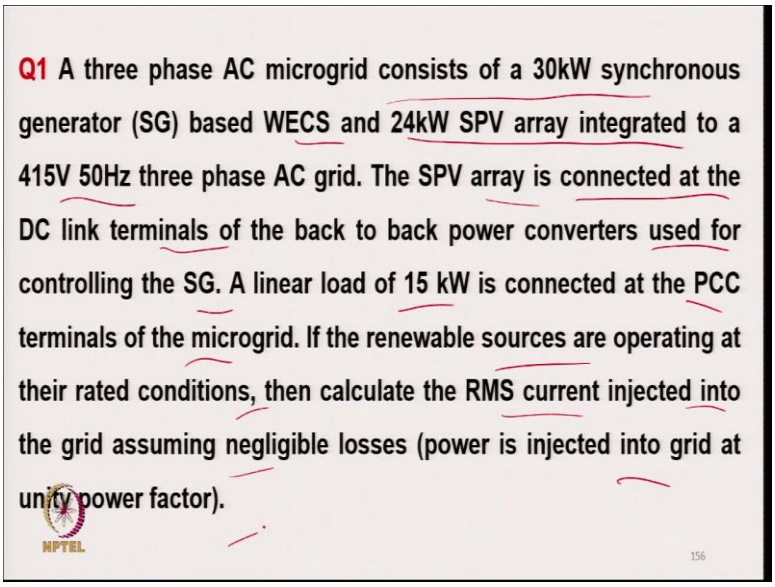

Three phase AC microgrid consists of 30 kilowatt synchronous generator based on wind power energy convergence 24 kilowatt solar PV array integrated to 415 volts 50 hertz three phase AC grid. And solar PV array is connected at the DC link terminal of the back to back connected power converter used for controlling the synchronous generator.

A linear load of fifteen kilowatt is connected at the PCC terminal of the microgrid and if renewable sources are operating at that rated condition. Then calculate the RMS current

injected into the grid assuming negligible losses power injected into grid at unity power factor.

(Refer Slide Time: 40:56)

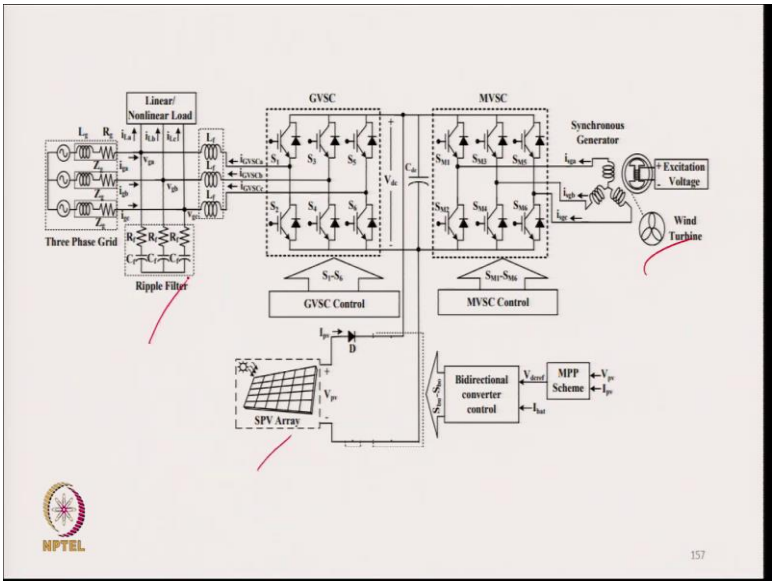

The solution to the numerical example is detailed in the screenshots herein.

(Refer Slide Time: 41:08)

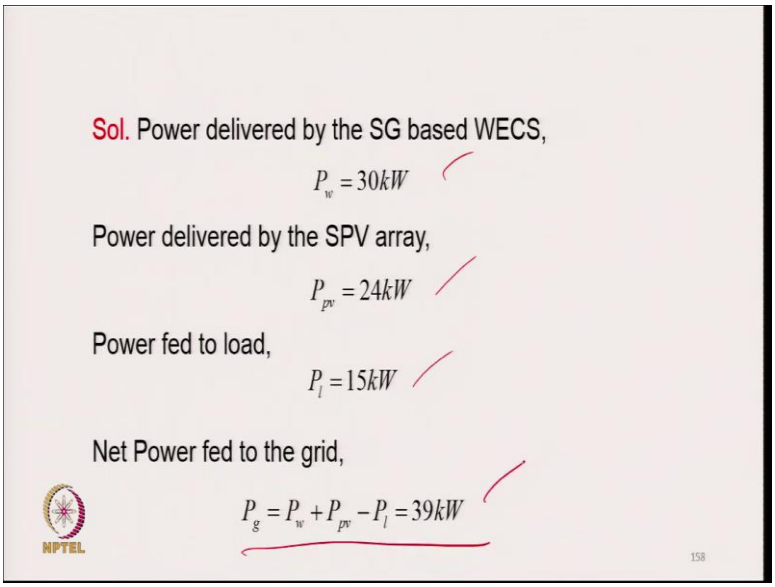

(Refer Slide Time: 41:17)

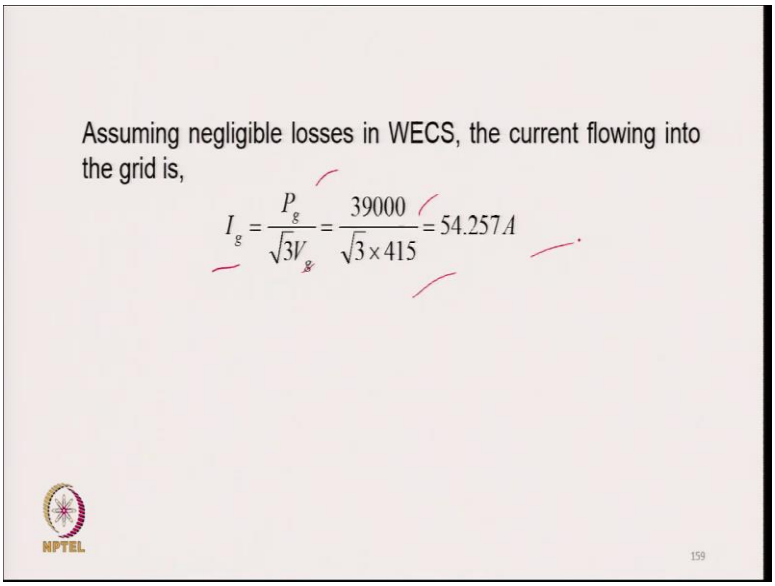

(Refer Slide Time: 41:23)

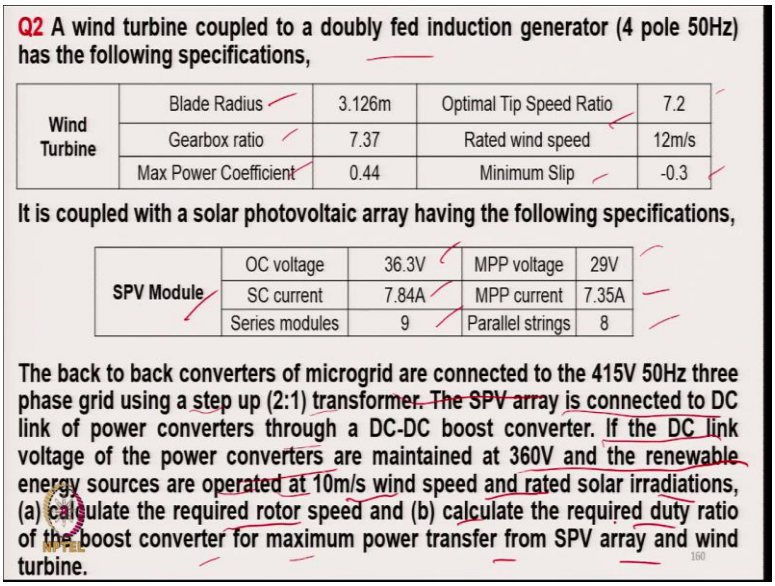

A wind turbine compared to doubly fed induction under 4 pole 50 hertz. These are typically that are of blade radius gearbox and maximum power coefficient slip maximum slip corresponding to your rated wind speed. And these are the PV array open circuit PV module current and MPPT voltage for PV module.

Back to back converters of microgrid connected to 415 volt 50 hertz three phase step up 2 to 1 transformer and SPV array connected to the DC link up through DC DC boost converter. And DC link voltage of the power converter are made at 360 volt with the

renewable research operator 10 meter per second wind speed and rated solar period. And calculate the required rotary speed, calculate the required duty ratio of the boost converter for maximum power from solar PVR and wind turbine.

(Refer Slide Time: 42:07)

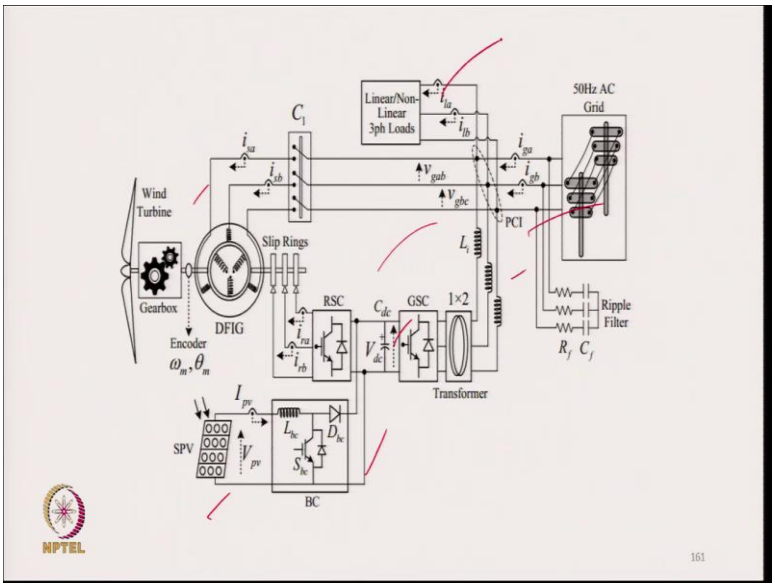

The solution to the numerical example is detailed in the screenshots herein.

(Refer Slide Time: 42:19)

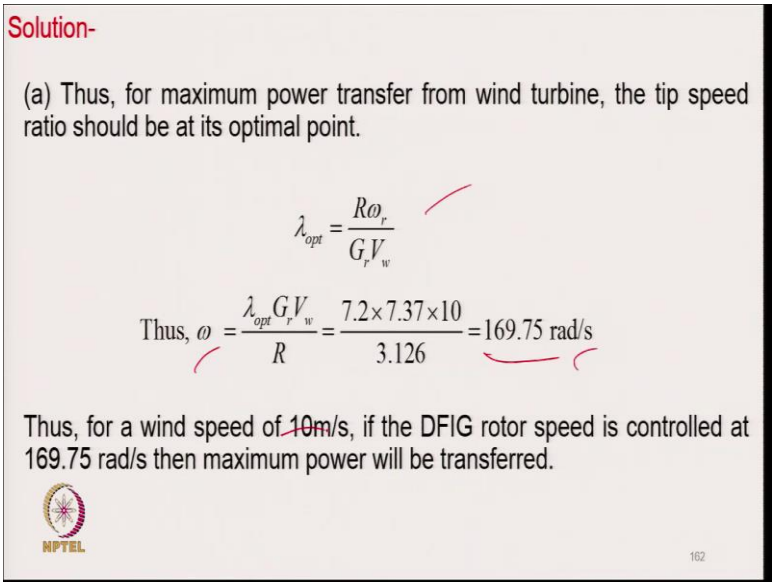

(Refer Slide Time: 42:28)

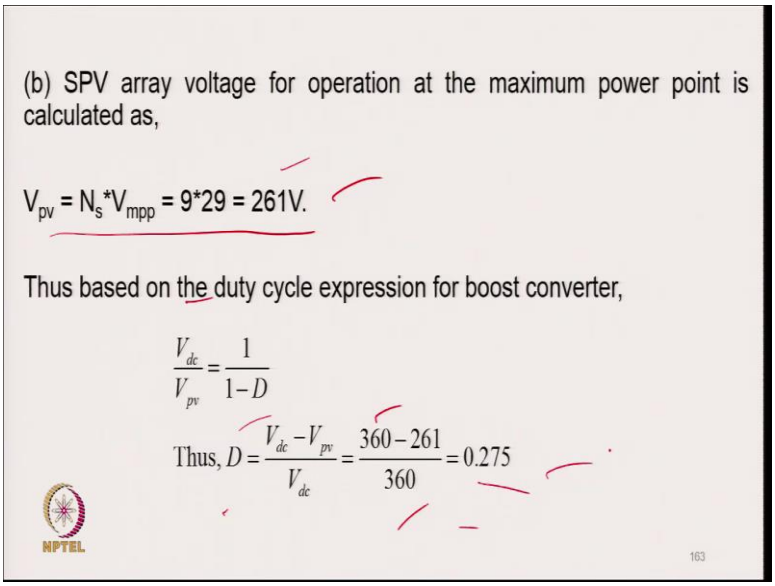

(Refer Slide Time: 42:43)

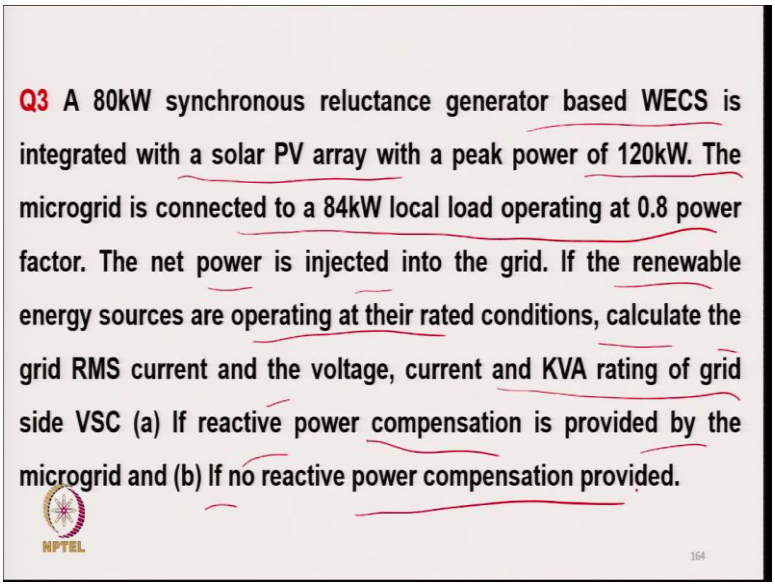

A 80 kilowatt synchronous reluctance generator base wind generator integrated system with the PV array with the peak power of 120 kilowatt. And the microgrid is connected to 84 kilowatt local load operating at 0.8 lagging power factor.

Net power is injected into the grid if the renewable energy source is operating at the rated condition calculate the grid RMS current and the voltage current. And KVA rating of the grid side voltage source converter a the reactive power compensation is provided by the microgrid and no reactive power compensation provided microgrid.

(Refer Slide Time: 43:15)

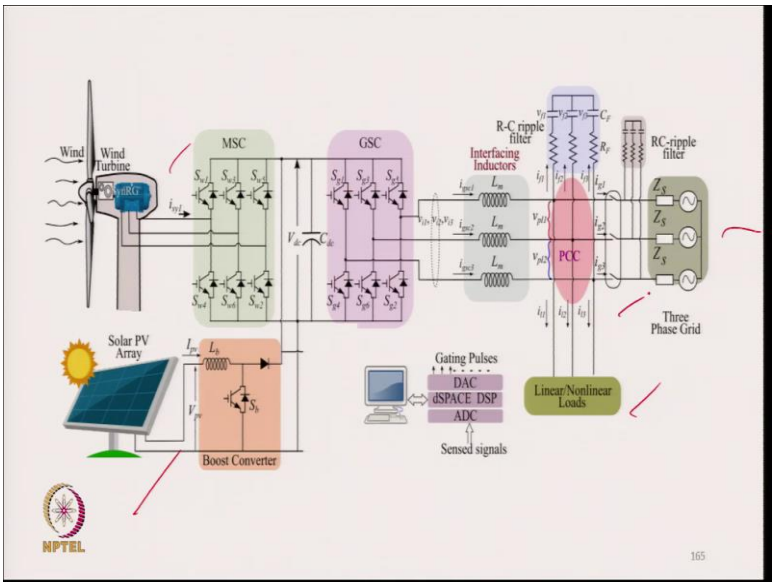

The solution to the numerical example is detailed in the screenshots herein.

(Refer Slide Time: 43:23)

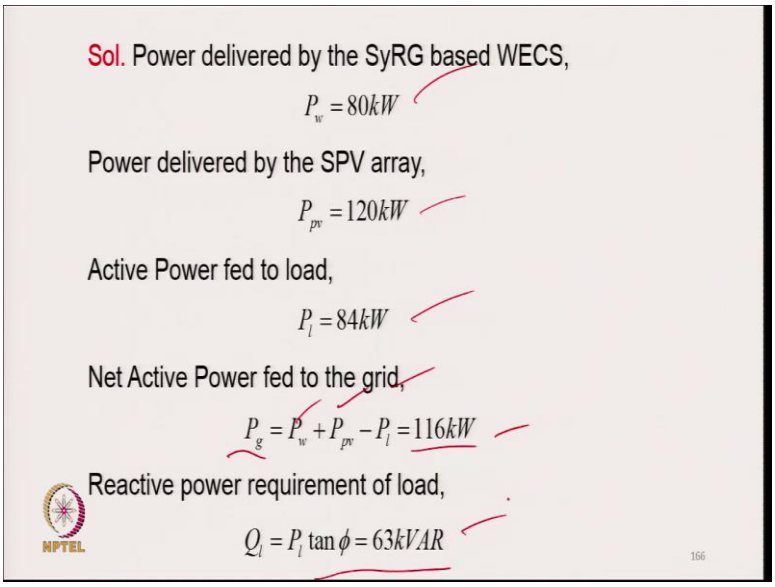

(Refer Slide Time: 43:42)

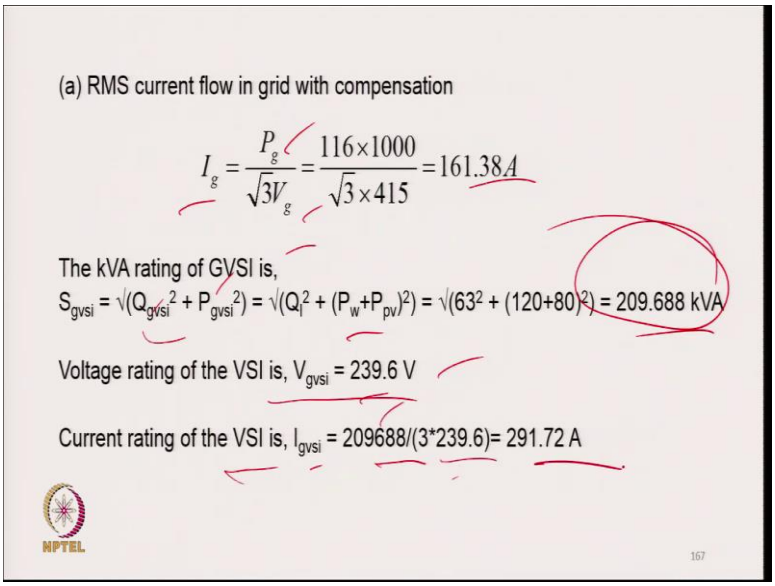

(Refer Slide Time: 44:06)

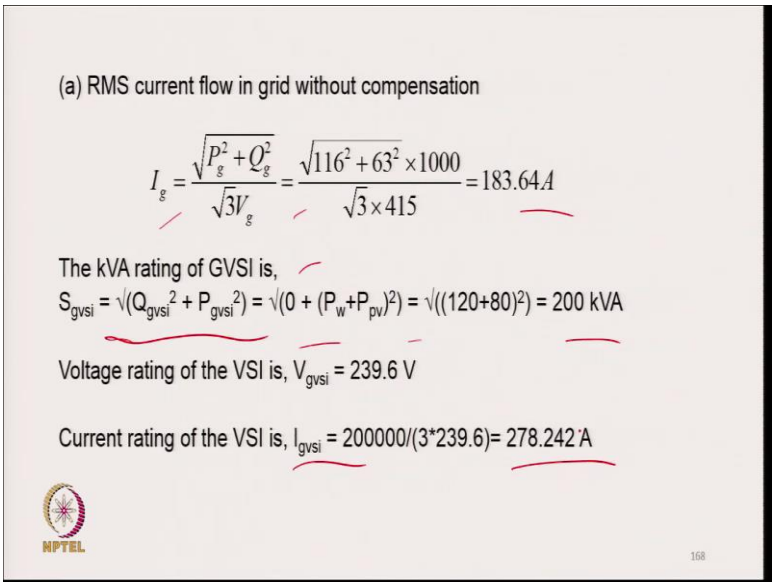

(Refer Slide Time: 44:25)

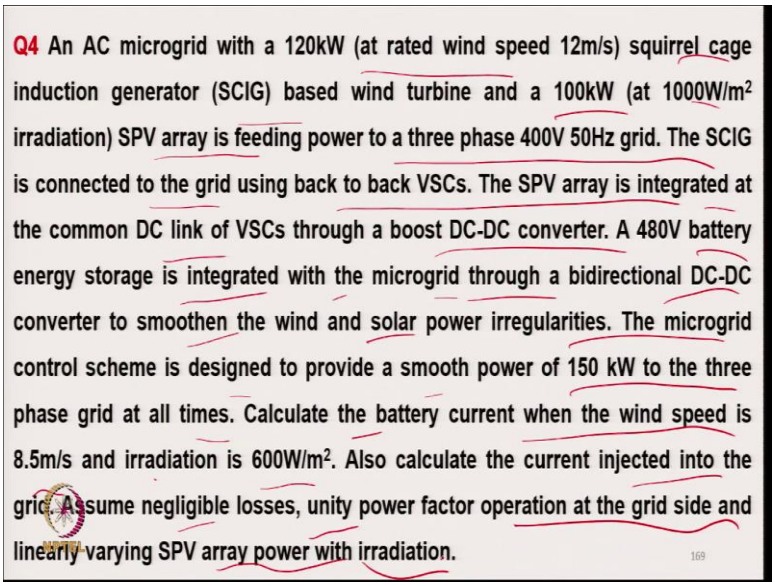

An AC microgrid with 120 kilowatt at rated wind speed of 12 meter per second is squirrel cage induction generator based on wind turbine. And a 100 kilowatt at 1000 (Refer Time: 44:37) solar PV range fitting power to the three phases of 400 volt 50 hertz squirrel. And squirrel cage generator to the grid using back to back voltage source converter and SPV array is integrated to the common DC link of VSC through boost convertor.

A 480 volt standard battery energy storage system integrated with the microgrid through bidirectional DC DC converter which smoothen the wind and solar irregularity. The microgrid control scheme is to provide a smooth power of 150 kilowatt to three phase grid at all time. Calculate the battery current when the wind speed is 8.5 meter per second and the solar radiation 600 watt per meter. Also, calculate the current injected into the grid also assume negligible losses unity power factor operation at the grid side can be varying the linear variation of solar PV power with irradiation.

(Refer Slide Time: 45:17)

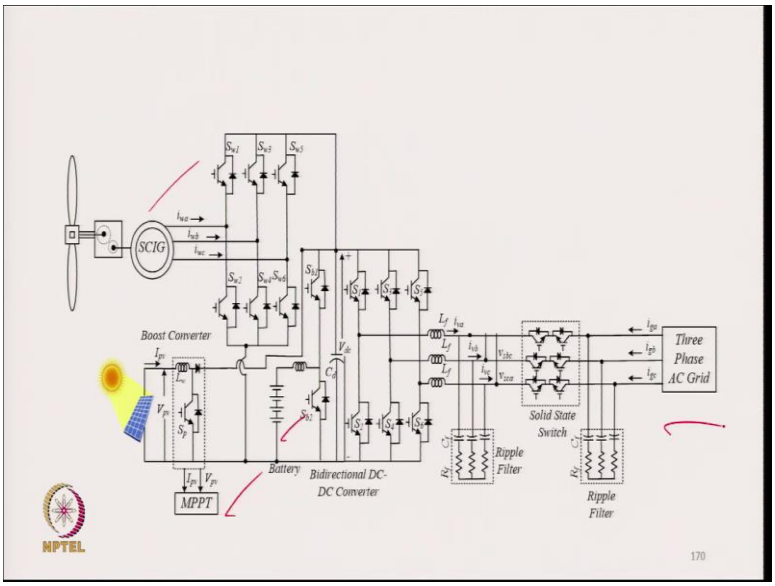

The solution to the numerical example is detailed in the screenshots herein.

(Refer Slide Time: 45:23)

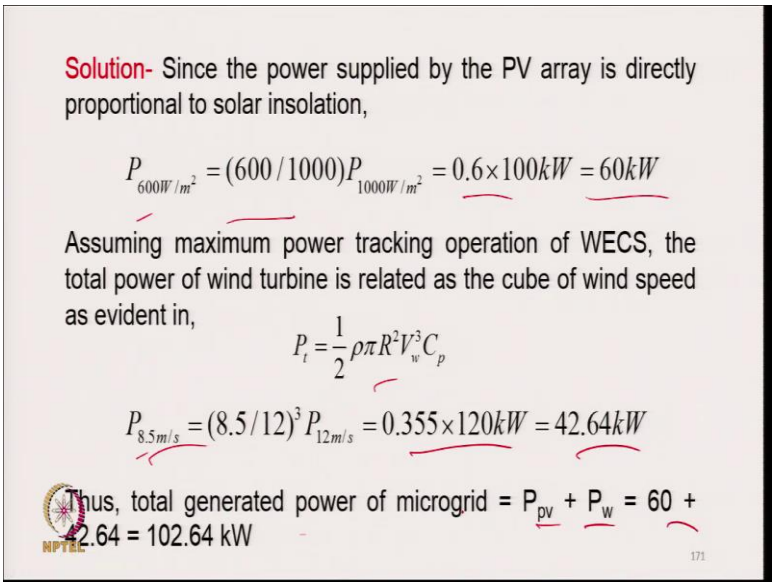

(Refer Slide Time: 45:42)

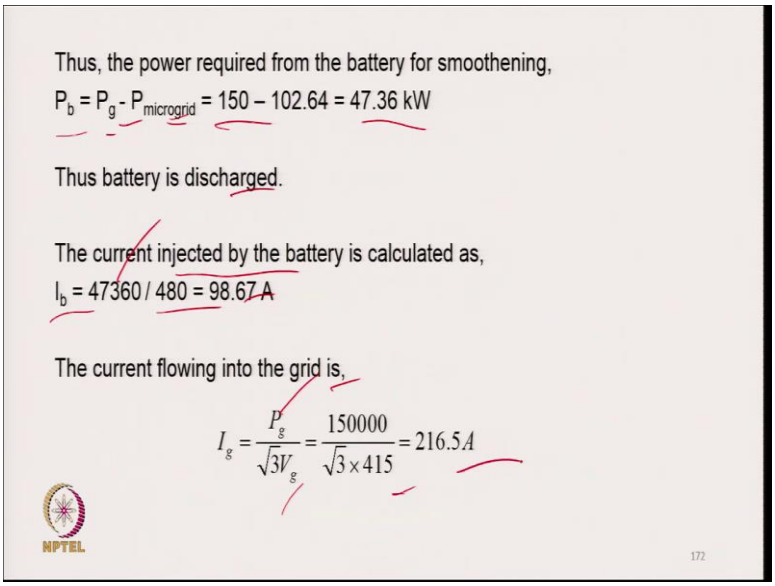

(Refer Slide Time: 46:07)

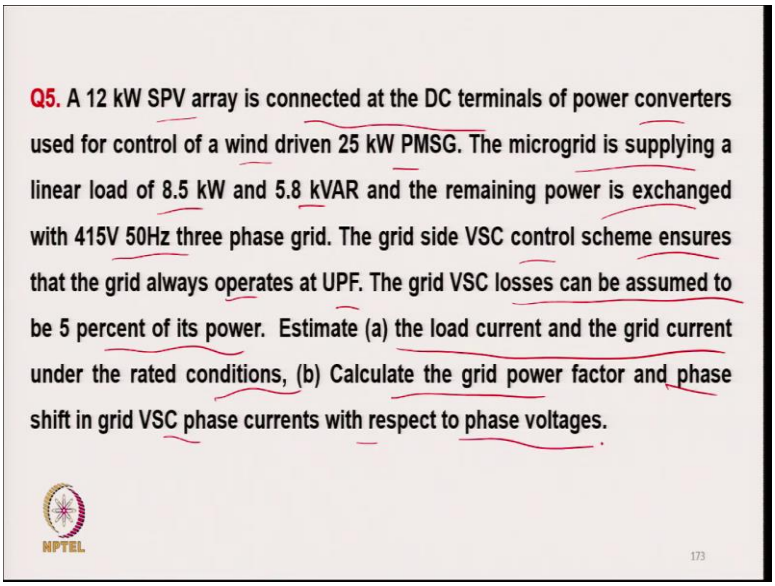

A 12 kilowatt solar PV array is connected to the DC terminal of power converter used for the control of wind driven 25 kilowatt permanent magnet synchronous generator. The microgrid is supplying the linear load of 8.5 kilowatt and 5.8 kVAR. And remaining power is exchanged with the 415 volt three phase grid the grid side voltage source converter ensure the grid always operate at UPF. And the grid voltage source converter losses can be assumed 5 percent of the estimate a the load current and the grid current under the rated condition b calculate the grid power factor and the phase angle shift between AC current with respect to the voltage.

(Refer Slide Time: 46:44)

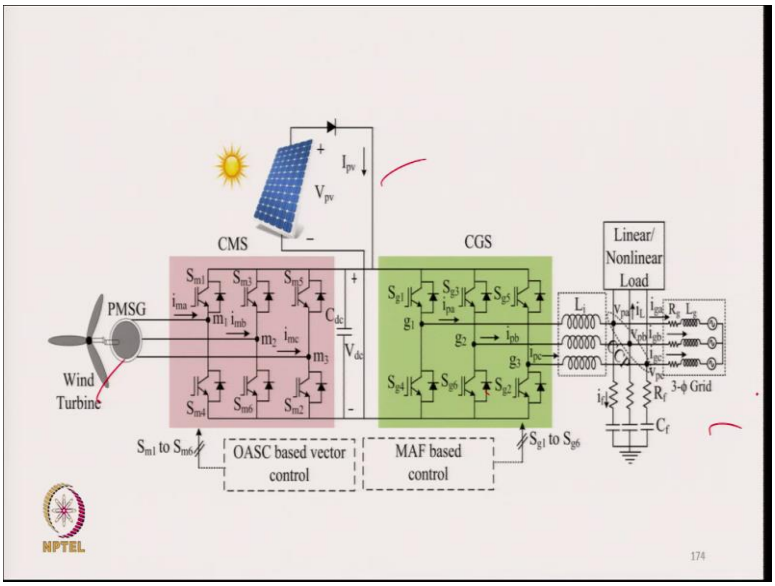

The solution to the numerical example is detailed in the screenshots herein.

(Refer Slide Time: 46:52)

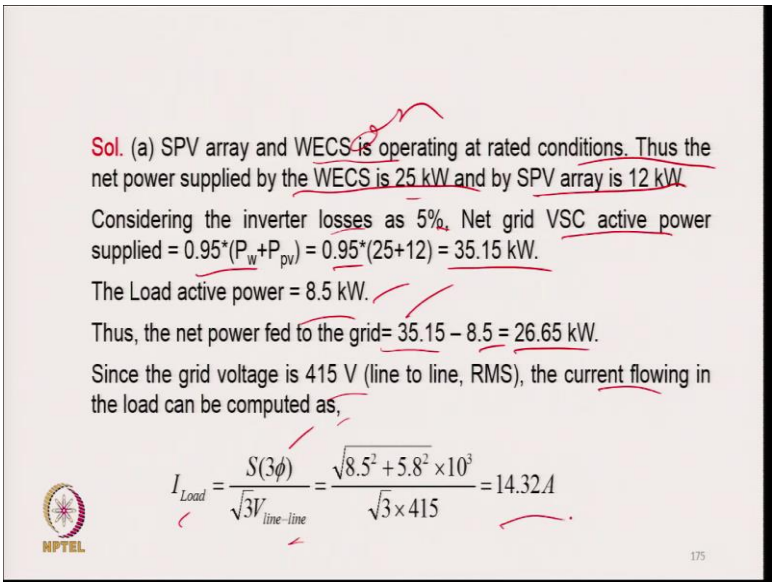

(Refer Slide Time: 47:32)

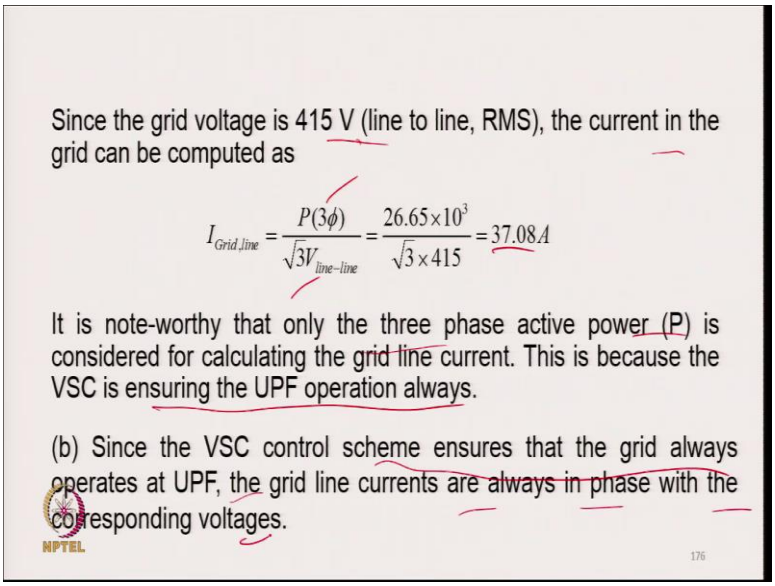

(Refer Slide Time: 47:51)

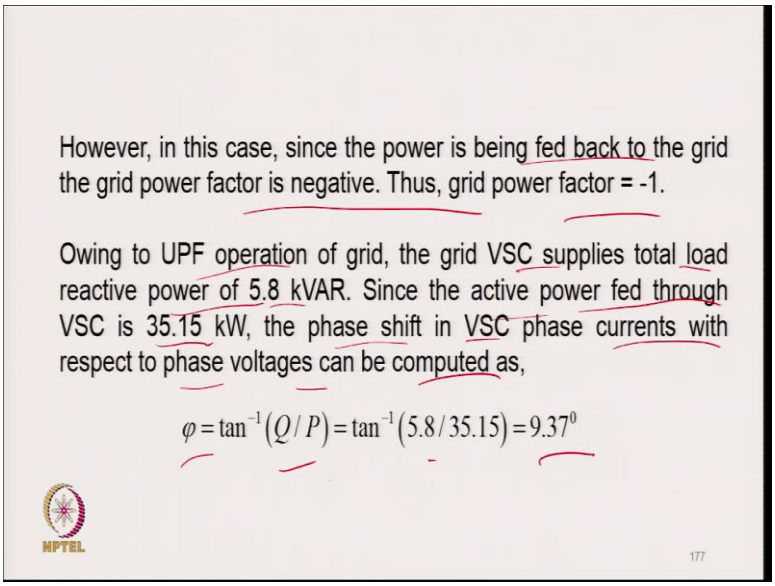

(Refer Slide Time: 48:17)

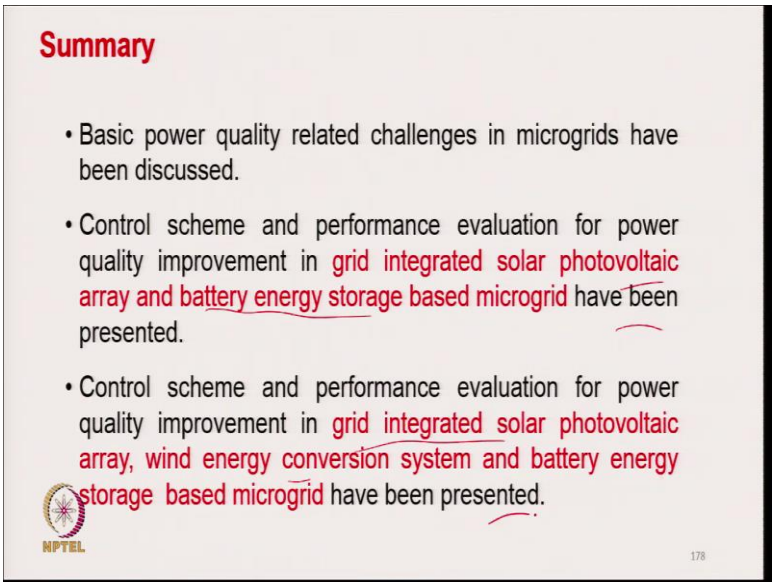

To summarize: Basic power quality relative challenges have been discussed. Control scheme and performance evaluation of power quality improvement grid integrated solar PV array battery base energy system based micro would have been presented. Control scheme and performance of evaluation of power quality improvement grid integrated and wind generation convergence system battery have been discussed.

(Refer Slide Time: 48:40)

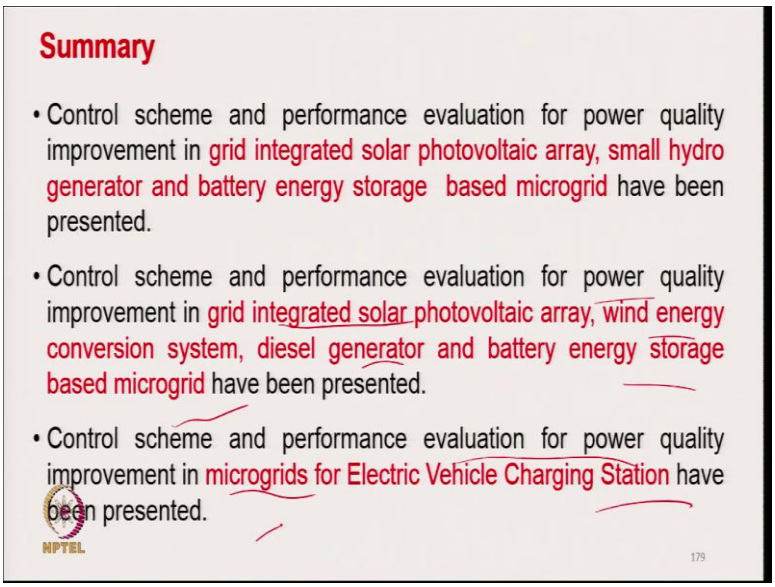

Control scheme and performance evaluation of power quality improvement grid integrated solar PV small hydro and battery energy storage system based microgrid are

presented. Control scheme performance evaluation of grid connected indicators solar PV wind energy conversion system DG set, battery energy storage microgrid have been I mean discuss. Control scheme and performance evaluation of power quality improvement with the electric vehicle charging station have been presented.

(Refer Slide Time: 49:06)

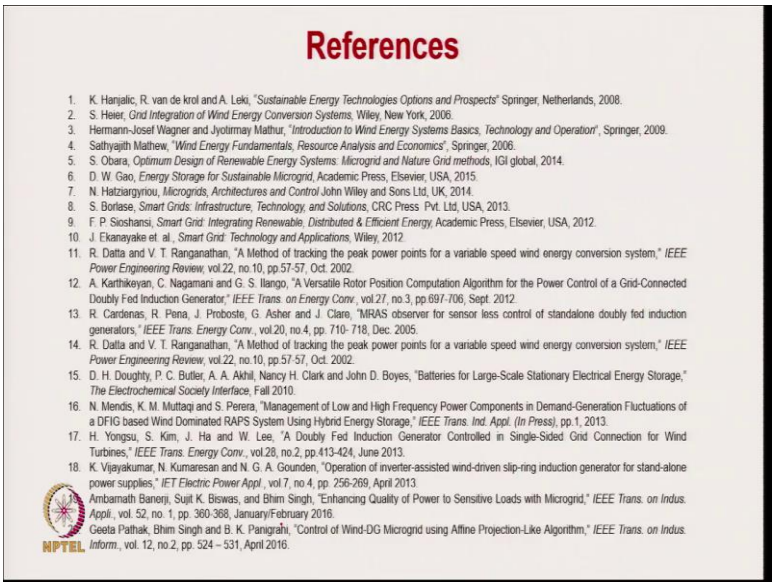

(Refer Slide Time: 49:07)

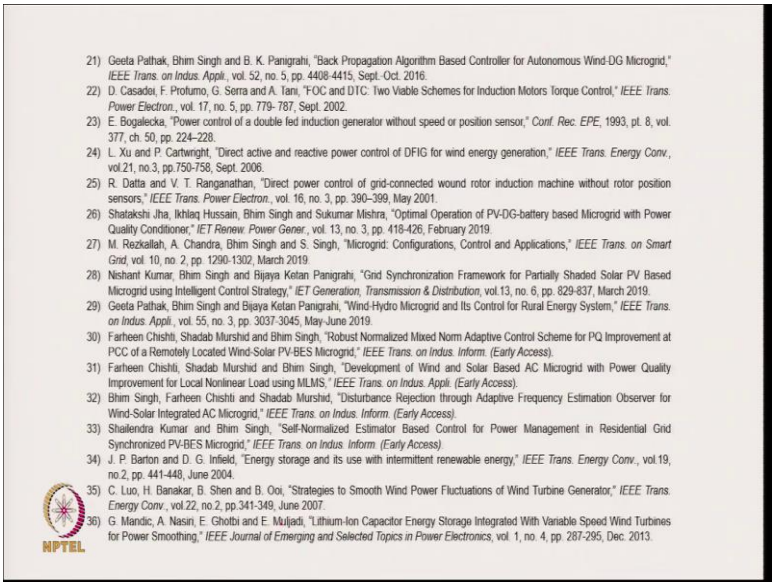

(Refer Slide Time: 49:08)

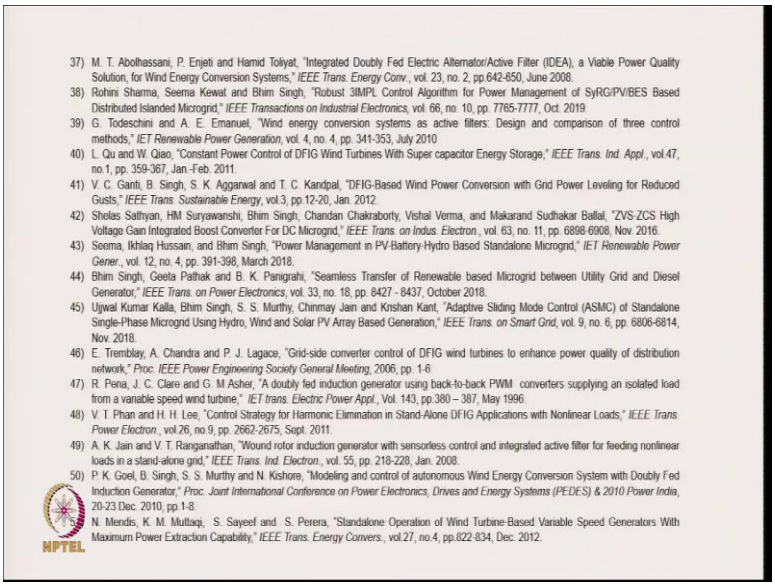

37) M. T. Abolhassani, P. Enjeti and Hamid Toliyat, "Integrated Doubly Fed Electric Alternator/Active Filter (IDEA), a Viable Power Quality Solution, for Wind Energy Conversion Systems," *IEEE Trans. Energy Conv.*, vol. 23, no. 2, pp.642-650, June 2008.
38) Rohini Sharma, Seema Kewat and Bhim Singh, "Robust 3IMPL Control Algorithm for Power Management of SyRG/PV/BES Based Distributed Islanded Microgrid," *IEEE Transactions on Industrial Electronics*, vol. 66, no. 10, pp. 7765-7777, Oct. 2019.
39) G. Todeschini and A. E. Emanuel, "Wind energy conversion systems as active filters: Design and comparison of three control methods," *IET Renewable Power Generation*, vol. 4, no. 4, pp. 341-353, July 2010.
40) L. Qu and W. Qiao, "Constant Power Control of DFIG Wind Turbines With Super capacitor Energy Storage," *IEEE Trans. Ind. Appl.*, vol.47, no.1, pp. 359-367, Jan.-Feb. 2011.
41) V. C. Ganti, B. Singh, S. K. Aggarwal and T. C. Kandpal, "DFIG-Based Wind Power Conversion with Grid Power Leveling for Reduced Gusts," *IEEE Trans. Sustainable Energy*, vol.3, pp.12-20, Jan. 2012.
42) Sholas Sathyan, HM Suryawanshi, Bhim Singh, Chandan Chakraborty, Vishal Verma, and Makarand Sudhakar Ballal, "ZVS-ZCS High Voltage Gain Integrated Boost Converter For DC Microgrid," *IEEE Trans. on Indus. Electron.*, vol. 63, no. 11, pp. 6898-6908, Nov 2016.
43) Seema, Ikhlaq Hussain, and Bhim Singh, "Power Management in PV-Battery-Hydro Based Standalone Microgrid," *IET Renewable Power Gener.*, vol. 12, no. 4, pp. 391-398, March 2018.
44) Bhim Singh, Geeta Pathak and B. K. Panigrahi, "Seamless Transfer of Renewable based Microgrid between Utility Grid and Diesel Generator," *IEEE Trans. on Power Electronics*, vol. 33, no. 18, pp. 8427 - 8437, October 2018.
45) Ujjwal Kumar Kalla, Bhim Singh, S. S. Murthy, Chinmay Jain and Krishan Kant, "Adaptive Sliding Mode Control (ASMC) of Standalone Single-Phase Microgrid Using Hydro, Wind and Solar PV Array Based Generation," *IEEE Trans. on Smart Grid*, vol. 9, no. 6, pp. 6806-6814, Nov. 2018.
46) E. Tremblay, A. Chandra and P. J. Lagace, "Grid-side converter control of DFIG wind turbines to enhance power quality of distribution network," *Proc. IEEE Power Engineering Society General Meeting*, 2006, pp. 1-6.
47) R. Pena, J. C. Clare and G. M Asher, "A doubly fed induction generator using back-to-back PWM converters supplying an isolated load from a variable speed wind turbine," *IET trans. Electric Power Appl.*, Vol. 143, pp.380 – 387, May 1996.
48) V. T. Phan and H. H. Lee, "Control Strategy for Harmonic Elimination in Stand-Alone DFIG Applications with Nonlinear Loads," *IEEE Trans. Power Electron.*, vol.26, no.9, pp. 2662-2675, Sept. 2011.
49) A. K. Jain and V. T. Ranganathan, "Wound rotor induction generator with sensorless control and integrated active filter for feeding nonlinear loads in a stand-alone grid," *IEEE Trans. Ind. Electron.*, vol. 55, pp. 218-228, Jan. 2008.
50) P. K. Goel, B. Singh, S. S. Murthy and N. Kishore, "Modeling and control of autonomous Wind Energy Conversion System with Doubly Fed Induction Generator," *Proc. Joint International Conference on Power Electronics, Drives and Energy Systems (PEDES) & 2010 Power India*, 20-23 Dec. 2010, pp.1-8.
51) N. Mendis, K. M. Muttaqi, S. Sayeef and S. Perera, "Standalone Operation of Wind Turbine-Based Variable Speed Generators With Maximum Power Extraction Capability," *IEEE Trans. Energy Convers.*, vol.27, no.4, pp.822-834, Dec. 2012.

(Refer Slide Time: 49:08)

52) Anjeet Verma and Bhim Singh, "Multi-objective Reconfigurable Three Phase Off-Board Charger for EV," *IEEE Trans. on Indus. Appli.*, vol. 55, no. 4, pp. 4192-4203, July-Aug. 2019.
53) Bhim Singh, Seema Kewat and Anjeet Verma, "Islanded Distributed Generation System with Feed-Forward PR-EFLL Control for AC-Electric Vehicle Charger," *Accepted for publication in IET Power Electronics.*
54) N. Mendis, K. M. Muttaqi, S. Sayeef and S. Perera, "Standalone Operation of Wind Turbine-Based Variable Speed Generators With Maximum Power Extraction Capability," *IEEE Trans. Energy Convers.*, vol.27, no.4, pp.822-834, Dec. 2012.
55) Shailendra Kumar and Bhim Singh, "Dual Mode Control of Utility Interactive Microgrid," *Accepted for publication in IET Renewable Power Generation.*
56) S. Sahoo, S. Mishra, S. Jha and B. Singh, "A Cooperative Adaptive Droop Based Energy Management & Optimal Voltage Regulation Scheme for DC Microgrids," *IEEE Trans. on Indus. Electron. (Early Access).*
57) Miloud Rezkallah, Sanjeev Singh, Ambrish Chandra, Bhim Singh, M. Tremblay, M. Saad, and H. Geng, "Comprehensive Controller Implementation for Wind-PV-Diesel based Standalone Microgrid," *Accepted for publication in IEEE Trans. on Indus. Appli.*
58) N. Saxena, I. Hussain, B. Singh and A. L. Vyas, "Implementation of a Grid-Integrated PV-Battery System for Residential and Electrical Vehicle Applications," *IEEE Trans. on Indus. Electron.*, vol. 65, no. 8, pp. 6592-6601, Aug. 2018.
59) Arun Kumar Verma, Bhim Singh and D.T. Shahani, "Grid to Vehicle and Vehicle to Grid Energy Transfer using Single-Phase Half Bridge Boost AC-DC Converter and Bidirectional DC-DC Converter," *International Journal of Engineering, Science and Technology*, vol. 4, no. 1, pp. 46-54, 2012.
60) Arun Kumar Verma, Bhim Singh and D.T. Shahani, "New topology for management of bi-directional power flow between vehicle and grid with reduced ripple current at unity power factor," *International Journal of Power Electronics*, vol. 5, no. 3-4, pp. 216-235, 2013.
61) Arun Kumar Verma, Bhim Singh, D.T Shahani and Chinmay Jain, "Grid Interfaced SPV Smart Building with Bidirectional Power Flow between Grid and Electric Vehicle with Improved Power Quality," *Journal of Electric Power Components and Systems*, vol.44, no.5, pp.480-494, February 2016.
62) A. Verma and B. Singh, "Control of vehicle-to-home operation of electric vehicle with seamless transition capabilities," *IEEMA Engineer Infinite Conference (eTechNxT)*, New Delhi, 2018, pp. 1-6.
63) S. Puchalapalli, S. K. Tiwari, B. Singh and P. K. Goel, "A Microgrid Based on Wind Driven DFIG, DG and Solar PV Array for Optimal Fuel Consumption," *IEEE Power India International Conference (PIICON)*, Kurukshetra, India, 2018, pp. 1-6.
64) S. Puchalapalli and B. Singh, "A Grid Interactive Microgrid Based on Wind Driven DFIG and Solar PV Array with Regulated Power Flow Functionality," *IEEE India International Conference on Power Electronics (IICPE)*, JAIPUR, India, 2018, pp. 1-6.
65) Deepu Vijay M, Bhim Singh and G Bhuvaneswari, "Effective Utilisation of Solar Energy Conversion System with Energy Storage in AC Microgrid," *IEEE International Conference on Power Electronics, Drives and Energy Systems (PEDES 2018)*, at Indian Institute of Technology Madras in Chennai, Tamilnadu, India, 18-21 Dec. 2018.

And these are the some of the references.

Thank you.